

# Variable-Density Groundwater Flow

Vincent E.A. Post and Craig T. Simmons



THE  
GROUNDWATER  
PROJECT

# *Variable-Density Groundwater Flow*

*The Groundwater Project*

i

*Vincent E.A. Post*

*Hydrogeologist,  
Edinsi Groundwater,  
Nederhorst den Berg, The Netherlands*

*Craig T. Simmons*

*Professor,  
Flinders University,  
Adelaide, South Australia, Australia*

*Variable-Density  
Groundwater Flow*

*The Groundwater Project  
Guelph, Ontario, Canada2  
Version 2, January 31, 2023*

All rights reserved. This publication is protected by copyright. No part of this book may be reproduced in any form or by any means without permission in writing from the authors (to request permission contact: [permissions@gw-project.org](mailto:permissions@gw-project.org)). Commercial distribution and reproduction are strictly prohibited.

Groundwater-Project (The GW-Project) works are copyrighted and can be downloaded for free from [gw-project.org](http://gw-project.org). Anyone may use and share [gw-project.org](http://gw-project.org) links to download GW-Project's work. It is not permissible to make GW-Project documents available on other websites nor to send copies of the documents directly to others. Kindly honor this source of free knowledge that benefits you and all those who want to learn about groundwater.

Copyright © 2022 Vincent E.A. Post, Craig T. Simmons (The Authors)

Published by the Groundwater Project, Guelph, Ontario, Canada, 2022.

Post, Vincent E.A.

Variable-Density Groundwater Flow / Vincent E.A. Post and Craig T. Simmons - Guelph, Ontario, Canada, 2022.

92 pages

ISBN: 978-1-77470-046-4

DOI: <https://doi.org/10.21083/978-1-77470-046-4>

Please consider signing up for the GW-Project mailing list to stay informed about new book releases, events and ways to participate in the GW-Project. When you sign up for our email list it helps us build a global groundwater community. [Sign up](#).

Citation: Post, V.E.A. and C.T. Simmons, 2021, [Variable-Density Groundwater Flow](#). The Groundwater Project, Guelph, Ontario, Canada. <https://doi.org/10.21083/978-1-77470-046-4>.



*Domain Editors*: Eileen Poeter and John Cherry

*Board*: John Cherry, Paul Hsieh, Ineke Kalwij, Stephen Moran, Everton de Oliveira and Eileen Poeter

*Steering Committee*: John Cherry, Allan Freeze, Paul Hsieh, Ineke Kalwij, Douglas Mackay, Stephen Moran, Everton de Oliveira, Beth Parker, Eileen Poeter, Ying Fan, Warren Wood, and Yan Zheng.

*Cover Image*: Post and Simmons, 2022

## Dedication

This book is dedicated to the pioneers of variable-density groundwater flow research, and especially to our mentors Robin A. Wooding, D. A. Nield, John W. Elder, and Henk Kooi.

# Table of Contents

<b>VARIABLE-DENSITY GROUNDWATER FLOW</b> .....	<b>I</b>
<b>AUTHORS</b> .....	<b>II</b>
<b>COPYRIGHT</b> .....	<b>III</b>
<b>DEDICATION</b> .....	<b>IV</b>
<b>TABLE OF CONTENTS</b> .....	<b>V</b>
<b>THE GROUNDWATER PROJECT FOREWORD</b> .....	<b>VII</b>
<b>FOREWORD</b> .....	<b>VIII</b>
<b>PREFACE</b> .....	<b>IX</b>
<b>ACKNOWLEDGMENTS</b> .....	<b>X</b>
<b>1 INTRODUCTION</b> .....	<b>1</b>
<b>2 WHAT CAUSES GROUNDWATER DENSITY VARIATIONS?</b> .....	<b>4</b>
<b>3 QUANTIFYING GROUNDWATER FLOW IN THE PRESENCE OF DENSITY VARIATIONS</b> .....	<b>7</b>
3.1 EQUIVALENT FRESHWATER HEAD .....	10
<i>Horizontal Flow</i> .....	12
<i>Vertical Flow</i> .....	13
<b>4 TYPES OF DENSITY FOR GROUNDWATER FLOW</b> .....	<b>16</b>
4.1 FREE CONVECTION .....	16
4.2 STABLE AND UNSTABLE DENSITY CONFIGURATIONS .....	18
4.3 TRANSPORT PROCESSES IN GROUNDWATER .....	21
4.4 LANDFILL LEACHATE PLUME EXAMPLE .....	23
<b>5 DIMENSIONLESS NUMBERS</b> .....	<b>25</b>
5.1 MIXED CONVECTION RATIO .....	26
5.2 RAYLEIGH NUMBER .....	28
5.3 WOODING NUMBER .....	32
5.4 SHERWOOD NUMBER .....	34
5.5 NUSSELT NUMBER .....	35
<b>6 MATHEMATICAL MODELING</b> .....	<b>36</b>
6.1 GOVERNING EQUATIONS .....	36
6.2 THE ELDER PROBLEM .....	39
6.3 PREDICTABILITY OF CONVECTIVE FLOW PATTERNS .....	44
<i>Homogeneous Systems</i> .....	48
<i>Heterogeneity</i> .....	51
<b>7 SELECTED RESEARCH TOPICS</b> .....	<b>56</b>
7.1 FIELD SCALE DETECTION OF FREE CONVECTION .....	56
7.2 CHEMICAL REACTIONS IN VARIABLE-DENSITY FLOW SYSTEMS .....	61
7.3 FUTURE RESEARCH DIRECTIONS .....	64
<b>8 EXERCISES</b> .....	<b>66</b>
EXERCISE 1 .....	66
EXERCISE 2 .....	66
EXERCISE 3 .....	66
EXERCISE 4 .....	67
EXERCISE 5 .....	67

EXERCISE 6 ..... 68

EXERCISE 7 ..... 68

EXERCISE 8 ..... 68

**9 REFERENCES ..... 69**

**10 BOXES..... 82**

    BOX 1 - FREE CONVECTION CAKE ..... 82

*Ingredients* ..... 82

*Preparation* ..... 83

**11 EXERCISE SOLUTIONS ..... 84**

    SOLUTION EXERCISE 1 ..... 84

    SOLUTION EXERCISE 2 ..... 84

    SOLUTION EXERCISE 3 ..... 84

    SOLUTION EXERCISE 4 ..... 85

    SOLUTION EXERCISE 5 ..... 86

    SOLUTION EXERCISE 6 ..... 87

    SOLUTION EXERCISE 7 ..... 87

    SOLUTION EXERCISE 8 ..... 87

**12 NOTATIONS ..... 88**

**13 ABOUT THE AUTHORS ..... 91**

**MODIFICATIONS TO ORIGINAL RELEASE ..... A**

## The Groundwater Project Foreword

The Year 2022 marks an important year for groundwater because the United Nations Water Members and Partners have chosen the theme of this year's March 22 World Water Day to be: "Groundwater: making the invisible visible". The goal of the Groundwater Project (GW-Project) is in sync with this theme.

The GW-Project, a registered charity in Canada, is committed to contributing to advancement in groundwater education and brings a unique approach to the creation and dissemination of knowledge for understanding and problem-solving. The GW-Project operates the website <https://gw-project.org/> as a global platform for the democratization of groundwater knowledge, founded on the principle that:

*"Knowledge should be free and the best knowledge should be free knowledge." Anonymous*

The mission of the GW-Project is to promote groundwater learning. This is accomplished by providing accessible, engaging, high-quality, educational materials, free-of-charge online in many languages, to all who want to learn about groundwater. In short, providing essential knowledge tools for developing groundwater sustainably for humanity and ecosystems.

This is a new type of global educational endeavor in that it is based on the volunteerism of professionals from different disciplines and includes academics, consultants and retirees. The GW-Project involves many hundreds of volunteers associated with more than 200 organizations from 27 countries and six continents, with growing participation.

The GW-Project is an ongoing endeavor and will continue with hundreds of books being published online over the coming years, first in English and then in other languages, for downloading wherever the Internet is available. An important tenet of the GW-Project books is a strong emphasis on visualization via clear illustrations that stimulate spatial and critical thinking to facilitate absorption of information.

The GW-Project publications also include supporting materials such as videos, lectures, laboratory demonstrations, and learning tools in addition to providing, or linking to, public domain software for various groundwater applications supporting the educational process.

The GW-Project is a living entity, so subsequent editions of the books will be published from time to time. Users are invited to propose revisions.

We thank you for being part of the GW-Project Community. We hope to hear from you about your experience with using the books and related material. We welcome ideas and volunteers!

The Groundwater Project Steering Committee

May 2022

vii

## Foreword

In textbooks published about hydrogeology over the decades, the emphasis is on the flow of groundwater based on the assumption that the groundwater has a spatially constant density. This common conceptualization of groundwater systems gives the impression that in nature groundwater behaves as if this assumption is generally valid. However, this is not the case. The assumption is a convenience for teaching and textbook purposes, and to justify simpler calculations. The inclusion of variable density in the consideration of groundwater behavior adds complexity for which understanding requires time and effort beyond what can be included in most groundwater courses and consulting projects. In nature, there are many circumstances where density effects are sufficiently strong that the character of the groundwater flow system is entirely different from the case where density effects are absent. Including the influence of variable density in evaluating groundwater systems has profound consequences for groundwater flow and transport behavior, because it results in a completely different flow regime, with much faster and more effective mixing, over larger spatial scales, and shorter time scales.

Density effects occur in groundwater when there is a significant contrast in the density of water masses from different sources. One example is where fresh groundwater below land flows toward the coast where salt water occurs in the aquifer below the sea. Another example is where groundwater flows through a chemically reactive zone in which minerals dissolve adding mass to the water. This creates a density contrast between the geochemically altered water and the ambient groundwater. An additional example is where groundwater is contaminated by a source such as a landfill or septic system and the dissolved constituents increase the density of the water forming a plume that sinks into the ambient groundwater flow system. Yet another example is where a zone of groundwater is heated, perhaps by localized geothermal activity deep in the earth causing convective flow cells to form in the groundwater system.

This book presents the theory of variable-density flow and provides many examples based on published field and laboratory studies as well as numerical model simulations showing that density variations can result in complex patterns of salinity and/or temperature distribution in groundwater.

The authors, Dr. Vincent Post in the Netherlands and Dr. Craig Simmons in Australia have published extensively on topics related to variable-density groundwater flow including numerical simulations, as well as laboratory and field studies, giving them a balanced viewpoint of the topics. This book describes the approaches, tools, techniques, and methods for conceptualizing, understanding, predicting, modeling and measuring variable-density groundwater flow behavior. The graphs and simulation results in this book provide the reader with an informed basis for evaluating circumstances for which variable density can be important to groundwater flow and envisioning how the flow system will deviate from constant density systems.

John Cherry, The Groundwater Project Leader  
Guelph, Ontario, Canada, May 2022

## Preface

Differences in groundwater density are caused by variations in solute concentrations and/or temperature. Density-driven flow is important across a range of groundwater settings but its significance and complexity are sometimes underestimated. This book summarizes the main causes for, and manifestations of density-driven flow, in groundwater systems. Techniques used to understand, conceptualize, model, predict, and measure density-driven flow in groundwater are described.

Theoretical and experimental matters (including field-based investigations) are dealt with. Guidelines for assessing when density effects become important and corrections that are needed to correctly infer groundwater flow in systems where the density varies are discussed. The book highlights the difficulties and possibilities of simulating variable-density groundwater systems using numerical models. It also discusses some areas of ongoing research and debate and describes the challenges and opportunities for measuring density-driven flow directly in field-based groundwater settings.

## Acknowledgments

We deeply appreciate the thorough and useful reviews of and contributions to this book by the following individuals:

- ❖ Eileen Poeter, Colorado School of Mines, Colorado, USA;
- ❖ Ekkehard Holzbecher, German University of Technology in Oman, Germany;
- ❖ John M. (Jack) Sharp, Department of Geological Sciences, The University of Texas, Austin, Texas, USA;
- ❖ Harald Klammler, Federal University of Bahia, Brazil;
- ❖ Everton de Oliveira, Sustainable Water Institute, Brazil; and,
- ❖ Fred Marinelli, Ensero Solutions, Fort Collins, Colorado, USA.

We are grateful to Amanda Sills, Juliana Apolonio, Gabriel Amorim, and Beatriz Andrade of the Groundwater Project for their oversight and copyediting of this book. Special thanks go to André Nogueira and Rita Parente for sharing the vegan version of the ‘free convection cake’ recipe found in the back of this book.

# 1 Introduction

Groundwater movement is driven by hydraulic head gradients but under many circumstances, density variations exert an important control on the flow as well. This book describes variable-density groundwater flow and discusses when and why density-driven flow is important, and how it can be detected, quantified, and modeled. It also describes historical achievements and future challenges for this specialization within groundwater hydrogeology.

The ancient Greeks already wondered about the role of density in groundwater flow as shown by the following excerpt that is taken from the English translation by Hett (1957) of Aristotle's "Problems".

*"Why does not salt-water flow easily? Is it because what is heavy tends to be stationary? Now salt water is heavy so that salt water only flows easily when it is hot. For hot things contain a lightness in themselves, which masters the heaviness due to the salt for what is hot is lighter. Moreover, water which flows easily percolates through the earth and, as it percolates, the densest and heaviest part remains behind, while the light and pure part is separated. For salt water is heavy and fresh water light. This is why water which flows easily is fresh. The same cause explains why salt water becomes sweeter by moving and changing its position for it becomes lighter and less strong because of the movement."*

"Problems" was assembled by Aristotle's followers over a period between the third century BC (Before Christ) to the sixth century AD (Anno Domini), so it is not clear when exactly the scholars of the time began such early discussions of variable-density groundwater flow problems, and how insights evolved. But the paraphrased text above shows that they already had an understanding of the effect of salinity and temperature on density. As can be inferred from the second part, they thought that the density of groundwater would decrease during groundwater flow, as the soil filtered out the solutes. This reflects the widely held belief at the time that fresh groundwater formed out of seawater by filtration and condensation processes in the subsurface (Brutsaert, 2005). This belief, which is now known to be generally false, was maintained for centuries and it was not until the 18<sup>th</sup> century that alternative hypotheses started to emerge (Post et al., 2018b). The French clergyman and scholar Labat, for example, attributed the occurrence of fresh water on a small Caribbean islet to the infiltration of rainwater in the soil (Labat, 1724). He also explained that due to its lower density, fresh groundwater will float on top of saline groundwater.

Other scholars also understood that the difference in density between seawater and fresh water had to be taken into account to understand the salinity distribution in coastal

aquifers. A major scientific advancement was the formulation of the hydrostatic pressure equilibrium between fresh water and seawater. During the first half of the 19<sup>th</sup> century, publications emerged which drew attention to the analogy of the pressure equilibrium between fresh and saline groundwater in an aquifer with that in a U-tube (Boblaye, 1833; Du Commun, 1828; Inglis, 1817). A sketch of such a U-tube and the physical interpretation in terms of the freshwater-saltwater interface is given in Figure 1. The works by Drabbe and Badon Ghijben (1889) and Herzberg (1901, 1888) linked the quantitative relationship  $y = 40h$  (often referred to as “Ghijben Herzberg principle”; see caption of Figure 1) to the shape of a freshwater lens in a coastal aquifer. In other words, if the water table is found at 1 masl (meters above sea level), the interface between fresh and saline groundwater is at 40 mbsl (meters below sea level).

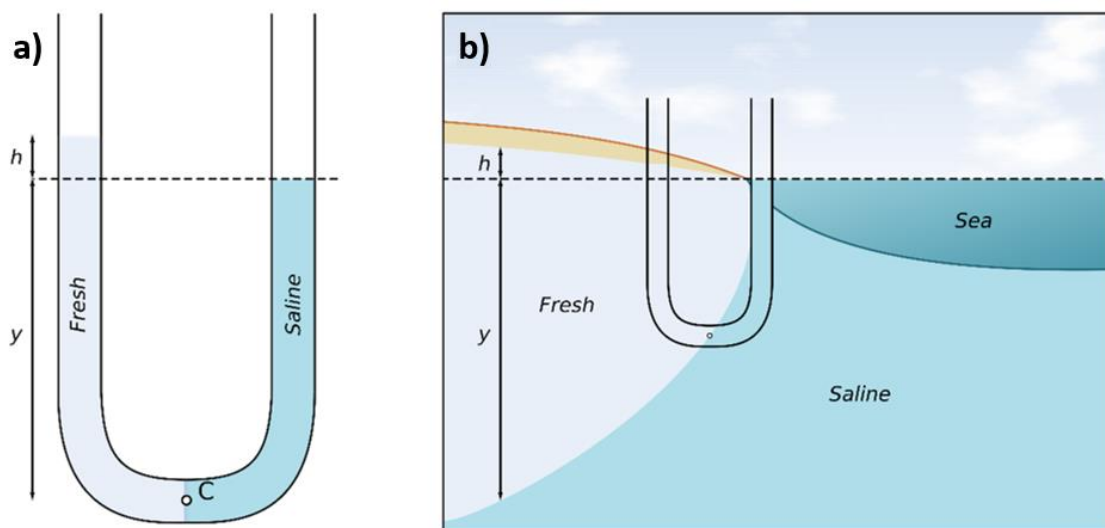


**Figure 1** – a) The hydrostatic pressure between fresh and saline water in a U-tube. When both fluids are at rest, the pressure exerted by the column of fresh water at point C is equal to the pressure exerted by the column of saline water at point C. Because the density of the fresh water is lower than the density of the saline water, a taller column of fresh water is needed to exert the same pressure. b) The U-tube analogy is applied to a coastal aquifer. In this case,  $h$  is equal to the water table elevation above mean sea level, and  $y$  is the depth to the freshwater-saltwater interface below mean sea level. For seawater ( $\rho = 1025 \text{ kg m}^{-3}$ ) and fresh water ( $\rho = 1000 \text{ kg m}^{-3}$ ), the hydrostatic equilibrium relationship between  $h$  and  $y$  is approximately  $y = 40h$ .

The nineteenth-century work was primarily concerned with hydrostatic conditions. The field of variable-density flow (dynamic conditions) emerged from classical fluid mechanics. Even the most cursory examination of the literature quickly reveals that the field of convection evolved from one concerned primarily with the heating of fluid layers in the early 1900s (Bénard, 1900; Rayleigh, 1916) to include porous media in the 1940s (Horton and Rogers, 1945; Lapwood, 1948). Wooding (1969, 1963, 1962, 1959) and Bachmat and Elrick (1970) provided some of the earliest work on solute-driven convective instability in porous media. The studies emerging from classical fluid mechanics find application in hydrogeology for geothermal systems, in which the temperature differences have an

important influence on the density. In deep sedimentary basins, both salinity differences and temperature differences cause variations in groundwater density. Nield (1968) provided some of the earliest work on thermohaline convection where flow is driven by both heat and solute gradients.

Interestingly, some already recognized the importance of convective flow phenomena for groundwater systems even before their physics became well understood. This includes the Dutch engineer Jan Versluys who gave a public lecture in 1918 in Delft, the Netherlands, that was later published (Versluys, 1918). The first publication contains a sketch of a cross section across the Dutch coastal area (Figure 2) that shows how Versluys pictured the evolving groundwater salinity distribution after the sea invaded the area during the Holocene sea-level rise. He drew columns of salt water (horizontal hatching) extending down from the inundated land surface in between remnant bodies of fresh groundwater (vertical hatching). In an explanatory note he wrote (translated from Dutch by the authors):

*“The... earth layers still contained fresh water, yet the seawater with a higher specific weight, infiltrated into them, and expelled the fresh water upward. The specific weight of seawater is significantly higher than of fresh water. Therefore, once the seawater had entered some distance, it had to penetrate at an ever-greater velocity. Thus, columns of salt water must have sunk down into the soil for some period of time, which had to experience large diversions because of clay layers. Such details are not indicated in this plate [...] At great depth, the salt water also spread landward, as indicated in plate 3.”*

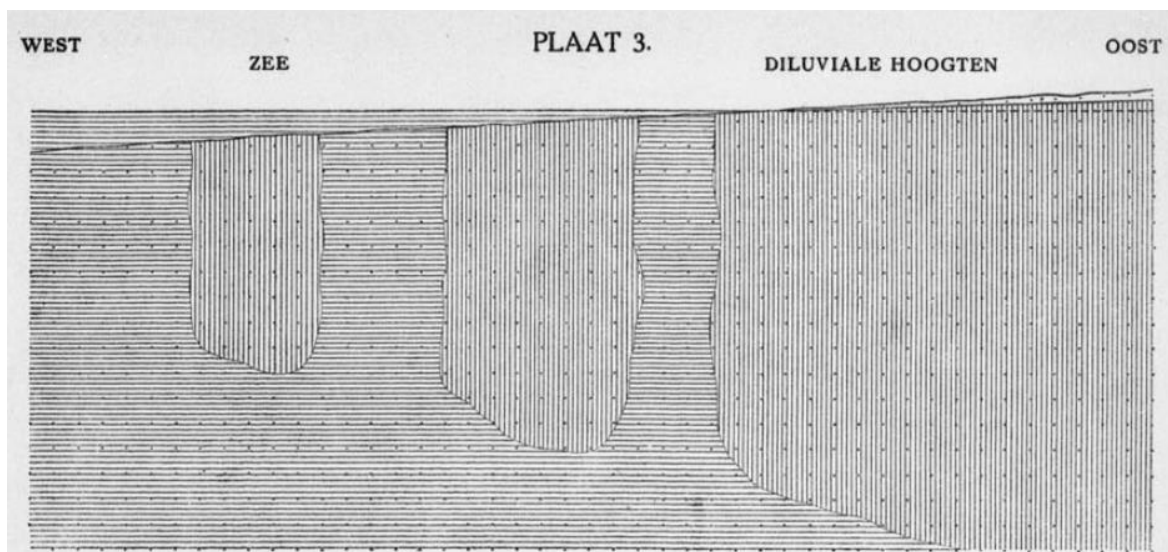


**Figure 2** - Schematic cross section by Versluys (1918) showing the distribution of fresh (vertical hatching) and saline (horizontal hatching) groundwater during an inundation of a freshwater aquifer by seawater. The depth scale is unknown, but the length scale would be tens of kilometers. Translations: “Plaat” is drawing or plate, “Zee” is sea, “Oost” is east (west is left untranslated) and “Diluviale hoogten” is an old-fashioned name for the fluvial sand deposits in the east part of the Netherlands that are above sea level.

In retrospect his conceptual model was largely correct, albeit that salt water does not accelerate as it sinks. He also understood that clay layers were less susceptible to salinization and that fresh water could be preserved in them. He argued that the fresh and saline waters would mix and that in the process their chemistry would alter. In discussing these aspects, he was listing a suite of research topics that would be studied in the century that followed his address. These include:

- What flow patterns evolve when a dense fluid overlies a lighter one?
- How do fluids of different densities mix?
- What is the resulting solute concentration or temperature distribution?
- At what rate and over what timescales do these processes operate?
- At what level of detail can predictions be made about density-driven flow?
- What is the role of geological heterogeneities?
- How does the flow impact the chemical composition of the groundwater and vice versa?

This book explores the answers to these questions by presenting an overview of the current state of knowledge of variable-density flow in groundwater systems. The book starts by discussing the dependence of the density of water on salinity and temperature. Then the role of density variations in groundwater flow processes is introduced. There are various ways to study density-driven flow. A lot of work is based on laboratory experiments and computational models, but it has proven very challenging to study variable-density flow and transport processes in the field. This book will deal with all of these methods, as well as highlight topics of ongoing research, debate and controversy. Section 8 contains exercises that illustrate application of some of the theoretical concepts.

## 2 What Causes Groundwater Density Variations?

Fluid density varies as the concentration, temperature and, to a much lesser extent fluid pressure, vary. Figure 3 shows the dependence of the density of water as a function of salt mass fraction (the mass of solutes divided by the total mass of the solution) and temperature at atmospheric pressure. At low solute concentrations, the water density ( $\rho$ ) is around  $1000 \text{ kg m}^{-3}$ , although this depends somewhat on the temperature. Typically, seawater has a salt mass fraction of around  $35 \text{ g kg}^{-1}$  with a density of approximately  $\rho = 1025 \text{ kg m}^{-3}$ .

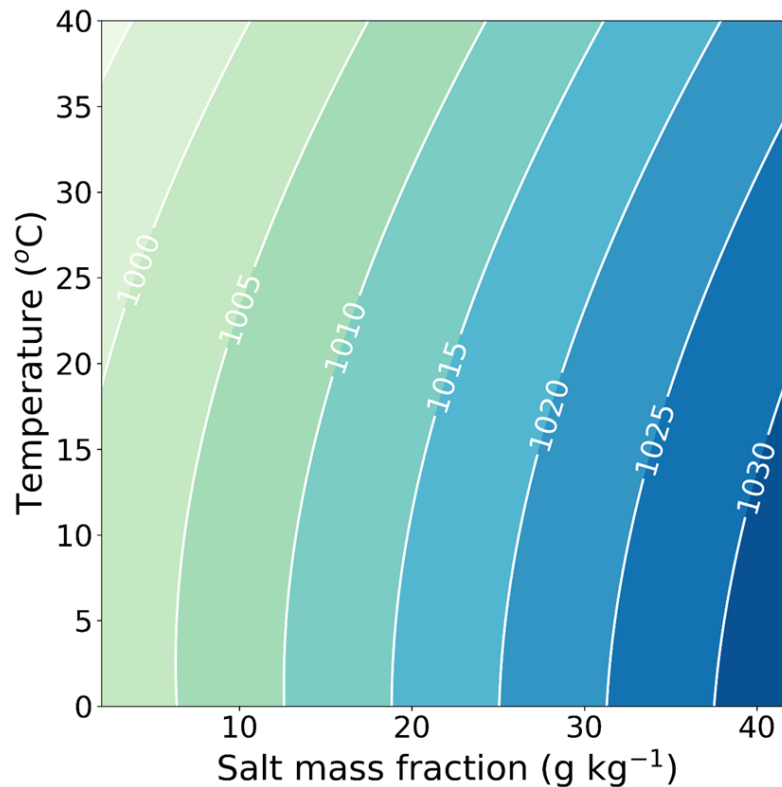


**Figure 3** - Contour lines of the density ( $\rho$  in  $\text{kg m}^{-3}$ ) of mixtures of seawater and fresh water as a function of temperature and salt mass fraction according to the international thermodynamic equation of seawater (IOC, 2010).

The values shown in Figure 3 are based on the international thermodynamic equation of seawater (TEOS-10) which was developed to determine the density of the world's oceans (IOC, 2010). As it turns out, it can also be used to approximate the density of groundwater in coastal aquifers (Post, 2012). Figure 4 shows the relationship between the specific conductance ( $SC_{20}$ , the electrical conductivity of water at a specific temperature, 20 °C in this case) and the density ( $\rho_{20}$ , also at 20 °C). The black line is the relationship according to the TEOS-10 and the data points are for samples from different groundwater systems. The samples from Portugal are from a sandy coastal aquifer in which mixing is the main process that determines the water composition, without significant changes in the chemistry by chemical reactions. These samples closely follow the theoretical relationship. Seawater has a specific conductance of approximately  $SC_{20} = 47 \text{ mS cm}^{-1}$ . The samples from Portugal with higher specific conductance values represent evaporated seawater (from evaporation ponds for salt production) and they too follow the TEOS-10 relationship, as long as salinity does not get too high. Samples with  $SC_{20} > 125 \text{ mS cm}^{-1}$  deviate significantly from the theoretical values because the TEOS-10 loses its validity at these salinity values. One reason is that the TEOS-10 relationship simply cannot be extrapolated too far outside the salinity range for which it was developed (the oceans). The other is that at these salinity levels, minerals like calcite and gypsum start to precipitate, changing the relative

proportions of the solutes, thus rendering the TEOS-10 fitting parameters invalid (Pawlowicz, 2012).

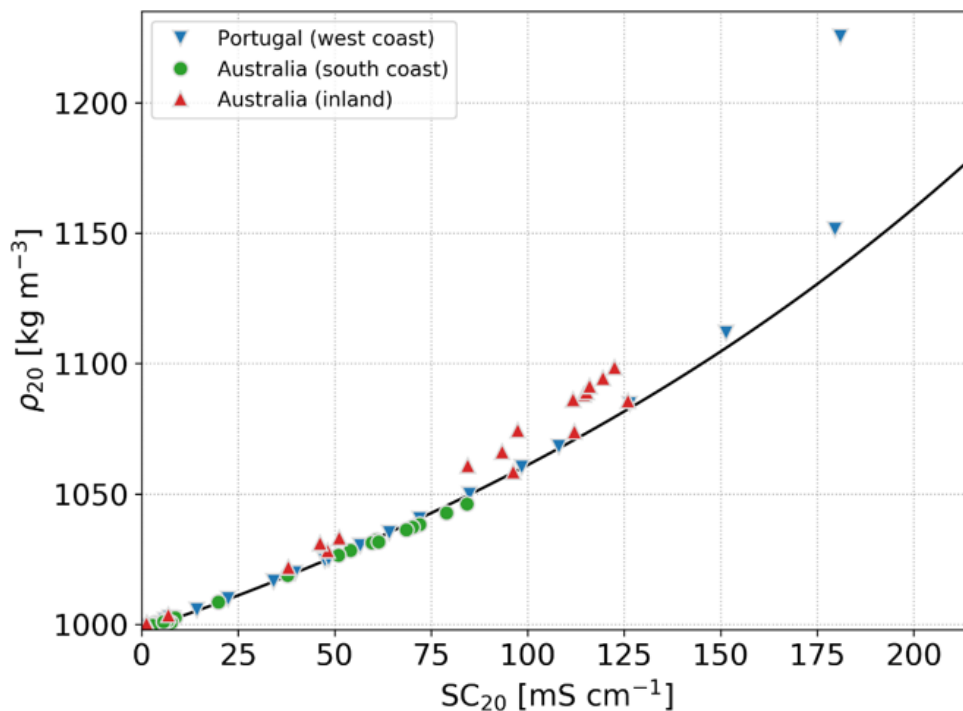


**Figure 4** - The density ( $\rho_{20}$ ) plotted against the specific conductance ( $SC_{20}$ ) of water samples from different groundwater systems. The solid line is the theoretical relationship according to the TEOS-10. Deviations from theoretical values occur because TEOS-10 loses its validity at salinity values above those of seawater for which the relationship was developed and because at these salinity levels minerals such as calcite and gypsum start to precipitate, changing the relative proportions of the solutes, thus rendering the TEOS-10 fitting parameters invalid. Inland Australia samples are courtesy of Margaret Shanafield.

The latter holds for the data points from the Australian south coast, which plot just below the TEOS-10 line. In this case, the relative proportions of the ions deviate significantly from seawater due to chemical reactions in the aquifer, which caused the groundwater to be depleted in magnesium and sulphate. The data points for the Ti Tree Basin in inland Australia on the other hand, plot above the TEOS-10 line. Their chemical composition differs from seawater-freshwater mixtures in that they contain a lot more sulphate.

The above examples show that some care must be exercised when selecting a relationship for a particular area as the chemical characteristics of the water can have an important influence. There are various relationships between salinity and density, and a useful overview has been presented by Adams and Bachu (2002). The TEOS-10 is a complex algorithm and special software is required to perform the density calculation as indicated by Figure 3 and Figure 4. More information can be found at [TEOS-10 software website](#)<sup>↗</sup>.

### 3 Quantifying Groundwater Flow in The Presence of Density Variations

The description of groundwater flow in variable-density systems is considerably more complex than in constant-density systems. While field measurements of hydraulic head conveniently allow for an assessment of groundwater flow direction and magnitude for constant-density systems, hydraulic head measurements cannot be used for flow calculations without making allowance for buoyancy effects in variable-density systems. Without citing anyone or any literature, it was casually remarked in a Dutch report (DZRD, 1936) that “It is known that the measured head of water with a high chloride content requires a correction” [paraphrased translation from Dutch by the authors]. Nevertheless, the use of hydraulic head measurements in a variable-density groundwater system still leads to confusion or even misinterpretation to this day.

Some basic intuition about the effect of density on the flow field can be gained by considering a confined aquifer with an impermeable base in which fresh water and salt water are separated by a vertical interface at time zero (Figure 5a).

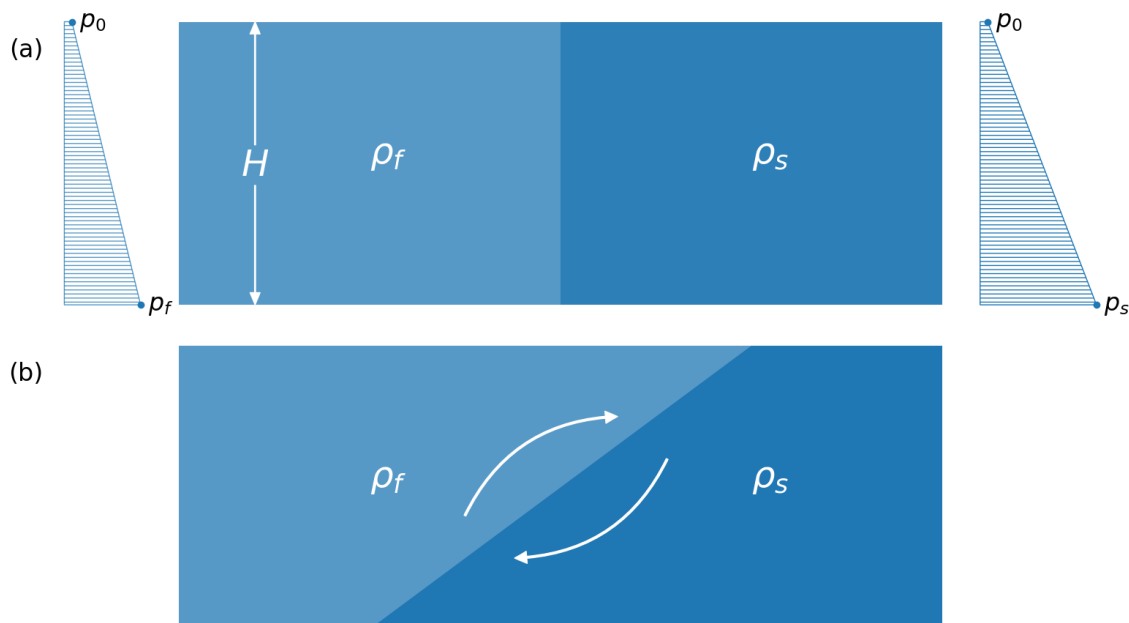


**Figure 5** - The effect of density on the flow field in a confined aquifer. a) Fresh and salt water are at rest and separated by a vertical interface at time zero. b) Rotating flow (clockwise) established under initially hydrostatic conditions. The base of the triangle in a) is much wider for the salt water than for the fresh water, to indicate that the freshwater pressure  $p_f$  at the aquifer bottom is greater than the saltwater pressure  $p_s$  because  $\rho_s > \rho_f$ . (After Santing, 1980).

All the system boundaries are closed, so there can be no inflow or outflow of water. Under the prevailing hydrostatic conditions at time  $t=0$ , the groundwater pressure  $p$  increases with depth according to Equation 1.

$$p = p_0 - \rho g z \quad (1)$$

where:

$p$  = pressure (M/(LT<sup>2</sup>)), e.g., kg m<sup>-1</sup> s<sup>-2</sup>

$p_0$  = pressure at the top of the aquifer where  $z = 0$  (M/(LT<sup>2</sup>)), e.g., kg m<sup>-1</sup> s<sup>-2</sup>

$\rho$  = groundwater density (M/L<sup>3</sup>), e.g., kg m<sup>-3</sup>

$g$  = gravitational acceleration (L/T<sup>2</sup>), e.g., m s<sup>-2</sup>

$z$  = elevation relative to a datum, which in this case is the top of the aquifer where  $z = 0$  and  $z$  is positive upward, thus there is a minus sign in the equation because  $p$  increases with depth (L), e.g., m

Assume that the groundwater density on the freshwater side of the interface is  $\rho_f = 1000 \text{ kg m}^{-3}$  and on the saltwater side it is  $\rho_s = 1025 \text{ kg m}^{-3}$ . The pressure thus increases faster with depth on the saltwater side than on the freshwater side (Figure 5a). The horizontal pressure difference gives rise to a flow, which in this example will be from the right to the left. Because the pressure difference between the freshwater and saltwater domains increases with depth, the initial flow will have the greatest magnitude at the base of the aquifer, and the interface will thus tend to rotate. As a result, the flow of fresh water above the interface will have to be from left to right to compensate for the displacement of the salt water along the aquifer base from right to left. The flow of the fresh water is thus in the opposite direction as the salt water (Figure 5b), resulting in a clockwise rotation of the initially vertical interface.

In reality, the description of the flow in an aquifer with a non-horizontal interface is far more complex (Bakker et al., 2004; Verruijt, 1980), but this simple example demonstrates that the presence of density differences gives rise to rotational flow. If this is the case, the hydraulic head is no longer suitable to describe the groundwater flow. The formal proof for this, which relies on determining whether the so-called curl (a property of a vector field that indicates rotational movement) of the force field is zero, can be found in Hubbert (1957).

The fact that the flow field is not irrotational means that measurements of hydraulic head cannot be directly compared to infer flow directions or magnitudes. Instead, flow calculations must be based on the general form of Darcy's law, which is shown in Equation 2 (Bear, 1972).

$$\vec{q} = -\frac{k}{\mu} (\nabla p - \rho \vec{g}) \quad (2)$$

where:

- $\vec{q}$  = specific discharge (L/T), e.g., m s<sup>-1</sup>  
 $k$  = intrinsic permeability (L<sup>2</sup>), e.g., m<sup>2</sup>  
 $\mu$  = dynamic viscosity of the groundwater (M/(LT)), e.g., kg m<sup>-1</sup> s<sup>-1</sup>  
 $\nabla$  = gradient operator and represents the rate of change of a variable ( $p$  in this case) per unit of distance in the  $x$ ,  $y$  and  $z$  direction  
 $\vec{g}$  = gravitational acceleration vector (L/T<sup>2</sup>), e.g., m s<sup>-2</sup>

When  $\rho$  is spatially constant, Equation 2 may be written as Equation 3.

$$\vec{q} = -\frac{k}{\mu}\nabla(p + \rho g z) = -\frac{\rho g k}{\mu}\nabla\left(\frac{p}{\rho g} + z\right) = -K\nabla\left(\frac{p}{\rho g} + z\right) \quad (3)$$

In the expression after the third equal sign, the parameters before the gradient operator were replaced by  $K$  (m s<sup>-1</sup>) the hydraulic conductivity. The term within the last set of parentheses is the hydraulic head  $h$  (m) as shown in Equation 4.

$$h = z + h_p = z + \frac{p}{\rho g} \quad (4)$$

where:

$$h_p = \text{pressure head (L), e.g., m}$$

The first term in Equation 4,  $z$ , is the elevation head, which determines the groundwater's potential energy (per unit of weight) due to its position in the Earth's gravitational field. In practice it is simply the elevation of the piezometer screen relative to a standard datum, usually mean sea level. The pressure head is a measure of the energy of groundwater because of its pressure above a reference pressure. The value of  $p$  is gage pressure, for which the atmospheric pressure is taken as the reference pressure. Inserting Equation 4 into Equation 3 gives Equation 5.

$$\vec{q} = -K\nabla h \quad (5)$$

Equation 5 is the familiar form of Darcy's law based on the hydraulic head gradient. However, given that the step from Equation 2 to 3 relies on the assumption that the density is spatially constant, the hydraulic head gradient is not suitable to quantify groundwater flow in variable-density groundwater flow systems. The hydraulic head form of Darcy's law (Equation 5) is strictly applicable to constant density systems.

### 3.1 Equivalent Freshwater Head

To emphasize the location-dependence of the hydraulic head, pressure and density values, Lusczynski (1961) suggested adding a subscript  $i$  to the parameters in Equation 4 as shown in Equation 6.

$$h_i = z_i + h_{p,i} = z_i + \frac{p_i}{\rho_i g} \quad (6)$$

where:

$h_{p,i}$  = pressure head for a piezometer at location  $i$  containing a fluid column with density  $\rho_i$ , so it is the height of the fluid column above the  $z_i$  coordinate (L), e.g., m, which is typically taken as the center of the piezometer screen

Lusczynski referred to this hydraulic head,  $h_i$ , as the *point water head*. The point water head is the hydraulic head that would be measured in a piezometer screened at point  $i$  and filled with groundwater having a density  $\rho_i$ . Groundwater often leaks into piezometers and observation wells along their length at unscreened locations, so the density of the standing water may not be the same as the groundwater at the screen (Post et al., 2018a; Post and von Asmuth, 2013), but for the discussion that follows, it is assumed that the water inside the piezometer has the same density as the groundwater at the screen. It is also useful to note that in systems with density variations caused by temperature differences, the density of the water inside of the piezometer will vary with depth because the stagnant water inside the standpipe achieves thermal equilibration with the surrounding rock, which gets warmer with increasing depth.

As shown in Figure 6, consider two piezometers completed at the same depth in an aquifer containing salt water, that sense the same pore water pressure ( $p_i$ ). Figure 6a is a piezometer with a fluid column having the same density as the groundwater at the screen ( $\rho_i$ ). Figure 6b is a piezometer that has a fictitious fluid column composed of fresh water ( $\rho_f$ ). As illustrated by Equation 6,  $h_{p,i} = p_i / \rho_i g$ , so the density of the water inside the piezometer determines the height to which the water rises. For a given groundwater pressure  $p$ , a taller water column is needed for fresh water than for salt water. Warm water requires a taller column than cold water. In freshwater systems, where the depth of investigation does not exceed a hundred meters or so below the surface, spatial density differences caused by temperature differences are usually small enough to be ignored. But in variable-density groundwater systems, such as coastal aquifers and near salt lakes, the relationship between  $h_p$  and  $p$  will not be the same for all piezometers.

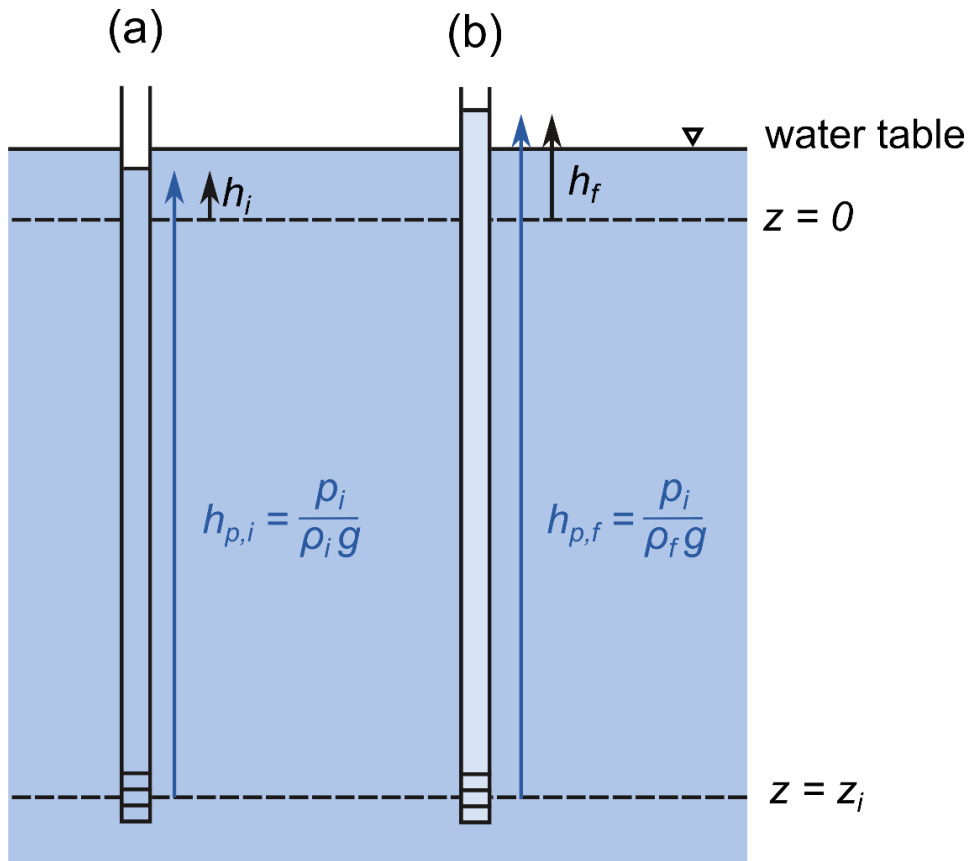


**Figure 6** - a) Point water head for a system with water density greater than freshwater density and b) equivalent freshwater head for the piezometer located at (a). The pressure and density at elevation  $z_i$  are  $p_i$  and  $\rho_i$ .

To compare measured hydraulic heads from different piezometers, they must all be referenced to the same density. The freshwater head  $h_f$  is the head that would be measured if the piezometer were filled with fresh water instead of groundwater with a higher density (Figure 6b). The choice of a reference density is arbitrary, but the density of fresh water is most commonly used. Analogous to the definition of hydraulic head, the freshwater head can be expressed as the sum of the elevation and the freshwater pressure head (Equation 7).

$$h_f = z_i + h_{p,f} = z_i + \frac{p_i}{\rho_f g} \quad (7)$$

In Equation 7,  $\rho_f$  is used to convert  $p_i$  to a length of freshwater column  $h_{p,f}$ . Rearranging Equation 6 results in Equation 8.

$$p_i = (h_i - z_i)\rho_i g \quad (8)$$

Inserting Equation 8 into Equation 7 yields the relation between the point water head and the freshwater head (Equation 9).

$$h_f = z_i + (h_i - z_i) \frac{\rho_i}{\rho_f} \quad (9)$$

Since  $h_f - z_i = h_{p,f}$  and  $h_i - z_i = h_{p,i}$ , Equation 10 is valid.

$$h_{p,f} = h_{p,i} \frac{\rho_i}{\rho_f} \quad (10)$$

Equation 10 shows that fresh water would rise to a higher level in a piezometer if it replaced denser water (i.e.,  $\frac{\rho_i}{\rho_f} > 1$ ). This result is consistent, as it should be, with the U-tube analogy in Figure 1.

With all hydraulic heads expressed as freshwater heads, care must still be taken to calculate the flow, as the freshwater head gradient does not indicate flow in the same way as the hydraulic head gradient in single-density systems. Consider for example the saltwater part of the aquifer in Figure 5 under the stagnant conditions at time  $t = 0$ . The equivalent freshwater head on the saltwater side is expressed by Equation 11.

$$h_f = z_i + (h_i - z_i) \frac{\rho_s}{\rho_f} \quad (11)$$

Because there is no flow,  $h_i$  is constant and Equation 11 can be differentiated with respect to  $z$  to obtain Equation 12.

$$\frac{\partial h_f}{\partial z} = \frac{\rho_f - \rho_s}{\rho_f} = \frac{1000 - 1025}{1000} = -0.025 \quad (12)$$

This outcome shows that there is a vertical freshwater head gradient in a stagnant body of saline groundwater. Based on the density values for seawater and fresh water, there is an increase of the freshwater head by 2.5 cm per meter of depth increase. It would therefore be a mistake to consider this value of the freshwater head gradient as an indication for vertical flow. One cannot expect to replace  $h$  with  $h_f$  in Equation 5 and expect to get the correct direction and magnitude of flow.

An implication that follows from this example is that in a variable-density system horizontal flow cannot be calculated from the horizontal freshwater head gradient if the piezometers are screened at different elevations. After all, the freshwater head increases with depth in a variable-density system even under stagnant conditions. The freshwater head gradient provides information about horizontal flow only if the screens are positioned on the same horizontal plane.

## Horizontal Flow

The correct use of the freshwater head gradient in flow calculations can be derived from Darcy's law as given by Equation 2. To simplify the analysis, it is assumed that the permeability is homogeneous and isotropic so that  $k$  has no spatial or directional dependency and can be written as a scalar. Because the vector  $\vec{g}$ , which represents the Earth's gravitational acceleration, has no components in the  $x$  and  $y$ -direction (i.e., it is zero in the horizontal plane), the horizontal components of the specific discharge vector  $\vec{q}$ , as defined by Equation 2, are shown by Equations 13 and 14.

$$q_x = -\frac{k}{\mu} \frac{\partial p}{\partial x} \quad (13)$$

$$q_y = -\frac{k}{\mu} \frac{\partial p}{\partial y} \quad (14)$$

Rearranging and differentiating Equation 7 with respect to  $x$  and  $y$  and inserting the result into Equations 13 and 14 yields the horizontal flow components as a function of the freshwater head gradient as shown in Equations 15 and 16.

$$q_x = -\frac{k\rho_f g}{\mu_f} \frac{\mu_f}{\mu} \frac{\partial h_f}{\partial x} = -K_f \frac{\mu_f}{\mu} \frac{\partial h_f}{\partial x} \quad (15)$$

$$q_y = -\frac{k\rho_f g}{\mu_f} \frac{\mu_f}{\mu} \frac{\partial h_f}{\partial y} = -K_f \frac{\mu_f}{\mu} \frac{\partial h_f}{\partial y} \quad (16)$$

For many applications of practical interest  $\frac{\mu_f}{\mu} \cong 1$ , so it can be omitted, although this approximation is not likely to be accurate in geothermal systems with elevated temperature because water viscosity decreases by nearly a factor of 4 from 20 °C to 100 °C. The parameter  $K_f = \frac{k\rho_f g}{\mu_f}$  is the freshwater hydraulic conductivity, for which deviation of a few percent from the hydraulic conductivity at the ambient groundwater density is an acceptable simplification given the large uncertainty about the magnitude of  $K$  in a field setting.

## Vertical Flow

Recalling, once again, that the positive  $z$ -direction is taken upward (against gravity), the component of the specific discharge vector in the vertical direction is given by Equation 17, where  $q_z$  is positive in the +  $z$  direction.

$$q_z = -\frac{k}{\mu} \left( \frac{\partial p}{\partial z} + \rho g \right) \quad (17)$$

For flow in the vertical direction, Equation 7 can be rearranged and differentiated with respect to  $z$ . Inserting the result into Equation 17 yields Equation 18.

$$q_z = -\frac{k\rho_f g}{\mu_f} \frac{\mu_f}{\mu} \left( \frac{\partial h_f}{\partial z} + \frac{\rho - \rho_f}{\rho_f} \right) = -K_f \frac{\mu_f}{\mu} \left( \frac{\partial h_f}{\partial z} + \frac{\rho - \rho_f}{\rho_f} \right) \quad (18)$$

The term between the parentheses is the sum of the freshwater head gradient and a buoyancy term  $\frac{\rho - \rho_f}{\rho_f}$ . It is useful to note that  $\frac{\partial h_f}{\partial z}$  in Equation 18 differs from that of Equation 12 which is applied to a stagnant system where  $q_z = 0$ . The practical application of Equation 18 can be illustrated by the example (depicted in Figure 7 and Table 1) of a freshwater aquifer that overlies a saltwater aquifer and is separated from it by an aquitard. Flow across the aquitard is upward. The vertical flow rate is rather small (0.1 m yr<sup>-1</sup>) and lateral groundwater flow along the base of the freshwater aquifer is sufficiently high to keep the groundwater fresh. The results shown in the figure were calculated using a

numerical model built into SEAWAT (Langevin and Guo, 2006), so this is a synthetic case, but it serves to illustrate some important points. First, it is useful to note how the point water head varies vertically just below the top of the aquitard: it decreases with depth in the first meter or so. Without knowledge of the groundwater density, taking the hydraulic head gradient at face value as an indicator of the flow direction would lead to the incorrect conclusion that flow was downward in the aquitard. Next, it is useful to note that the vertical point water head gradient in the saltwater aquifer is notably smaller than in the aquitard because of the aquifer's higher hydraulic conductivity ( $K_f = 1 \text{ m d}^{-1}$  versus  $K_f = 0.01 \text{ m d}^{-1}$ ). The freshwater head increases with depth at all depths, but at a lower rate in the lower aquifer than in the aquitard. This example once more shows that a simple comparison of freshwater or point-water heads in two wells may not provide the correct direction of vertical flow.

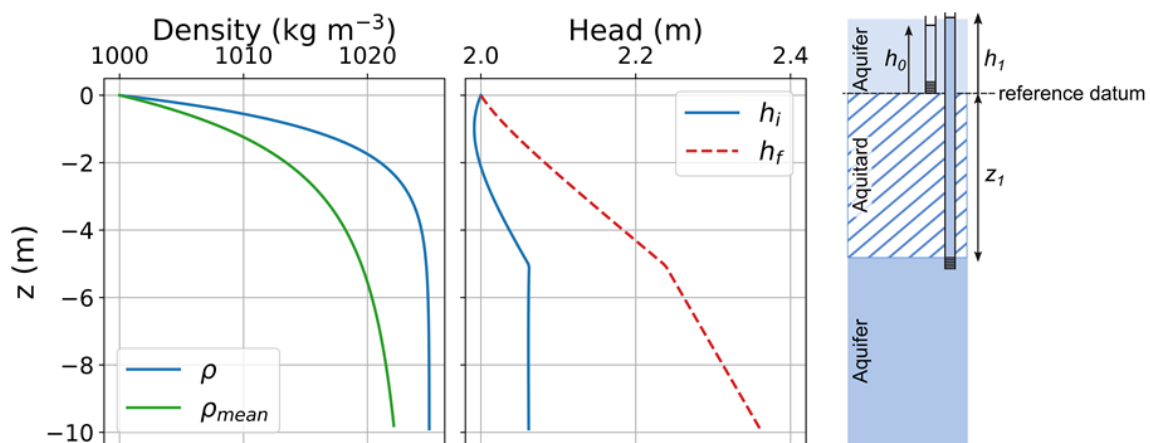


**Figure 7** – Comparison of the point water head,  $h_i$ , and the equivalent freshwater hydraulic head,  $h_f$ , in a system with vertically upward flow from a saltwater aquifer through an aquitard to a freshwater aquifer. The graph on the left shows the density ( $\rho$ ) as a function of height  $z$ , as well as the mean density ( $\rho_{mean}$ ) between 0 and  $z$ .

**Table 1** - Data associated with Figure 7.

$z_i$	$h_i$	$\rho_i$	$h_f$
m	m	$\text{kg m}^{-3}$	m
0	2	1000	2
-5	2.06	1024.7	2.24

Table 1 lists data required to do the hydraulic head corrections for two piezometers, one that is screened at the base of the freshwater aquifer and the other screened directly below the aquitard. The aquitard is five meters thick. The freshwater heads were calculated using Equation 9. The specific discharge  $q_z$  can be calculated using the difference form of Equation 18 to obtain Equation 19.

$$q_z = -K_f \left( \frac{\Delta h_f}{\Delta z} + \frac{\rho_{mean} - \rho_f}{\rho_f} \right) \quad (19)$$

The difficulty is that the density  $\rho$  in the buoyancy term is the mean density over the interval  $\Delta z$ , which has been emphasized by replacing  $\rho$  from Equation 18 with  $\rho_{mean}$  in Equation 19. For this synthetic example,  $\rho_{mean}$  is known as it can be calculated from the given density distribution with depth ( $\rho_{mean} = \frac{1}{z} \int_0^z \rho dz$ ). The green line in Figure 7 indicates that over the interval 0 to -5 m,  $\rho_{mean} = 1019.5 \text{ kg m}^{-3}$ , so  $q_z$  can be calculated as follows.

$$q_z = -0.01 \times \left( \frac{2-2.24}{0-(-5)} + \frac{1019.5-1000}{1000} \right) = -0.01 \times (-0.048 + 0.0195) = 2.9 \times 10^{-4} \text{ m d}^{-1}$$

Negative elevations are used in the calculation of the freshwater head gradient and  $q_z$  is a positive number because the flow is directed upward.

More often than not, the mean density distribution between two piezometer screens is not known, and the mean density is typically approximated by the mean of the densities of the two measurement points. In this case, this would yield  $\rho_{mean} = \frac{(1000+1024.7)}{2} = 1012.4 \text{ kg m}^{-3}$ , which would give  $q_z = 3.6 \times 10^{-4} \text{ m d}^{-1}$ . The estimated flux is in error by ~20 percent, but it could be argued that such an error dwarfs in comparison to the uncertainty of  $K_f$ . Post and others (2007) recommended taking the uncertainty of  $\rho_{mean}$  into account by considering the conceivable end members of the density distribution between the points of measurement, and Post and others (2018a) used borehole resistivity logs to determine  $\rho_{mean}$ .

Luszczynski (1961) introduced the concept of environmental head to facilitate the determination of vertical flow, which is indicated by the environmental head gradient. Despite this advantage, determining how to calculate the environmental head is not always trivial and its application has sometimes led to confusion. Readers may find more information about the environmental head in the original Luszczynski (1961) paper as well as in Post and others (2007). Guo and Langevin (2002) derived versions of Equations 15 through 18 for the general case when gravity is not perpendicular to the x-y plane. Use of these alternative equations is required when the coordinate system needs to be aligned with principal directions of permeability that are askew to the horizontal and vertical axes. Density effects in sloping aquifers further complicate the analysis and are discussed in Bachu (1995) and Bachu and Michael (2002). Moreover, the theoretical framework presented in this section can only be practically applied when the density field is in a steady state. If the fluid densities change in time, as in the examples of variable-density flow presented later in this book, numerical models can assist in the interpretation of flow and transport processes as discussed in Section 6.

## 4 Types of Density for Groundwater Flow

Groundwater density varies significantly with salinity and temperature as was shown in Figure 3 of Section 2. Where this is the case, there is the potential for variable-density flow to exist in many groundwater systems. Apart from coastal groundwater systems, which were mentioned in Section 1, density-driven flow can also be important in groundwater systems impacted by man, such as radioactive waste disposal sites (NEA, 1992), aquifer thermal energy storage systems (van Lopik et al., 2016), managed aquifer recharge schemes (Missimer et al., 2002; Ward et al., 2007), and finally waste disposal or contaminated sites (Zhang and Schwartz, 1995) where the contaminant plume is denser than the surrounding groundwater. Density-driven flow is also important on geological timescales in determining the development of ore deposits (Garcia-Fresca et al., 2012; Garven et al., 2003; Raffensperger and Garven, 1995), geochemical alteration of carbonate platforms (Garcia-Fresca et al., 2012; Jones et al., 2004; Wilson et al., 2001) and freshening and salinization of continental shelves due to global sea-level changes (Kooi et al., 2000a; Person et al., 2003). During the last decade or two, density-driven flow has also been studied extensively for the sequestration of carbon dioxide in subsurface reservoirs (Riaz et al., 2006; Ringrose et al., 2021).

### 4.1 Free Convection

The potentially substantial effect of density on groundwater flow is illustrated by the following experiment, which was conducted by Simmons and others (2002b) to study the impacts of unstable flow in a laboratory sand tank and is shown in Figure 8. The tank has dimensions of about 1.2 m by 1.2 m and is filled with homogeneous sand, saturated with fresh water at time  $t = 0$ . A calcium chloride plume of  $3000 \text{ mg L}^{-1}$  was introduced into the top of the sand tank. The plume was stained purple with a dye to allow visualization. Figure 8a shows the resulting plume at 150 minutes at which time the plume has moved fairly uniformly through the sand to about 25 to 30 cm depth. The process was repeated with a much higher concentration fluid introduced to the top of the tank. This time the calcium chloride solution had a concentration of  $300,000 \text{ mg L}^{-1}$ , so one hundred times more than the first low concentration plume. Figure 8b shows the resultant plume at 50 minutes (only one-third of the time of the result shown for the low concentration plume in Figure 8a). The difference between the results is striking and remarkable. In the case of the higher density plume, the plume displays substantial instability with dense lobes sinking in the tank under the influence of gravity. This process is often referred to as fingering due to the resemblance of the lobes with fingers. In between each sinking lobe, fresher water is upwelling. In just one-third of the time, the high-salinity plume has moved about three times the distance traversed by the low-salinity plume.

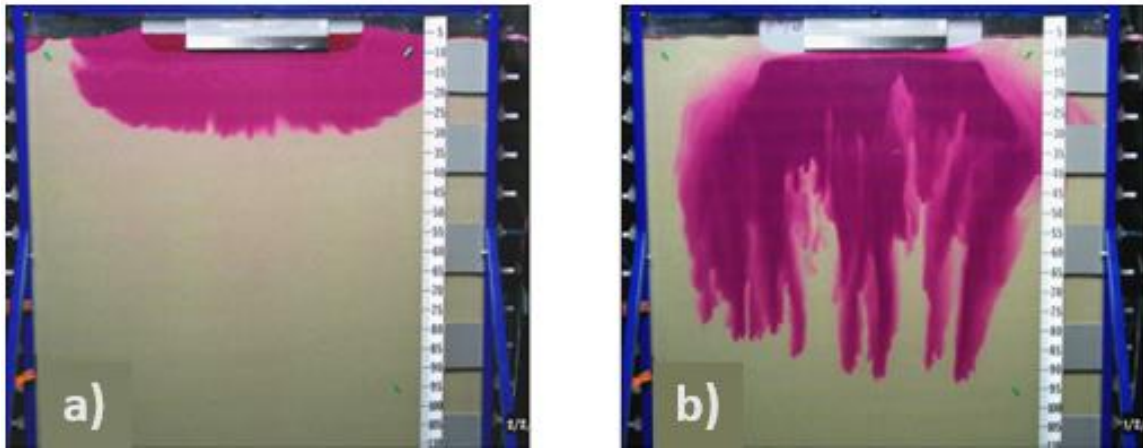


**Figure 8** - a) Plume in a sand tank:  $3 \text{ g L}^{-1}$   $\text{CaCl}_2$  after 150 min since the start of the experiment. b) Plume in a sand tank:  $300 \text{ g L}^{-1}$   $\text{CaCl}_2$  after 50 min since the start of the experiment. (From Simmons et al., 2002b). A video of the experiment is available [here](#).

This experiment illustrates the effect of density-driven flow simply and beautifully. It shows the development of gravitational instabilities and the profound implications of such instabilities for flow and transport, which are:

- an increase in the total quantity of solute involved in the solute transport process;
- a significant reduction of the time scales for mixing over similar spatial scales; and
- an increase in the distance of solute spreading.

In short, unstable, transient, density-driven flow is a rapid and effective spreading and mixing mechanism for solutes.

The flow shown in Figure 8b is driven purely by density variations and is called *free (or natural) convection*. The large density contrast in the experiment exacerbates the role of density. It would be a misconception though to associate density-driven flow with only high solute concentrations. Even low-density differences can exert a significant effect on the flow pattern. This was made clear in the famous Cape Cod tracer test, which involved the injection of a mixture of  $\text{Li}^+$  salts ( $\text{LiBr}$ ,  $\text{LiF}$  and  $\text{Li}_2\text{MoO}_4$ ) dissolved in water into a sand and gravel aquifer. The total concentration of dissolved solids was approximately  $890 \text{ mg L}^{-1}$  and the density difference  $\Delta\rho$  of the injected solution with the ambient groundwater varied between  $0.74$  and  $0.85 \text{ kg m}^{-3}$  (LeBlanc et al., 1991).

Numerical modeling confirmed that the density difference, albeit small, was sufficient to cause the injected plume to sink (at a rate higher than what would be expected due to rainfall recharge) during the early stage of the injection experiment (Zhang et al., 1998). During later stages, density-driven flow decreased in importance as the plume mixed with the ambient groundwater.

The downward flow rate associated with convective fingering tends to be much higher relative to the vertical flow rates in groundwater systems driven by topography and

rainfall recharge. The speed of finger descent ( $v_z$ ,  $\text{m s}^{-1}$ ) in systems without an ambient flow field was given by Wooding (1969) as Equation 20.

$$v_z = \frac{\Delta\rho g k}{4\mu n} \quad (20)$$

where:

$n$  = porosity (dimensionless)

For an aquifer with  $k = 10^{-11} \text{ m}^2$  and porosity 0.4 which is in the range of property values for a clean sand, this means that  $v_z \approx 2.5 \times \Delta\rho$  when expressed in  $\text{m y}^{-1}$ . So, if seawater floods a freshwater aquifer, salt fingers may be expected to sink at a rate of approximately  $2.5 \times 25 = 62 \text{ m y}^{-1}$ . Higher rates apply below sabkhas (flat areas that are regularly inundated where salts precipitate when water evaporates). For example, van Dam and others (2009) observed salt fingers that moved down 15 m in a seven-week period. It is interesting to compare such vertical flow velocities to those generated by groundwater recharge, which are on the order of millimeters per year in arid- and semi-arid regions, to typically one or two meters per year in humid regions. The speed of fingering in groundwater is a remarkable observation that defies conventional wisdom about the rate of groundwater processes. In more typical advection-driven situations, much smaller flow rates are usually encountered. In relative terms, fingering associated with free convection can be a remarkably fast groundwater process. Convective fingering, where it occurs, can completely alter the solute distribution in a short period of time.

## 4.2 Stable and Unstable Density Configurations

The Simmons and others (2002b) experiment provides an example of a potentially unstable density layering where higher density water overlies lower density water. The reason why the term “potentially unstable” is used (as opposed to unconditionally unstable) is that there are other factors, such as the permeability of the sediment and the background flow field, that determine whether gravitational instabilities as shown in Figure 8b will develop and amplify. These additional factors are considered in Section 5.

On the opposite side of the spectrum are stable density configurations, where the lower density fluid rests on top of higher density fluid. The difference between the two regimes is illustrated in this [video](#) , which is an animated version of the snapshot at 10,000 years shown in Figure 9. The temperature is color-coded. The left and right images show the temperature distribution in a  $500 \times 500 \text{ m}$  cross-section through a homogeneous aquifer with no external hydraulic head gradients to drive forced convection. In the unstable regime of Figure 9b, the temperature is fixed to  $1.5 \text{ }^\circ\text{C}$  along the top and the system is heated from below by a heat flux of  $100 \text{ mW m}^{-2}$ . Conditions like these occur, for example, below the bottom of the world’s oceans underlain by basalt aquifers (Fisher and Geoffrey,

2010). In the stable regime shown in Figure 9a, the upper and lower boundary conditions are reversed, so the temperature is fixed along the bottom and the heat flux is applied from above. Because the density of water decreases with increasing temperature (for pure water this is true above 4 °C but for seawater, this is true for all temperatures above freezing point) the warmer water over cooler water in the system on the left represents the stable regime. Because the groundwater is stagnant in Figure 9a, locations throughout the flow system where flow vectors would be plotted appear as dots (i.e., the groundwater has zero velocity, thus the flow vector has no magnitude nor direction). In the absence of flow, the rock and the groundwater convey heat only by conduction.

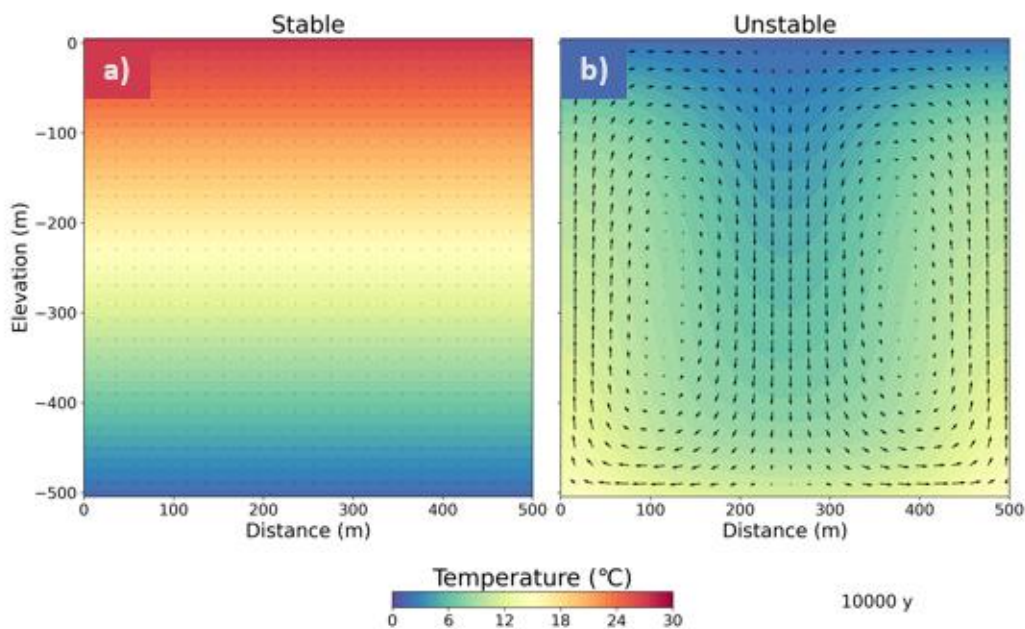


**Figure 9** - Stable and unstable temperature fields 10,000 years after heat was applied to the boundary. a) Heat conduction in a stable state where heat is applied to the top so water density is lower at the top; and, b) free convection cells in an unstable state where heat is applied to the bottom so water density is lower at the bottom. The Rayleigh number (discussed in Section 5.2) is on the order of  $Ra = 3 \times 10^2$ . [Video at this link](#) provides the animated version of this figure.

In the case of the unstable regime shown in (Figure 9b), the situation is entirely different. The [video at this link](#) shows that the system is initially stable as the aquifer is heated from below. Then, after approximately 2250 years, the horizontal temperature stratification is disrupted and the system transitions into a new regime in which there is vigorous, circulatory groundwater flow. Cold water is transported downward in the center of the aquifer and warm groundwater rises along the left and right boundaries. The video shows that the temperature distribution does not change after approximately 5000 years, nevertheless, the convective flow pattern persists as evidenced by the circulating particles. In Figure 9b, this flow pattern is shown by flow vectors, which in contrast to the stable case

of Figure 9a, are arrows with magnitude and direction indicating the groundwater is in motion.

The counter-rotating cells, shown in Figure 9b, are called *free convection cells*. Cooler water from the top of the aquifer descends to replace the warmer fluid that rises. Something similar happens when you heat water to cook or make a cup of tea. Just before the water starts to boil, you may recognize the water movement that is similar to the pattern displayed in Figure 9b, but because all the water has the same color, the convection cells can be hard to see. A clearer and more entertaining household example is the recipe for a marble cake. When alternate layers of vanilla and chocolate cake mix are carefully put more or less horizontally in a baking tray, the result after baking is a pattern where counter-rotating cells are formed in the baking process (Figure 10). It is noted that this example is not entirely representative of groundwater because of the phase change that occurs (from liquid to solid when baking a cake).



**Figure 10** - Free convection cake. [Box 1](#) provides the recipe.

A classic example of a stable density configuration is encountered in coastal aquifers. In this case, dense seawater water sits under less dense fresh groundwater, which creates a seawater wedge that can penetrate inland from the coast for some distance. Coastal aquifer hydrogeology is extensively treated in books (Bear et al., 1999; Cheng and Ouazar, 2004; Jiao and Post, 2019) as well as in literature reviews on this topic (Reilly and Goodman, 1985; Werner et al., 2017, 2013). The quintessential conceptual model of the salinity distribution and flow pattern in groundwater in an aquifer near the sea is depicted in Figure 11. It shows the results of a model simulation in which there is lateral inflow of fresh water across the left boundary, as well as across the top boundary of the landward part of the aquifer. On the seaward part of the aquifer, the hydraulic head along the top boundary is equal to sea level. The seawater wedge protrudes inland from the coast. As presented earlier in Figure 1, the higher pressure of saline compared with fresh groundwater at the same depth is responsible for the formation of the wedge. The rotational flow that was illustrated in Figure 5 can also be seen in Figure 11. It exists because the

groundwater that originates inland, mixes with the intruded seawater along the interface and carries with it some of the dissolved salt, which is lost from the system when the groundwater mixture discharges. To compensate for this loss of solutes, there must be a landward flow of seawater below the seafloor. This mechanism maintains the rotational flow cell that exists seaward of the interface.

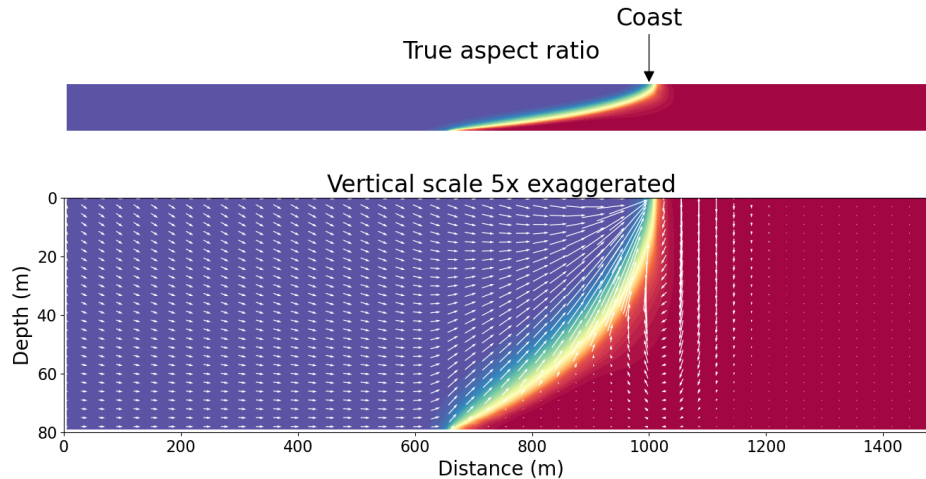


**Figure 11** - Salinity distribution and flow pattern in a coastal aquifer. The upper image shows the salinity distribution and is depicted at the true aspect ratio. The red color indicates seawater salinity, while the blue color depicts fresh water and varying salinity level between the two end members are shown by transitional colors in the mixing zone. The white arrows in the lower image represent the magnitude and direction of specific discharge vectors. An animated version of this figure is available at this [link](#). In the animated version, particles are periodically added to the left and top boundaries to reveal the flow pattern illustrated by the arrows in the still image.

### 4.3 Transport Processes in Groundwater

Before continuing this discussion, it is useful to review some of the most important terms related to groundwater transport processes, as there can be confusion in some cases. Hydrogeologists generally refer to the movement of groundwater simply as *flow*. In fluid mechanics, from which many insights about variable-density phenomena are derived, the flow of a fluid is referred to as *advection*. In hydrogeology, this term is generally used in a stricter sense and is understood to refer to the transport of solutes by flowing groundwater. Groundwater can also transport heat, and this is called *convection*, although the term is used quite liberally and can refer to advective flow as well. In the context of variable-density flow, the term convection tends to be used to indicate flow that arises as a consequence of density variations.

As solutes or heat are transported, initially steep concentration or temperature gradients become more diffuse. Spreading of solutes due to concentration differences is called *diffusion*. The equivalent process for heat transport driven by temperature gradients is called *conduction*.

The solute mass flux per unit area of the bulk porous medium due to diffusion is given by Fick's law and presented in Equation 21.

$$\vec{j}_C = -D_C \nabla C \quad (21)$$

where:

$$\vec{j}_C = \text{solute mass flux (M/(L}^2\text{T))}, \text{ e.g., kg m}^{-2} \text{ s}^{-1}$$

$$D_C = \text{solute diffusion coefficient in the porous medium (L}^2\text{/T)}, \text{ e.g., m}^2 \text{ s}^{-1}$$

$$C = \text{solute concentration (M/L}^3\text{)}, \text{ e.g., kg m}^{-3}$$

The porous medium diffusion coefficient  $D_C$  is lower than the diffusion coefficient in free water because the solutes have to move along a tortuous flow path in the connected pore space. For conduction, the heat (or energy) flux per unit area of the bulk porous medium is given by Fourier's law (Equation 22).

$$\vec{j}_e = -c_p D_T \nabla T = -k_T \nabla T \quad (22)$$

where:

$$\vec{j}_e = \text{heat flux (M/T}^3\text{)}, \text{ e.g., kg s}^{-3}, \text{ or W m}^{-2}$$

$$c_p = \text{volumetric heat capacity (M/(LT}^2\Theta\text{))}, \text{ e.g., kg}^2 \text{ m}^{-1} \text{ s}^{-2} \text{ K}^{-1}$$

$$D_T = \text{thermal diffusivity (L}^2\text{/T)}, \text{ e.g., m}^2 \text{ s}^{-1}$$

$$T = \text{temperature } (\Theta), \text{ e.g., K}$$

$$k_T = \text{thermal conductivity (M/(L}\Theta\text{))}, \text{ e.g., W m}^{-1} \text{ K}^{-1}, k_T = c_p D_T$$

Just like Equation 5, the flux in Equations 21 and 22 is the product of a proportionality constant and the gradient of a field variable. Because of their resemblance, these relationships are all called Fickian type equations or diffusion equations. There is a fundamental difference between solute and heat transfer because solutes can only move through the connected water-filled pore space, but heat is transmitted by conduction through the bulk, wet rock. That means that  $\vec{j}_C$  must be multiplied by the porosity  $n$  to obtain the net solute mass flux, i.e., the transported mass of solute per unit of surface area per unit of time. This is not necessary for the heat flux  $\vec{j}_e$  as long as  $k_T$  represents the bulk thermal conductivity (i.e., the net value for the groundwater and the rock material).

As Equations 21 and 22 show, diffusion and conduction operate when there is a concentration ( $\nabla C$ ) or temperature ( $\nabla T$ ) gradient, and assume no forced advection (i.e., there need not be physical movement of groundwater through the porous medium). Diffusion and conduction can be regarded as a "spreading" process in a system that is hydraulically stagnant. When groundwater is flowing, solutes will migrate in the flowing groundwater across a range of spatial scales while at the same time spreading by diffusion

(or in the case of heat, conduction). At the pore scale, water flows fastest through the pore centers but is stagnant at the pore wall. At the scale of a pore network, the flow path of water is tortuous due to the irregular shape of the connected pore space. At the scale of an aquifer, differences in permeability cause water to flow fast in some zones, and slow in others. These velocity variations at various scales cause spreading, which is referred to as *mechanical dispersion*. For most groundwater systems, the effects of mechanical dispersion tend to dominate over diffusion.

In combination, the combined process of diffusion and mechanical dispersion is called *hydrodynamic dispersion*,  $D_H$ . Hydrodynamic dispersion is commonly described in transport models using Equation 21, albeit with a hydrodynamic dispersion tensor replacing the diffusion coefficient  $D_C$ . The coefficients of mechanical dispersion are functionally related to the groundwater seepage velocity (that is, they have higher values for higher flow velocities) (Bear, 1972).

Flow driven by hydraulic head gradients is commonly called *forced convection*. Truly free convection, as in the Simmons and others (2002b) laboratory experiment of Figure 8 or the unstable heat flow example in Figure 9b, is rare in groundwater systems, where density-driven flow mostly occurs in the presence of background groundwater flow. A flow regime influenced by both forced and free convection is called *mixed convection*. Understanding the magnitude of the different driving forces in any given hydrogeological situation is critical, as is the need to appreciate the different flow processes that can occur in a variable-density flow system. These will affect the magnitude of the solute fluxes and the patterns and rates of plume migration. Comparison of time-length scales for the flow and transport processes discussed above can be useful when assessing the importance of density-driven flow in groundwater (Section 5).

#### 4.4 Landfill Leachate Plume Example

The relative importance of the transport processes discussed in the previous subsection changes with time, hence the type of convection regime (free, forced or mixed) changes with time as well. As dense plumes disperse and diffuse, density contrasts become smeared out, which diminishes the driving force for density-driven flow and increases the relative importance of forced convection. This can be illustrated using the case of a dense leachate plume infiltrating from a landfill into an aquifer with a background flow field. Figure 12 shows the concentration patterns that may develop, as calculated using a numerical model. Groundwater flow is from left to right, with inflow of pristine groundwater from the upgradient section of the aquifer to the left and as recharge from infiltration at the surface. A 100 m long landfill is located between 50 and 150 m. Chloride is often present in high concentrations in landfill leachate due to the presence of soluble salts in household waste. Infiltration through the landfill dissolves these salts which

increase the density of the recharge water in that zone. Color-coded concentration is used here to visualize spreading of the plume. Three different snapshots show the concentration pattern after 20 years of continuous leaching for leachate chloride concentrations of 250, 2500 and 10000 mg L<sup>-1</sup>, which will be referred to as the low-, medium- and high-density cases, respectively. These values are based on reported concentrations for Danish landfills (Christensen et al., 2001).

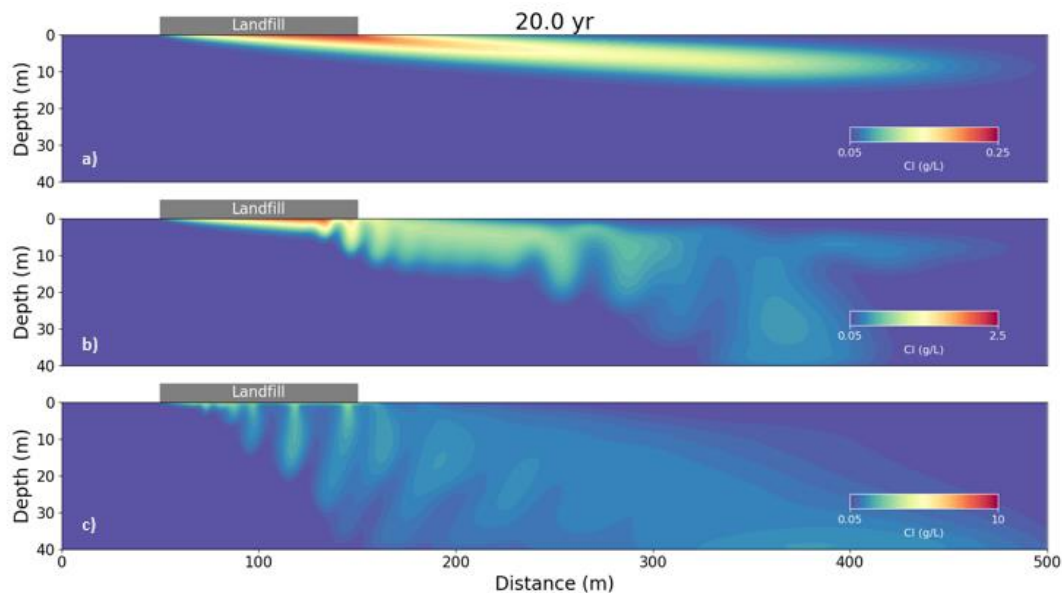


**Figure 12** - Three different snapshots of numerical simulations showing the concentration distribution of a landfill leachate plume with chloride concentrations for the low-, medium- and high-density cases of: a) 250 mg L<sup>-1</sup>; b) 2500 mg L<sup>-1</sup>; and, c) 10000 mg L<sup>-1</sup> after 20 years of continuous leaching. The animated version of this illustration is provided [here](#).

The difference between the three snapshots in Figure 12 illustrates again that density differences can have an enormous impact on the flow dynamics and hence the spreading of contaminants. For the low-density case (Figure 12a), the density contrast between the landfill leachate and the pristine groundwater is too low to cause any noticeable deviation from the plume spreading that might be expected under the prevailing flow conditions. As the plume emanates from the landfill, it gets pushed slightly deeper into the aquifer by the uncontaminated rainwater that recharges the aquifer downstream of the landfill. The peak concentrations decrease with distance downstream due to spreading caused by hydrodynamic dispersion.

For the medium-density case (Figure 12b), the plume thickness increases significantly, and lobes of contaminated groundwater have formed. This is the result of the downward flow caused by the negative buoyancy of the denser leachate plume. At a distance of almost 400 m, the plume even reaches the bottom of the aquifer, and in some places, the concentrations increase with depth. This is entirely counter-intuitive for a system in which the contaminant source is at the top of the aquifer, yet this situation is

sometimes observed under field conditions near landfills in Denmark (Christensen et al., 2001).

While the plume of the medium-density case has some resemblance to the low-density case just downstream of the landfill, the situation is entirely different for the high-density case (Figure 12c). There, the density contrast between the leachate and the groundwater is so high that convective fingering starts immediately below the landfill and while the lobes are entrained with the regional groundwater flow, the direction of spreading is strongly vertical. Interestingly, the peak concentrations are dissipated much more efficiently in the high-density case compared to the other two cases. This is because the formation of fingers leads to a larger contact area between the contaminated and pristine groundwater, which enhances mixing by dispersion and diffusion. While the positive effect is that the peak concentrations of the contaminants are attenuated, the adverse effect is that a much larger volume of groundwater becomes contaminated.

It is further interesting to note that the dissipation of mass strongly reduces the density contrast and hence the propensity for variable-density flow downstream of the landfill. The animated version of Figure 12 ([video](#) ) shows that once the plumes have reached the bottom of the aquifer and the concentrations have decreased, the migration is essentially horizontal as dictated by the regional flow field. Thus, the high-density case is free convection dominated under the landfill, but transitions to a forced convection mode once the driving force for density-driven flow is diminished. The low-density case is dominated by forced convection throughout. The medium case is an example of a mixed convection regime.

## 5 Dimensionless Numbers

Unstable density layering may not always give rise to convective flow. It depends on several factors. Instability tends to occur where the permeability of the geologic material is high (as in sand) or where density differences are large (e.g., beneath an evaporating salty lake). Diffusion (for solutes) or conduction (for heat) also play a role. Free convection will occur when small perturbations of the concentration or temperatures can grow into larger finger-like structures. Over time, diffusion and conduction will tend to suppress the formation of instabilities as these processes smear out concentration and temperature differences, and the onset of fingering thus depends on their ability to suppress the growth of perturbations. But how can we predict whether a system is stable or unstable, and what conditions determine this? Also, how can we determine the importance of density-driven flow relative to natural background flow in a mixed convection system?

One useful way to assess the importance of density driven flow in a groundwater system is to test the sensitivity of flow and transport behavior in a numerical groundwater

model. One can run the model with the density coupling turned on so that as the concentration or temperature field changes, the fluid density changes. This is called a density-variant solution or density-variant model. The density-variant model can be compared with the density-invariant model, in which concentration or temperature changes do not affect the density. If the results of the two cases are very similar or identical, one can conclude that density is likely an insignificant part of the system behavior. If there is a significant difference between the two cases, then one can conclude that density is an important factor and that this may warrant further investigation and inclusion in subsequent analyses. Section 6 discusses variable-density groundwater models in more detail.

Not all numerical codes have the option to consider density effects, and variable-density groundwater models are much more complex than constant-density models. Setting up a numerical model takes time and is not always easy nor trivial. Alternatively, dimensionless numbers can be used to assess the importance of density variations and serve as a useful starting point before more complex analyses are undertaken. Theoretical treatments are given in books such as Holzbecher (1998) and Nield and Bejan (2006). Only salient details are described in the following subsections.

## 5.1 Mixed Convection Ratio

As noted earlier, many if not most convective groundwater systems are mixed convection systems where forced convection (flow driven by pressure or hydraulic head gradients) and free convection (flow driven by density variations) co-exist. They work together to control the flow behavior and solute concentration (or heat) distributions. In such cases, it is often interesting and important to understand the relative strengths of free and forced convection in controlling the resultant flow and transport process.

The mixed convection ratio is a simple and effective way to understand this. It is the ratio of the density-driven convective flow velocity to the advective flow velocity and allows determination of the dominant driving mechanism. The simplest form of a mixed convection ratio is for vertical flow and can be derived from Equation 18, which shows that the magnitude of the vertical flow is proportional to the sum of the vertical freshwater head gradient and the relative density difference (Equation 23).

$$q_z \propto \frac{\partial h_f}{\partial z} + \frac{\rho - \rho_f}{\rho_f} \quad (23)$$

In practical applications, the gradient term is replaced by the difference form (Equation 19), which approximates the gradient by taking the freshwater head difference,  $\Delta h_f$ , between two points separated by a distance  $\Delta z$ . Recall that density  $\rho$  in Equation 23 is

the mean density between the two measurement points. The ratio of the two is the mixed convection ratio  $M$  (Equation 24).

$$M = \frac{\frac{\Delta\rho}{\rho_f}}{\left|\frac{\Delta h_f}{\Delta z}\right|} \quad (24)$$

where:

$$\Delta\rho = \rho_{mean} - \rho_f$$

For the example case of stagnant saline groundwater considered earlier  $\frac{\Delta h_f}{\Delta z} = \frac{\Delta\rho}{\rho_f}$ , so  $M = 1$ .

For density-invariant flow,  $M = 0$ . If  $M \gg 1$ , then free convection is dominant. If  $M \ll 1$ , then forced convection is dominant. For the example shown in Figure 7,  $M = \frac{0.0195}{0.048} = 0.4$ .

The definition of  $M$  according to Equation 24 applies to the analysis of vertical flow, but an equivalent mixed convection ratio can be defined to study instabilities in predominantly horizontal flow fields as well (Oostrom et al., 1992) as shown in Equation 25.

$$M' = \frac{K \frac{\Delta\rho}{\rho_f}}{q_x} \quad (25)$$

This form of the mixed convection ratio applies to the landfill example in Figure 12. Even though  $q_x$  varies spatially because there is groundwater recharge across the top of the aquifer (i.e.,  $q_x$  increases from left to right),  $M'$  can still be estimated if some effective  $q_x$  can be defined. In this case, it could be set to the specific discharge across the midpoint of the horizontal aquifer distance ( $x = 250$  m). The volumetric flow rate due to the recharge (which is  $0.5 \text{ mm d}^{-1}$ ) between  $x = 0$  and  $x = 250$  m is  $5 \times 10^{-4} \text{ m d}^{-1} \times 250 \text{ m} = 0.125 \text{ m}^2 \text{ d}^{-1}$ , which needs to be augmented by the inflow rate across the left boundary which was  $0.5 \text{ m}^2 \text{ d}^{-1}$  for this example. Assuming that the horizontal flow is distributed equally over the thickness of the aquifer gives  $q_x = (0.5 + 0.125)/40 = 0.016 \text{ m d}^{-1}$ . The hydraulic conductivity was  $K = 25 \text{ m d}^{-1}$ , and  $\frac{\Delta\rho}{\rho_f}$  equates to  $3.25 \times 10^{-4}$ ,  $3.25 \times 10^{-3}$  and  $1.3 \times 10^{-2}$ , for the low, medium, and high-density cases, respectively. Inserting these values into Equation 25 yields corresponding values for  $M'$  of 0.52, 5.2 and 20.8. The values are all above the critical threshold of  $M' \approx 0.3$  defined by Oostrom and others (1992), so one would expect the plume to be unstable for all density contrasts considered, yet the low-density case in Figure 12 is stable. One likely reason for this is that there is recharge across the top boundary, which is different from the experimental conditions in Oostrom and others (1992). Moreover, the Oostrom and others (1992) criterion was based on laboratory experiments, in which the physical heterogeneities that trigger instabilities are much more pronounced than in the

numerical simulation of the landfill leachate plume, in which small numerical roundoff errors form the triggering instabilities. This aspect is discussed in more detail in Section 6.

Mixed convection ratios have been used by various authors to assess the relative importance of free and forced convection in regional flow systems. For example, Illangasekare and others (2006) used it to infer the main driving force of aquifer salinization in Sri Lanka following the December 26, 2004 tsunami, while Holzbecher (2005) used it to determine the effect of regional flow on the flow pattern and salinity distribution near salt lakes. Mixed convection ratios can be formulated for more complex flow conditions as well. For example, Ward and others (2009) give expressions for  $M$  for radial flow fields.

## 5.2 Rayleigh Number

The mixed convection ratio is useful for determining the strength of the density driving force relative to the forced convection driving force. In systems where there is initially no flow, but a concentration or temperature difference exists, the onset of instability is determined by the value of a nondimensional number called the Rayleigh number ( $Ra$ ). It was named in the honor of Lord Rayleigh, who published some of the earliest work in classical fluid mechanics dealing with unstable flows in his paper “*On convection currents in a horizontal layer of fluid when the higher temperature is on the underside*” (Rayleigh, 1916). The Rayleigh number is the ratio between buoyancy-driven forces that drive free convection to forces (caused by diffusion and dispersion) that act to dissipate it, (e.g., Simmons et al., 2001). For a system that extends infinitely in the horizontal direction, with impermeable top and bottom boundaries between which a density difference of  $\Delta\rho$  is maintained (Figure 13) the Rayleigh number is defined as shown in Equation 26.

$$Ra = \frac{\Delta\rho g k H}{\mu D} \quad (26)$$

where:

$\Delta\rho$  = density difference across the layer ( $M/L^3$ ), e.g.,  $kg\ m^{-3}$

$H$  = thickness of the layer ( $L$ ), e.g.,  $m$

$D$  = diffusion coefficient ( $L^2/T$ ), e.g.,  $m^2\ s^{-1}$

for solutes,  $D = nD_C$ , porosity times molecular diffusion coefficient

for heat,  $D = D_T$ , thermal diffusion coefficient

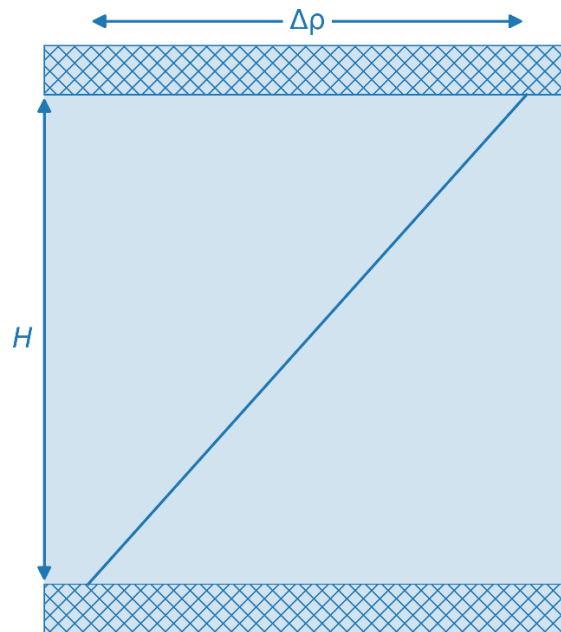


**Figure 13** - Schematic representation of the horizontally infinite system used to define the Rayleigh number, with impermeable top and bottom boundaries where a density difference  $\Delta\rho$  exist over the height  $H$ . The diagonal line indicates a linear variation in fluid density between the bottom and top boundaries with higher density at the top.

It is important to consider the different meanings of  $D$  in Equation 26 for solutes and heat as discussed in subsection 4.3. For solutes, diffusive transport can take place only through the water-filled pore space and therefore includes the effects of porosity (the fraction of the cross-sectional area across which diffusion occurs due to the presence of solids) and tortuosity (the longer transport pathway compared to diffusion in free water due to the tortuous path lines caused by the irregular geometry of the pore space). For heat, conduction is both through the water-filled pores and the rock itself, and therefore  $D_T$  is an averaged thermal diffusivity determined by the thermal characteristics of the water and the rock (Ingebritsen et al., 2006).

For Rayleigh numbers greater than some critical Rayleigh number  $Ra_c$ , gravity induced instability will occur in the form of waves in the boundary layer that develop into fingers or plumes. These fingers sink downward under gravitational influence. This critical Rayleigh number defines the transition between diffusive transport (at lower than critical Rayleigh numbers) and free convective transport by density-driven fingers (at higher than critical Rayleigh numbers). In the most basic sense, for  $Ra$  less than  $Ra_c$  the system is stable. For  $Ra$  greater than  $Ra_c$ , the system is unstable. For infinitely long, parallel domains, with upper and lower boundaries that are impermeable and remain at a constant temperature or concentration), and no forced horizontal advection, the critical Rayleigh number is

$Ra_c = 4\pi^2$ . For other boundary condition types, different values of  $Ra_c$  apply (Nield, 1968; Nield and Bejan, 2006).

Table 2 summarizes the main differences between groundwater systems and the experimental settings in classical fluid mechanics where convection theory was developed. It is immediately evident that there are significant differences between the physical conditions in these systems. These are also reflected in the nature of the implicit and explicit assumptions that are made, or can be reasonably made, in each case. An obvious problem arises when theoretical work developed under idealized and simplified conditions is applied to more complex settings that are typically encountered in groundwater applications.

**Table 2** - Some of the explicit and implicit assumptions made in the study of free convection systems in both traditional fluid mechanics (left column) and the study of groundwater hydrology (right column).

Traditional fluid mechanics	Groundwater hydraulics
<ul style="list-style-type: none"> <li>• Steady-state assumptions</li> <li>• Homogeneous layers</li> <li>• Length scale = layer thickness</li> <li>• Simple chemistry / fluids</li> <li>• Molecular diffusion</li> <li>• Rayleigh number predicted a priori</li> <li>• Known <math>Ra_c</math></li> <li>• Laboratory scale, simple boundary conditions</li> </ul>	<ul style="list-style-type: none"> <li>• Transient</li> <li>• Heterogeneous</li> <li>• Length scales ambiguous</li> <li>• Complex geochemistry / fluid-matrix</li> <li>• Dispersion greater than diffusion</li> <li>• Cannot determine Rayleigh number a priori</li> <li>• Unknown <math>Ra_c</math></li> <li>• Field scale, complex boundary conditions</li> </ul>

Simmons and others (2001) and Simmons (2005) described some of the problems using the Rayleigh number in natural groundwater systems. The criteria for extremely simple boundary and layer conditions in traditional fluid mechanics (e.g., an infinite horizontal homogeneous layer with perfect constant concentration upper and lower boundaries) are unlikely to be applicable to most groundwater situations. As Table 2 highlights, one reason for this is that natural systems are not at steady state, the hydraulic properties are heterogeneous, a representative length scale is difficult to define (Rees et al., 2008; Riaz et al., 2006) and the critical Rayleigh number  $Ra_c$  is rarely known in a natural groundwater setting.

Despite these limitations, some insight into the role of free convection in groundwater systems can be obtained by observing the range of Rayleigh numbers as a function of  $\Delta\rho$  and  $k$  (Figure 14). Since the range of permeability values for geologic materials is many orders of magnitude, so is the range of possible Rayleigh numbers, which is why the log of  $Ra$  was contoured. Figure 14 shows separate plots for solutes and heat because solutes and heat have vastly different values of  $D$  (which were taken as  $D = D_c = 5 \times 10^{-10}$  and  $D = D_T = 1.4 \times 10^{-6} \text{ m}^2 \text{ s}^{-1}$ , respectively). Moreover, the density range associated with solute concentration differences tends to be larger than for temperature differences, which is why the range on the vertical axes of Figure 14a and Figure 14b differ.

Finally, solute gradients can be much higher than common temperature gradients, so different values of  $H$  were chosen to draw the graphs of Figure 14a and 14b. Several general conclusions can be drawn from the graphs:

- density differences created by temperature differences require a higher permeability for instability to set in than density-differences created by solute concentrations;
- for permeable aquifer materials (e.g., sand and gravel), even small density contrast can lead to unstable convection;
- the actual value of the density contrast  $\Delta\rho$  required for onset of unstable conditions is sensitive only within a relatively narrow range of permeabilities (as inferred from the steep vertical trajectory of the white line); and,
- for materials with very low permeability (like clay), the density differences caused by variations in solute concentration or temperature in groundwater systems are not large enough to cause instability.

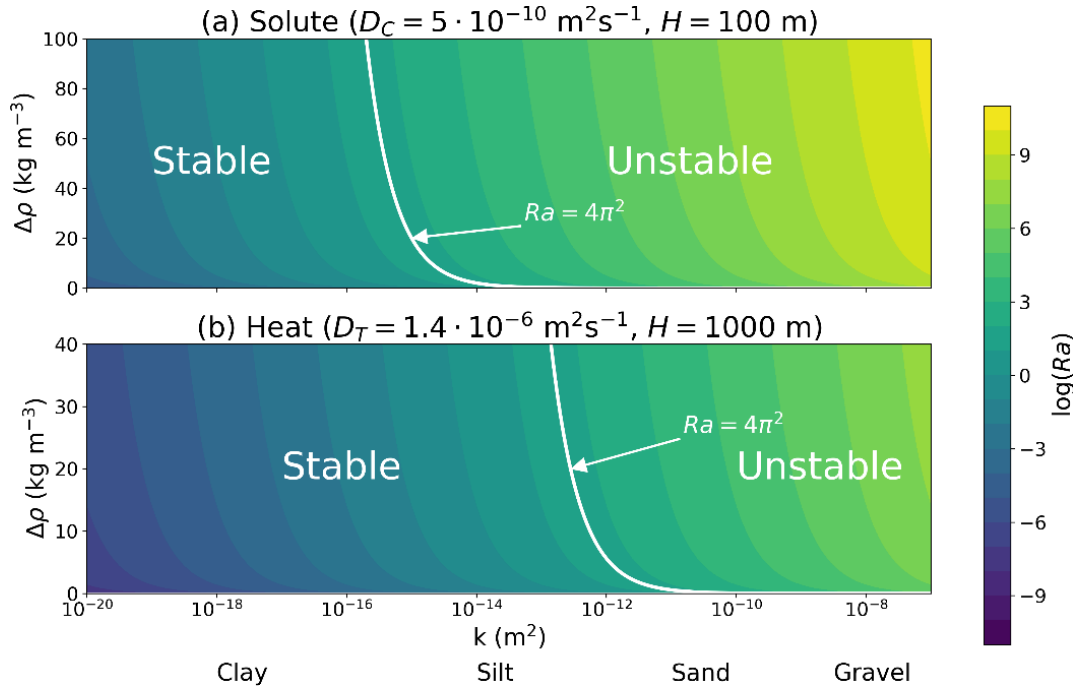


**Figure 14** - The Rayleigh number (note the decadal log scale) as a function of permeability  $k$  and density contrast  $\Delta\rho$  for: a) solutes, and b) heat. The white line indicates the combination of  $k$  and  $\Delta\rho$  values where  $Ra = 4\pi^2$ . For dissolved solids, a density difference of  $100 \text{ kg m}^{-3}$  is roughly equivalent to the difference between fresh water and water with  $150 \text{ g NaCl kg}^{-1}$ . For heat, at standard pressure, a density difference of  $40 \text{ kg m}^{-3}$  is roughly equivalent to the difference between fresh water at  $4 \text{ }^\circ\text{C}$  and  $98 \text{ }^\circ\text{C}$ . The labels below the graphs indicate where the  $k$  values of common unconsolidated aquifer materials occur on the permeability log scale based on Freeze and Cherry (1979; page 29).

An important caveat must be made for the discussion in the previous paragraph because the use of the solute molecular diffusion coefficient  $D_C = 5 \times 10^{-10} \text{ m}^2 \text{ s}^{-1}$  is not

appropriate for aquifers in which solute spreading also occurs by mechanical dispersion (as indicated in Table 2). In solute transport models, the effect of hydrodynamic dispersion is normally described using a dispersion coefficient ( $D_h$ ), which has the form  $D_h = \alpha v + D_c$ , where  $\alpha$  is the dispersivity (m) and  $v$  the groundwater seepage velocity ( $\text{m s}^{-1}$ ). Because of the directional dependence of the dispersion process,  $D_h$  is a tensor (as discussed further in Section 6.1) but this simple expression is useful to gain some insight into the relative magnitude of the molecular diffusion coefficient relative to the hydrodynamic dispersion coefficient. Considering a range of  $\alpha$  values from  $10^{-2}$  to 100 m, combined with a range of groundwater flow velocities  $v$  between 1 and  $10 \text{ m year}^{-1}$  yields a corresponding range of  $3.17 \times 10^{-10} < D_h < 3.17 \times 10^{-5} \text{ m}^2 \text{ s}^{-1}$ .

These values show that solute spreading by mechanical dispersion is more substantial than molecular diffusion and is usually the dominant spreading mechanism in natural groundwater systems. Unfortunately, incorporation of the mechanical dispersion into a Rayleigh number is non-trivial. An alternative Rayleigh number formulation was provided by Hidalgo and Carrera (2009, their Equation 2.18), who took the longitudinal dispersivity ( $\alpha_L$ , i.e., the dispersivity in the direction of flow), which reflects the character of the porous medium even though it only influences dispersion if groundwater velocity is greater than zero, and used it as the representative length scale (instead of  $H$ ) to estimate the onset of instability in an initially stagnant system as shown in Equation 27.

$$Ra' = \frac{\Delta \rho g k \alpha_L}{\mu (D + \alpha_L v)} \quad (27)$$

The onset time of free convection decreased with  $Ra'$  and it was found that the onset time could be up to two orders of magnitude shorter in dispersive systems than in purely diffusive systems. Laboratory experiments have confirmed the importance of mechanical dispersion in controlling the downward solute flux and the finger dimensions (Liang et al., 2018). In these experiments, which were conducted in homogeneous porous media, the dispersivity was a function of the grain size. In the field though, the dispersivity is controlled by the heterogeneity of the geological material, which spans a range of spatial scales. The relevance of mechanical dispersion in field settings, therefore, remains an unresolved issue because convective fingering is influenced by geological heterogeneity in a complex way. This is discussed in Section 6.3.

### 5.3 Wooding Number

As mentioned in the previous section, application of the Rayleigh number is limited to systems without a background flow field. Wooding (1960) analyzed the case of a boundary layer that grows by diffusion in the presence of a flow that opposes diffusion. Situations like these are found below the bottom of salt lakes that receive groundwater

input by upward seepage (Simmons et al., 2002; Simmons et al., 1999; Wooding et al., 1997), salt pans (Bauer et al., 2006) or where groundwater discharges into the ocean (Greskowiak, 2014). A stable boundary layer occurs when the diffusive flux equals the opposing advective flux (Figure 15).

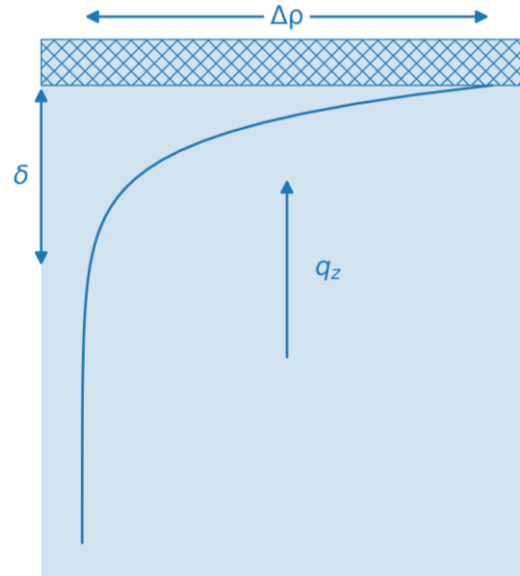


**Figure 15** - Schematic representation of a system with a flow component (upward in this image) in the opposite direction as diffusion (downward in this image), where a density difference  $\Delta\rho$  exists over the characteristic boundary layer thickness  $\delta$ . The hatched area is a zone of constant concentration that is higher than the initial concentration in the porous medium. The curved line represents the fluid density distribution below the hatched zone.

Wooding et al. (1997) defined the characteristic thickness  $\delta$  of the boundary layer as shown in Equation 28.

$$\delta = \frac{D}{q_z} \quad (28)$$

When  $H$  is replaced by  $\delta$  in Equation 26, the boundary layer Rayleigh number, or Wooding number, becomes Equation 29.

$$Ra^\delta = \frac{\Delta\rho g k \delta}{\mu D} = \frac{\Delta\rho g k}{\mu q_z} \quad (29)$$

Based on linear perturbation analysis, Wooding (1960) determined the value of the critical boundary Rayleigh number to be  $Ra_{cr}^\delta \approx 7$ . For values less than 7 which are situations with high  $q_z$  or low  $\Delta\rho$ , the boundary layer initially increases and then reaches a

stable thickness. For values greater than 7 which are situations with low  $q_z$  or high  $\Delta\rho$ , the boundary layer continues to increase and never stabilizes.

High values of  $q_z$  tend to stabilize the system, as shown in Figure 16. The colored lines mark the boundary between the stable and unstable regime for a range of values of  $q_z$  that may be encountered in groundwater systems. Fluxes of  $q_z > 0.1 \text{ m d}^{-1}$  are required to prevent instabilities from amplifying in the most permeable aquifers.

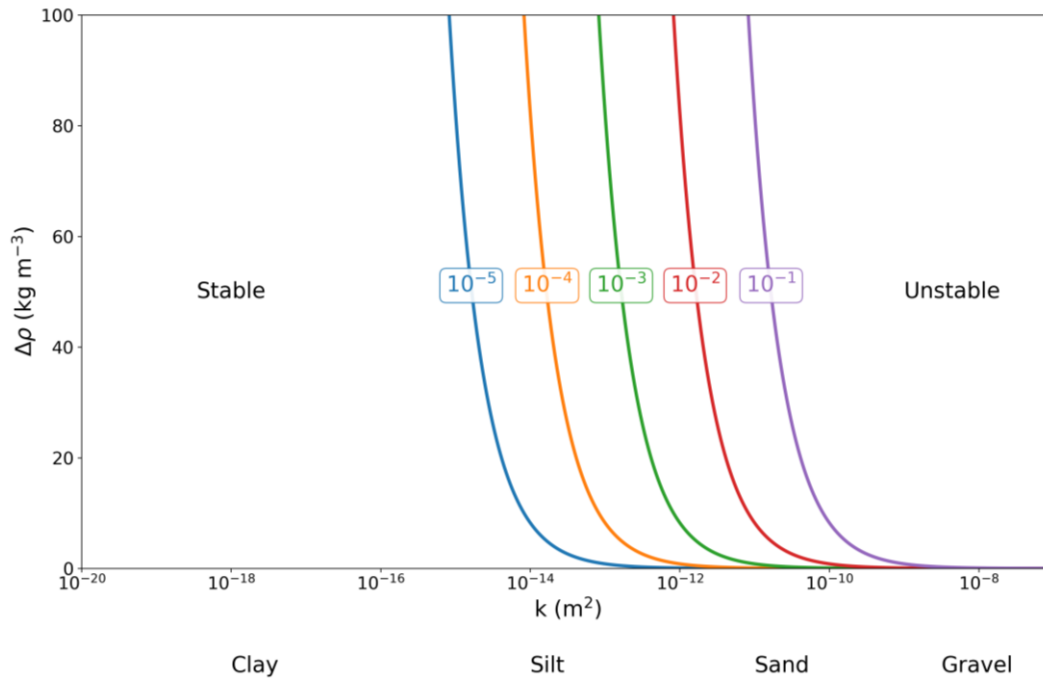


**Figure 16** - Boundaries between stable and unstable regimes for different values of  $q_z$  (in  $\text{m d}^{-1}$ ), indicated by colored lines. The lines are calculated according to Equation 29 with  $Ra = Ra_{cr}^{\delta} = 7$ . Stable conditions exist to the left, and unstable to the right, of each line marking the boundary between the regimes. Values of  $q_z$  well above  $0.1 \text{ m d}^{-1}$  would be required to maintain stable conditions in gravels for even small density differences.

## 5.4 Sherwood Number

The dimensionless Sherwood number ( $Sh$ ) is the ratio of the actual solute mass flux resulting from free convection to the solute mass flux resulting from diffusion and is given by Equation 30 (Prasad and Simmons, 2005).

$$Sh = \frac{Q_m H}{D_c \Delta C} \quad (30)$$

where:

$Q_m$  = mass flux across the source boundary ( $\text{M}/(\text{TL}^2)$ ), e.g.,  $\text{kg s}^{-1} \text{ m}^{-2}$

$\Delta C$  = concentration difference over the height  $H$  ( $\text{M}/\text{L}^3$ ), e.g.,  $\text{kg m}^{-3}$

For  $Sh < 1$ , transport is diffusive in the stable regime. For  $Sh > 1$  transport is in the unstable regime. As one moves from the stable to unstable density configuration, the associated physics become increasingly complicated as the diffusive transport gives way to convective fingering. The Sherwood number is a useful quantitative indicator for comparing the performance of numerical models of free convection (Niederer et al., 2019; Prasad and Simmons, 2005, 2003).

## 5.5 Nusselt Number

The Nusselt number ( $Nu$ ) is equivalent to the Sherwood number but applies to heat transport. It is defined in Equation 31 (Elder, 1967a).

$$Nu = \frac{Q_h H}{k_T \Delta T} \quad (31)$$

where:

$Q_h$  = heat flow across the source boundary ( $M/T^3$ ), e.g.,  $W m^{-2}$

$k_T$  = thermal conductivity ( $M/(L\theta)$ ), e.g.,  $W m^{-1}K^{-1}$

$\Delta T$  = temperature difference over the height  $H$  ( $\theta$ ), e.g.,  $K$

Laboratory and computational experiments have shown that there is a relationship between the Rayleigh number and the Nusselt number (Cheng, 1979). This is illustrated in Figure 17. If the Rayleigh number is below the critical value, there is no convective heat transfer and so  $Nu = 1$  (conductive heat transfer only). As the Rayleigh number increases, so does the Nusselt number, which means that more heat is being transported convectively. This is because at high Rayleigh numbers, the convective cells become slimmer and thereby more efficient in transferring heat. Modeling by Holzbecher (1996) showed that the exact relationship varies depending on the aspect ratio of the domain as illustrated in Figure 17, that is, the larger the height/width ratio, the higher the heat transfer at high Rayleigh numbers.

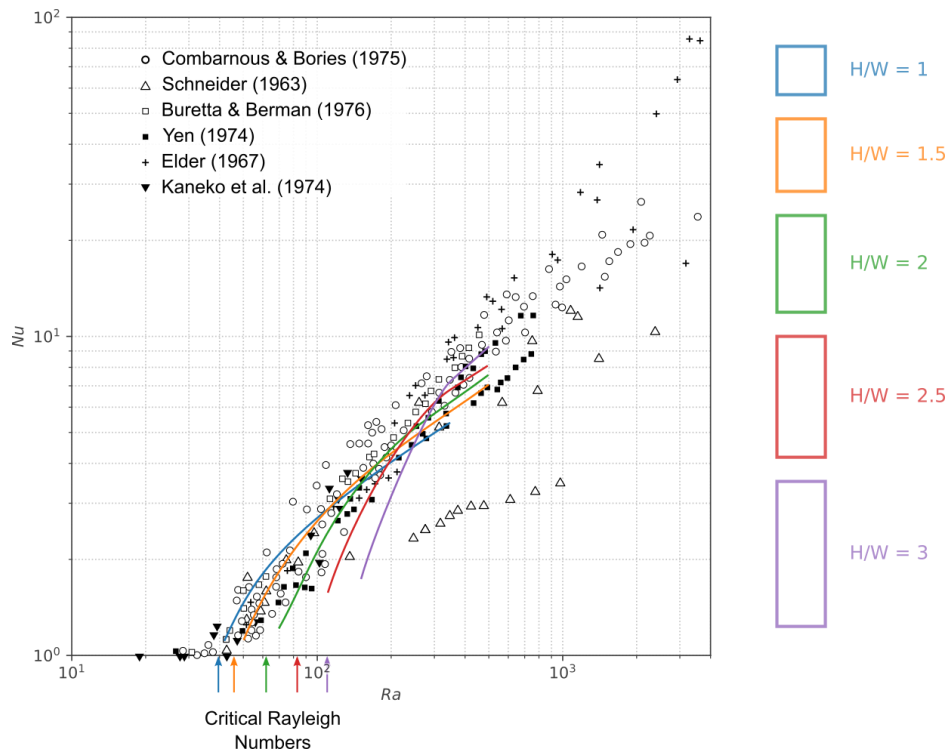


**Figure 17** - Relationship between the Rayleigh ( $Ra$ ) and Nusselt ( $Nu$ ) numbers originally published by Cheng (1978). The lines represent model-based relationships by Holzbecher (1996) for domains of different height/width ratios  $H/W$ , as shown schematically to the right of the graph. The critical Rayleigh number for each  $H/W$  value is indicated by an arrow below the horizontal axis. Original figure reprinted from *Advances in Heat Transfer*, 14, P. Cheng, *Heat Transfer in Geothermal Systems*, Copyright (1979), with permission from Elsevier. Model data courtesy of Ekkehard Holzbecher.

## 6 Mathematical Modeling

Numerical modeling of groundwater flow is a complex subject, and variable-density models are significantly more complex than constant-density models. An exhaustive discussion of all the details of these complexities is impossible here. Readers are referred to the works of, amongst others, Holzbecher (1998), Segol (1994), Voss (1999, 1984) and Zheng and Bennett (2002) for information on important aspects of variable-density flow such as governing equations, numerical methods, boundary conditions, initial conditions and parametrization. This section touches upon some of the basics and discusses the challenges associated with modeling unstable systems.

### 6.1 Governing Equations

For variable-density flow, the mass conservation equations for fluid (groundwater), mass and heat are the basis for numerical models. The mass balance equation for a compressible fluid in a saturated porous medium is shown in Equation 32.

$$\frac{\partial(n\rho)}{\partial t} = -\nabla \cdot (\rho \vec{q}) + \rho_{ss} q_{ss} \quad (32)$$

where:

$t$  = time (T), e.g., s

$\vec{q}$  = specific discharge as given by Equation 2 (L/T), e.g., m s<sup>-1</sup>

$\rho_{ss}$  = density of water source, or sink (M/L<sup>3</sup>), e.g., kg m<sup>-3</sup>

$q_{ss}$  = discharge rate per unit of volume of water source or sink (1/T), e.g., s<sup>-1</sup>

The term on the left of the equal sign represents the change in fluid mass per unit of time. The first term to the right of the equal sign represents the change in fluid mass due to differences between inflow and outflow, while the second term is the change in fluid mass due to a source or sink. In groundwater, this can be recharge, inflow from an adjacent aquifer or an extraction/injection well, for example.

The mass balance equation for a solute that instantaneously and linearly partitions between a dissolved phase at concentration  $C$  in the pores and an adsorbed phase on the rock surface is Equation 33.

$$\left(1 + \frac{\rho_b K_d}{n}\right) \frac{\partial(nC)}{\partial t} = -\nabla \cdot (\vec{q}C) + \nabla \cdot (n\overline{D}_{h,C} \cdot \nabla C) + q_s C_s \quad (33)$$

where:

$\rho_b$  = dry bulk density of the rock (M/L<sup>3</sup>), e.g., kg m<sup>-3</sup>

$K_d$  = distribution coefficient (L<sup>3</sup>/M), e.g., m<sup>3</sup> kg<sup>-1</sup>, which is the ratio of adsorbed mass and solute mass

$\overline{D}_{h,C}$  = solute dispersion tensor (L<sup>2</sup>/T), e.g., m<sup>2</sup>s<sup>-1</sup>, which includes the effect of both molecular diffusion and mechanical dispersion

$C_s$  = concentration associated with a source (M/L<sup>3</sup>), e.g., kg m<sup>-3</sup>

The heat balance equivalent for Equation 33 for temperature being at local instantaneous equilibrium between the pore water and rock matrix is Equation 34.

$$\left(1 + \frac{1 - n \rho_r c_s}{n \rho c}\right) \frac{\partial(nT)}{\partial t} = -\nabla \cdot (\vec{q}T) + \nabla \cdot (\overline{D}_{h,T} \cdot \nabla T) + q_s T_s \quad (34)$$

where:

$\rho_r$  = density of the rock (M/L<sup>3</sup>), e.g., kg m<sup>-3</sup>

$c$  and  $c_s$  = specific heat capacities of the groundwater and rock, respectively (ML<sup>2</sup>/(T<sup>2</sup>θ)), e.g., J K<sup>-1</sup> kg<sup>-1</sup>

$\overline{D}_{h,T}$  = tensor which includes the combined effects of thermal conduction and mechanical dispersion (L<sup>2</sup>/T), e.g., m<sup>2</sup>s<sup>-1</sup>

$T_s$  = temperature associated with a source (θ), e.g., K

The terms on the left of the equal sign in Equations 33 and 34 represent the change in solute mass or energy, respectively, per unit of time. For both equations, the terms on the right-hand side of the equal sign represent the change due to:

- advective solute/heat transfer;
- mechanical dispersion coupled with diffusion of a solute or conduction of heat; and,
- fluid entering or exiting the system.

Most numerical codes assume that density is a linear function of  $C$  and  $T$ , as well as pressure  $p$  for the range of conditions within the modeled region such that all of the derivatives have constant values (Equation 35).

$$\rho = \rho_0 + \frac{\partial \rho}{\partial C}(C - C_0) + \frac{\partial \rho}{\partial T}(T - T_0) + \frac{\partial \rho}{\partial p}(p - p_0) \quad (35)$$

where:

- $\rho_0$  = density of the fluid at initial concentration, temperature and pressure (M/L<sup>3</sup>), e.g., kg m<sup>-3</sup>
- $C_0$  = initial concentration of the groundwater (M/L<sup>3</sup>), e.g., kg m<sup>-3</sup>
- $T_0$  = initial temperature of the groundwater ( $\Theta$ ), e.g., K
- $p_0$  = initial fluid pressure (M/(L<sup>1</sup>T<sup>2</sup>)), e.g., kg m<sup>-1</sup> s<sup>-2</sup>

It should be noted that the slope  $\frac{\partial \rho}{\partial C}$  is constant over a large concentration and temperature range, but  $\frac{\partial \rho}{\partial T}$  is temperature-dependent over the range of temperatures of hydrogeological interest. The dependency of  $\rho$  on  $p$  is very small due to the low compressibility of water such that  $\frac{\partial \rho}{\partial p} \ll \frac{\partial \rho}{\partial C}$  and  $\frac{\partial \rho}{\partial p} \ll \frac{\partial \rho}{\partial T}$ . In fact, it is much smaller than the compressibility of most of the natural materials that make up aquifers, so it is usually not entered explicitly but combined with the elastic storage properties of the rock in the specific storage coefficient  $S_p$ . With the use of Equation 35, Equation 32 can be transformed into Equation 36 (Guo and Langevin, 2002; Jiao and Post, 2019).

$$\rho S_p \frac{\partial p}{\partial t} + \frac{\partial \rho}{\partial C} \frac{\partial C}{\partial t} + \frac{\partial \rho}{\partial T} \frac{\partial T}{\partial t} = -\nabla \cdot (\rho \vec{q}) + \rho_{ss} q_{ss} \quad (36)$$

Equations 33, 34 and 36, or their equivalents, form the governing equations of numerical codes for variable-density groundwater flow. In addition to these, numerical models rely on the pressure-based form of Darcy's law (Equation 2) to describe groundwater flow, Fick's law (Equation 21) for dispersive and diffusive solute mass transfer and/or Fourier's law for conductive heat transfer (Equation 22), as well as an equation of state like Equation 35. An inspection of the equations shows that they are coupled. That is, the solute concentration and temperature affect the density, the density affects the flow field, and the flow field alters the solute concentrations and temperatures. The governing equations for groundwater flow and solute transport, therefore, need to be

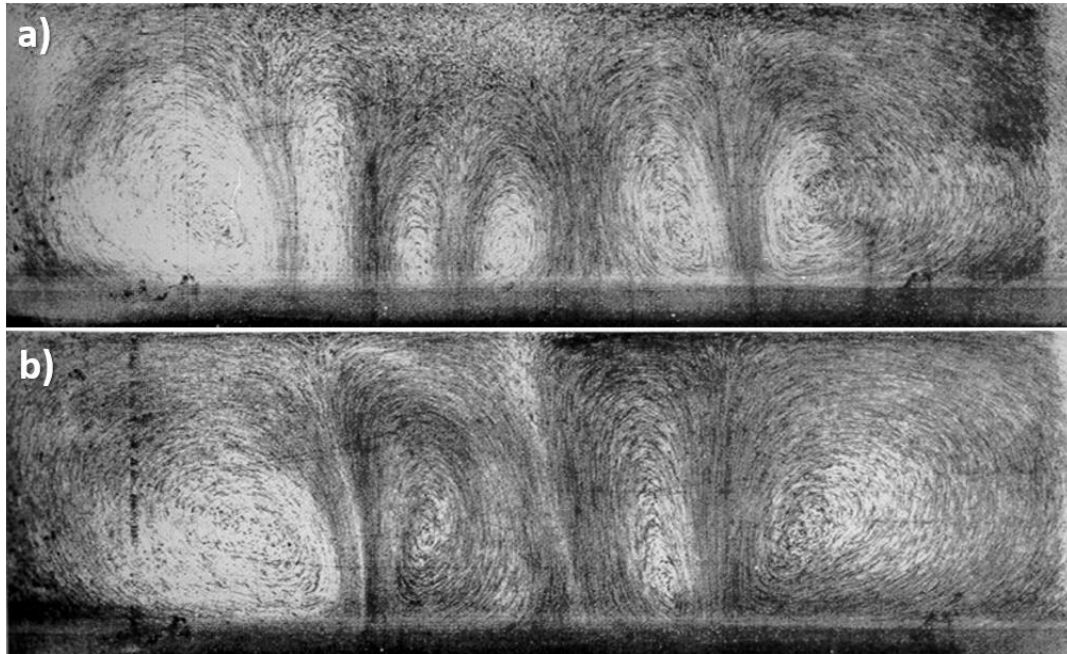
solved simultaneously for variable-density flow problems. Codes for variable-density flow are therefore inherently more complex than those for constant-density systems.

## 6.2 The Elder Problem

Because the governing equations are non-linear and coupled, analytical solutions are intractable and only exist for the simplest arrangements of convection cells. This means that numerical codes are not easily verified, i.e., the testing of their accuracy by comparing the numerical result to an analytical solution is generally not possible. In that case, alternative strategies are required, such as internal consistency testing (for example mass balance checks) and external consistency testing (Konikow et al., 1996). The latter involves comparing the results of different numerical codes against one another, which is known as benchmarking. A number of model benchmarks have been developed and applied over the years to test variable-density flow models. Information on these model benchmarks and test cases, including successes and limitations, can be found in the references noted in the following discussion and review papers (Diersch and Kolditz, 2002; Voss et al., 2010 and Simmons et al., 2010).

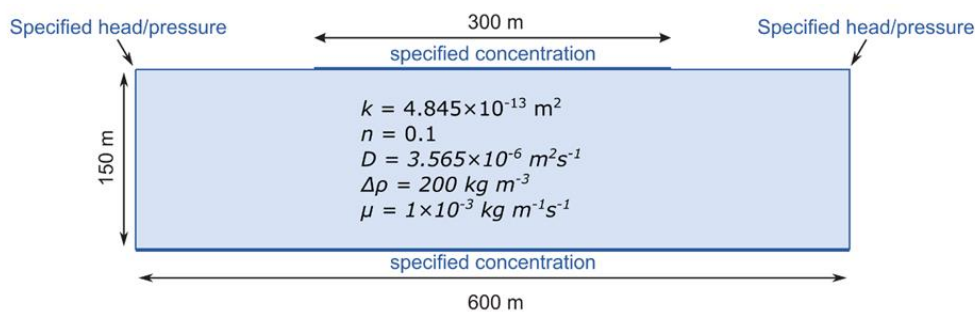
One of the most intensely studied and well-known benchmark problems for variable-density simulators is the Elder problem. It is based on pioneering work by John W. Elder in the Cavendish Laboratory at Cambridge. It was published in the *Journal of Fluid Mechanics* in 1967 (Elder, 1967b, 1967a), and two papers marking the 50<sup>th</sup> anniversary of Elder's work were published in 2017 (Elder et al., 2017; Simmons and Elder, 2017). What is remarkable is that he did not realize his work at Cambridge had gone on to become the basis for the benchmark problem that became famous in hydrogeology. Elder's original study was based on a thermal experiment conducted in a Hele-Shaw Cell. A Hele-Shaw cell consists of two closely spaced parallel plates, between which a fluid, or multiple fluids, are injected. Because the flow in the cell obeys Darcy's law, Hele-Shaw cells can be used to study flow in porous media (having an intrinsic permeability equal to  $k = \frac{a^2}{12}$  where  $a$  is the distance between the plates). Dispersive transport, however, cannot be studied (NEA, 1990).

In Elder's experiment, the fluid was heated from below across part of its base (a "short heater"). The fluid flow was visualized using suspended aluminum particles and the photographs of the results are shown in Figure 18 (Elder, 1967b). Six convection cells occur at early time (Figure 18a) and form four larger cells at later time (Figure 18b).



**Figure 18** - Elder’s original experimental results in a Hele-Shaw Cell (Elder, 1967b). A fluid is heated from below along part of the base of the Hele-Shaw cell. Elder used suspended aluminum particles to visualize the flow field. The photographs show transient natural convection at two different times: a) six convection cells at early time ( $T=0.025$  dimensionless time); and, b) four convection cells at later time ( $T=0.05$  dimensionless time). One dimensionless time unit ( $T$ ) in Elder’s experiment is  $2.4 \times 10^4$  seconds. Thus, (a) with dimensionless time of  $T=0.025$  corresponds to  $t=10$  minutes after the start of the experiment and (b) with  $T=0.05$  corresponds to  $t=20$  minutes after the start of the experiment. In Elder’s original Hele-Shaw cell experiment, plate spacing was 4.0 mm, depth of fluid 5 cm and width of the cavity 20 cm. Reprinted from Journal of Fluid Mechanics, 551, J.W. Elder, Transient convection in a porous medium, 609-623, Copyright (1967), with permission from Cambridge University Press.

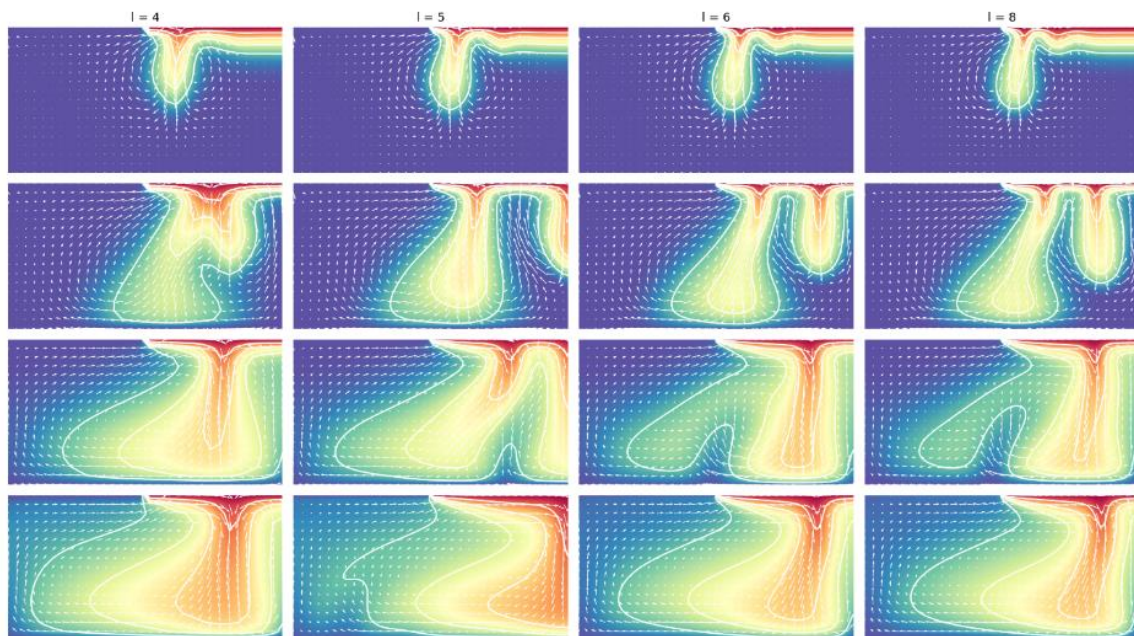
The solute analog was developed by authors including Diersch (1981), Voss and Souza (1987), and Holzbecher (1991). Figure 19 shows the boundary conditions for the solute analog of the Elder problem. Rather than heating from below, the solute analog has solute entering from above. The Rayleigh number is  $Ra = 400$ . It was considered part of the OECD (Organisation for Economic Co-operation and Development) Hydrocoin Project which was designed to test numerical simulators as part of the modeling required for nuclear waste repositories (NEA, 1992).



**Figure 19** - Dimensions, boundary conditions and parameter values of the solute variant of the Elder problem as proposed by Voss and Souza (1987).

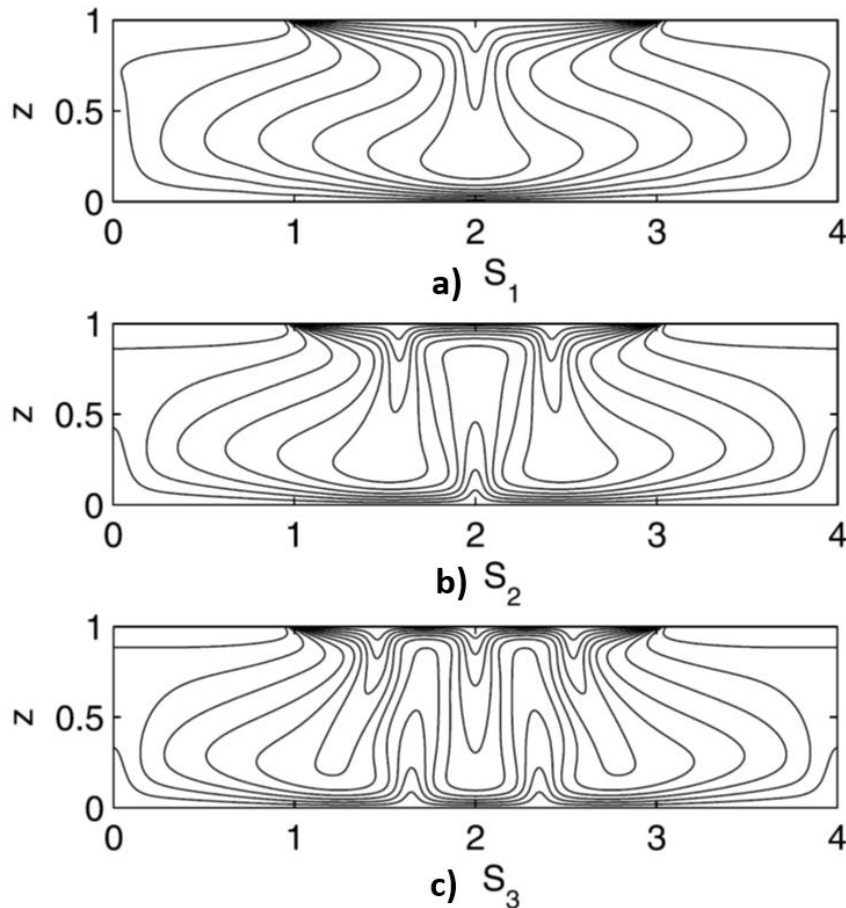
The Hydrocoin Project made it clear that as different numerical codes were used to simulate the Elder problem, their results were generally similar, but there were differences in the details. That is, even though the codes roughly predicted the same fingering pattern, the solute concentration fields were not exactly the same. Moreover, the project concluded that the results were sensitive to the grid discretization (NEA, 1992, 1990). Later on, both points became a topic of intensive research, which revealed that the differences between the models occurred to the differences in the nature and number of cells and whether there was a central downwelling or upwelling (Diersch and Kolditz, 2002).

Figure 20 gives an example of varying results as a function of the level of numerical grid resolution. The results were calculated using SEAWAT (Langevin and Guo, 2006) based on the grid refinement approach by Frolkovič and De Schepper (2000). The grid refinement,  $l$ , determines the number of nodes according to  $2^{2l+1}$ . As the grid is refined, the nature and number of convection cells changes, and there can be upwelling or downwelling below the center of the “short heater”. This variation in the flow direction was summarized by Diersch and Kolditz (2002). They found that different authors reported different results depending on the numerical code and the level of mesh discretization.



**Figure 20** - The Elder problem results ( $Ra=400$ ) as grid level,  $l$ , is varied. Small  $l$  is a coarser grid and larger  $l$  is finer grid. The number of cells is  $2^{2l+1}$ . Lower rows represent later time.

Frolkovič and De Schepper (2000) noted that their models evolved to one of three plume configurations as they were run long enough to reach steady solutions. These are shown in Figure 21 and are called the single plume ( $S_1$ ), double plume ( $S_2$ ) and triple plume ( $S_3$ ) solutions. Johannsen (2003) found the range of Rayleigh numbers over which these different steady convection solutions could come into being.



**Figure 21** - The Elder problem results. Three, steady-state, stable convection states are found using different numerical models and different levels of mesh discretization. These are the single plume ( $S_1$ ), double plume ( $S_2$ ) and triple plume ( $S_3$ ) solutions. Reprinted from *Water Resources Research*, 45(4), M. Van Reeuwijk and others, Insights from a pseudospectral approach to the Elder problem, Copyright (2009), with permission from John Wiley and Sons.

The question that arose was if these different steady-state convection solutions were real or numerical artifacts? To resolve the issue, Van Reeuwijk and others (2009) used a pseudospectral method to solve the Elder problem. This method eliminates all sources of numerical discrepancy, to obtain uncontaminated insights. The use of a pseudospectral method avoids all truncation errors associated with differentiation. The Van Reeuwijk and others (2009) results confirmed the earlier results from Johannsen (2003) and Frolkovič and De Schepper (2000): at  $Ra = 400$  three stable steady-state solutions co-exist. Hence, the ambiguities are physical rather than numerical. This regime is called the triple plume solution, denoted  $S_3$ , and exists when  $Ra > 172$ . A double plume solution,  $S_2$ , exists when  $76 < Ra \leq 172$ , as noted by Johannsen (2003). Below  $Ra = 76$ , there is only one stable steady state ( $S_1$ ). Van Reeuwijk and others (2009) therefore suggested the use of a low Rayleigh number solution for benchmark studies. This particular variant of the Elder problem, which has  $Ra = 60$ , is called the Low Rayleigh Number Elder problem.

Grid convergence is used to assess the performance of groundwater models of constant-density systems where the numerical errors tend to get smaller as the grid is refined. The studies by Van Reeuwijk and others (2009), Johannsen (2003) and Frolkovič and De Schepper (2000) led to the insight that the usual notion of grid convergence does not apply to the Elder problem, nor to numerical models of free convection models more generally, because it is impossible to expect to find a single answer when the physical system being simulated can reach more than one state under identical conditions, that is, there are multiple valid solutions.

The studies of the Elder and other benchmark problems have shown that there can be significant variability in results for the same problem when using different numerical software codes. The results of numerical simulations of free convection are sensitive to solution schemes used in the model. One critical aspect is the generation of heterogeneities that control the onset of convective fingering. Small perturbations of the concentration or temperature are required to trigger the unstable behavior, and in a numerical code these are caused by round-off error unless they are somehow prescribed by the modeler. Knowing how to prescribe perturbations is not trivial and the result of the simulation is inevitably dependent to at least some extent on the method selected for introducing perturbations.

In addition to the aforementioned issues associated with discretization, the physical dimensions of the boundary layer and the plume dimensions limit the maximum model cell dimensions (Kooi et al., 2000b). Fingers form once a boundary layer reaches a critical thickness, hence the vertical discretization of a numerical model must be such that the cell height,  $\Delta z$ , is less than  $\delta_{cr}$  where  $\delta_{cr}$  is the critical boundary layer thickness (Section 5.3). With  $\Delta z > \delta_{cr}$  a boundary layer is created that is numerically unstable, hence the onset of fingering is simulated unrealistically early. Moreover, the cell width  $\Delta x$  must be smaller than the instabilities that form, the size of which depends on the critical boundary layer thickness. For example, for a boundary layer that is compressed by an upward flux (Section 5.3), (Kooi et al., 2000b) recommended that  $\Delta x$  be smaller than the critical instability wavelength, hence they presented Equation 37 in contrast to Equation 29.

$$\Delta x < \left( \frac{\lambda_{cr}}{8} \approx 2\delta_{cr} = \frac{2Ra_{cr}^{\delta}\mu D}{\Delta\rho gk} \right) \quad (37)$$

The fact that  $k$  is in the denominator can mean that  $\Delta x$  can become impractically small for permeable layers (Post and Kooi, 2003). For this reason, the results of regional-scale models (with model grid cell dimensions typically on the order of 10 to 10<sup>2</sup> m) in which fingering occurs should always be interpreted with extreme caution.

## 6.3 Predictability of Convective Flow Patterns

As the example of the Elder problem showed, numerical solutions can be plagued by bifurcations. Bifurcation means that the convection regime can transition to a different steady state. Transient oscillatory behavior means no steady state exists; the flow and transport field keep changing and thus go in and out of different modes. The flow and transport field does not settle into one steady solution. Only modest hydraulic conductivity and density differences are required to achieve a Rayleigh number in excess of what is required for transient oscillatory behavior ( $Ra_c \approx 240-300$ ). Rayleigh numbers in many practical groundwater problems of interest are much higher. Post and Kooi (2003) reported values on the order of  $10^5 < Ra < 10^6$  for coastal aquifers in the Netherlands and van Dam and others (2009) estimated that the Sabkha aquifer in Abu Dhabi has  $Ra > 10^4$ .

The complex physics associated with convective processes raises important questions about the predictive ability of numerical models:

- What, if anything, can reasonably be predicted about fingering processes associated with free convection?
- How uncertain are those predictions likely to be?
- What features are physical reality (bifurcations, oscillatory behavior) and what are numerical artifacts?

Figure 22 provides preliminary insight regarding the answers to these questions. It shows the results of a laboratory tank experiment that was originally published by Post and Simmons (2010). In the original photographs of the experiment, showing the salinity distribution at different times, the view of the left part of the tank has been replaced by the results of the numerical model to facilitate assessment of the similarities and differences between numerical model results and physical systems. An accompanying [video](#)  shows the time-lapse sequence that provides more detail. The experiment was conducted to investigate free convection in the presence of heterogeneity, in this case, a low-permeability layer embedded into more permeable sand. Initially, the tank contained fresh water. As salt water was introduced from the source box at the top, then free convection occurred.

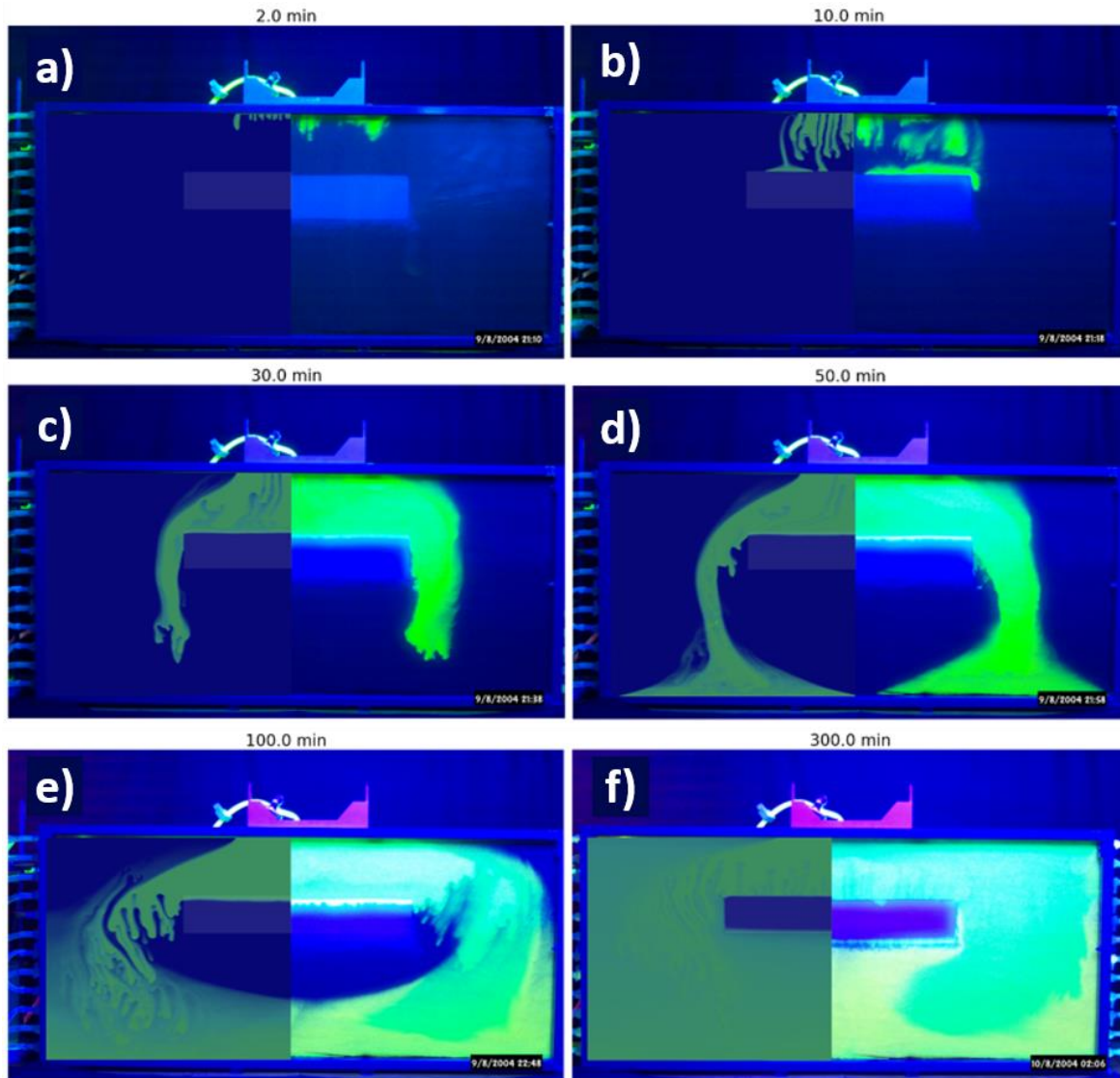


**Figure 22** - Comparison between the numerical model and laboratory tank results by Post and Simmons (2010). Numerical model results (left half of tank) are overlain on the photographs in a comparable color scheme as the laboratory experiment (right half of tank). Results are shown after a) 2, b) 10, c) 30, d) 50, e) 100, and f) 300 minutes. This [video](#) provides the animated version.

The hypothesis prior to conducting the experiment was that once the salt water reached the top of the low-permeability layer, fingers would develop in this layer but with a larger wavelength than the fingers that formed in the sand. In the laboratory experiment, this “re-fingering” did indeed occur. Interestingly, however, in the end, the low-permeability layer became salinized from below, instead of above where the salt source was located. The reason is that fresh water became entrapped below the low-permeability layer and the fresh water’s positive buoyancy caused it to drift upward, thereby pushing out the newly formed fingers and drawing in salt water from below. The video also shows numerous small plumes of fresh water escaping through the top of the low-permeability layer, rapidly mixing with the salt water.

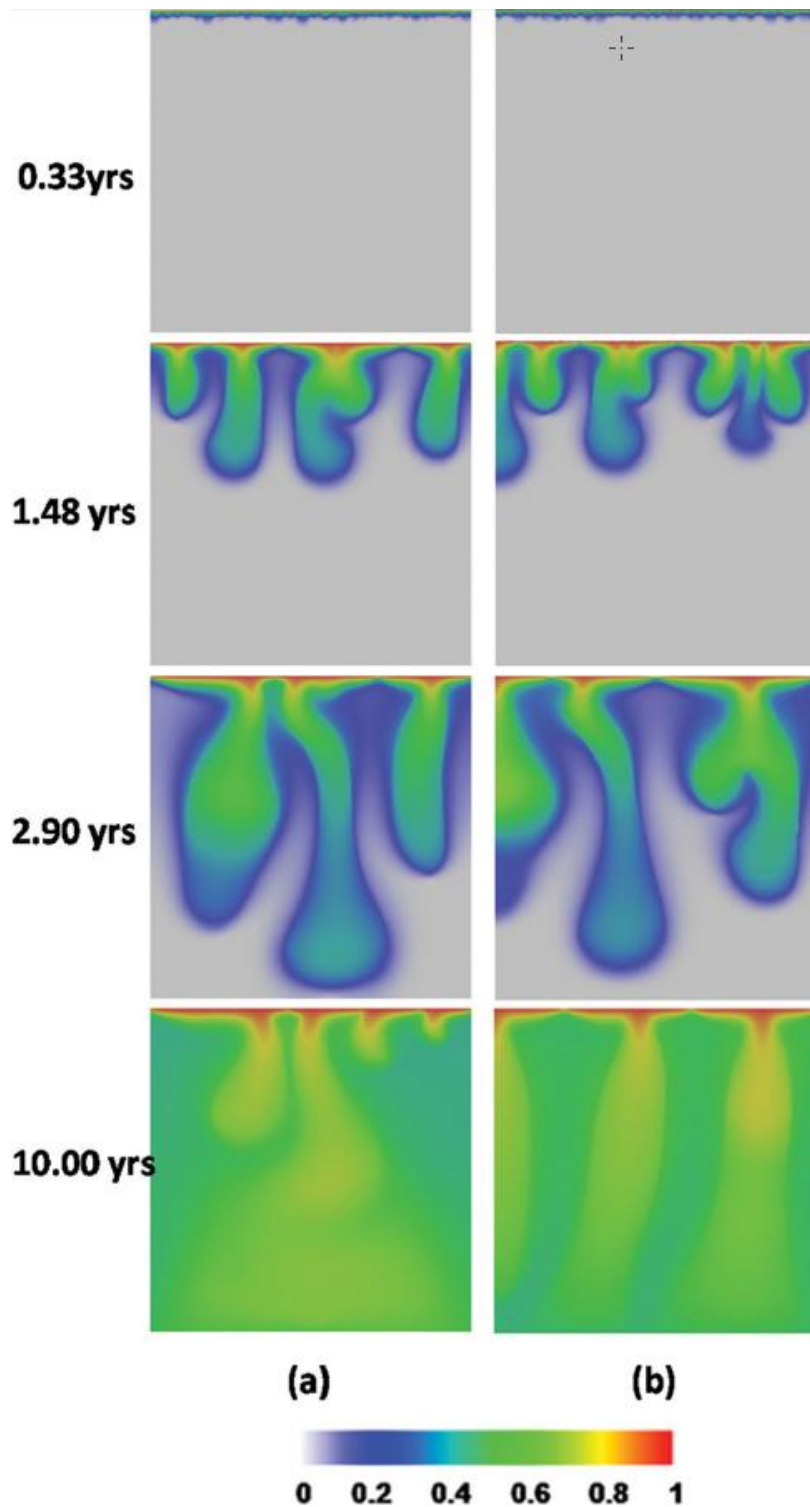
Features observed in the tank that the numerical model replicated included: onset of free convection in the sand layer; horizontal spreading of the salt water along the top of the low-permeability feature; further descent of the salt water and its spreading along the bottom of the tank; and, upward drift of the fresh water and the salt water entering the low-permeability feature from below. Given the challenges with modeling free convection as listed above, this is a very encouraging result. At the same time, a comparison between the model and the laboratory results highlights some important differences. For example, the intricate smaller scale fingering pattern in the model was not observable in the tank. Also, the fingers that initially formed in the low-permeability layer in the tank, did not form in the model. These results illustrate that one can expect to have some success in simulating the overall behavior of free convective flow systems, but not the intricate details. This has also become apparent from some classical studies on convective flow phenomena. Combarous and Bories (1975) showed that despite variability and complexity in the precise details of the convection cells themselves, similarity exists in geometrical structures, bifurcations, and transient oscillatory regimes as a function of Rayleigh number and slope of a layer (Figure 23). This suggests that some variables (e.g., approximate number of fingers, average speed of descent, and total mass of a plume) lend themselves more readily to prediction whereas exact number and locations of fingers are not easily predicted. Further to this, the data compilation of Cheng (1979) as shown in Figure 17 revealed that the convective flux (as indicated by the Nusselt number) is a function of the Rayleigh number of the system regardless of the details of the structure of the convection pattern itself.



## Homogeneous Systems

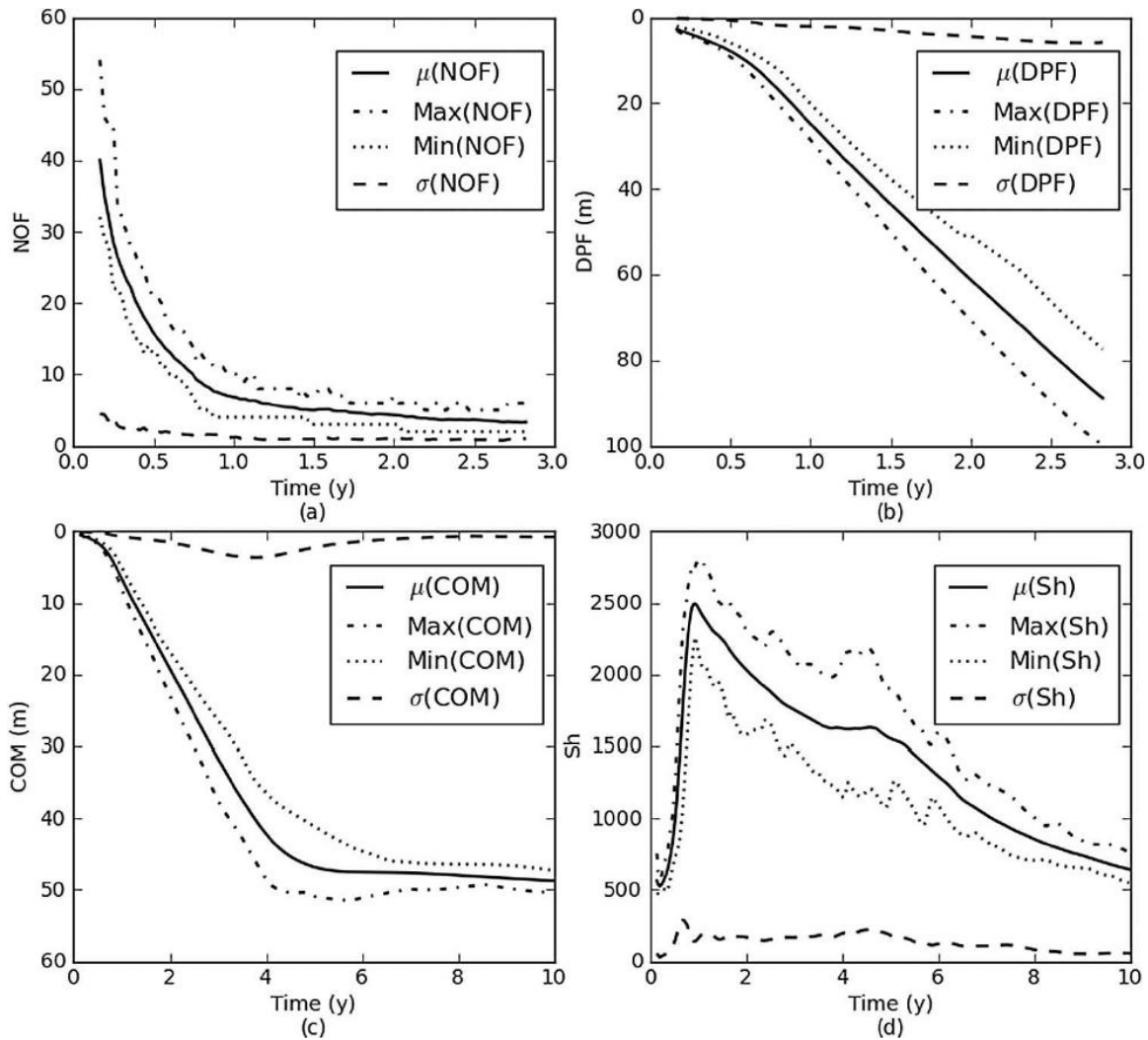
Based on the foregoing discussion, questions arise regarding what one can and cannot expect to be able to simulate and predict using models. Xie and others (2012) examined the predictability and uncertainty of free convection processes in homogeneous systems by considering quantitative indicators to represent plume behavior. These included the smaller-scale details of the fingering patterns themselves (e.g., number of fingers, deepest plume front) and the larger-scale features (e.g., vertical center of solute mass, total solute mass, and solute flux through the source zone). Many stochastic realizations, with the same fluid and solid properties but with random perturbations of the source concentration, were run to examine the plume dynamics and the range of quantitative indicators.

Figure 24 shows two such realizations selected randomly from the set of statistically equivalent realizations tested. Visual inspection reveals that the precise finger locations vary in space and time. The number of fingers themselves is different, but not very different. The bottom tips of the fingers at any given time appear, on average, to have descended to a similar level. In other words, there are features that appear to be reasonably consistent between the realizations. These are not entirely random and non-reproducible results so there is some level of predictive capacity that can be afforded in the analysis free convection behavior.



**Figure 24** - Finger patterns from two realizations (a and b), differing in source concentration, at four different times. Despite the difference in finger patterns, finger penetration rate and the number of fingers, the general character of the simulations (a) and (b) are comparable. (Figure and caption modified from Xie, et al., 2012. Reprinted from *Water Resources Research*, 48(2), Y. Xie and others, Prediction and uncertainty of free convection phenomena in porous media, Copyright (2012), with permission from John Wiley and Sons.

This is further illustrated in Figure 25, which shows the evolution of statistical features (i.e., mean and standard deviation) of four diagnostics with time for all of the stochastic realizations. These are “microscopic indicators” (i.e., number of fingers, NOF, and depth of penetration of the deepest finger, DPF) and “macroscopic indicators” (i.e., center of mass, COM, and the Sherwood number,  $Sh$ ). The maximum and minimum values of these diagnostic variables are also plotted for comparison. All indicators display some level of variability. This confirms previous studies (Bachmat and Elrick, 1970; Mazzia et al., 2001; Schincariol and Schwartz, 1990; and van Reeuwijk et al., 2009) that exact reproducibility is neither possible nor should be expected.



**Figure 25** - The evolution of statistical features (mean  $\mu$  and standard deviation  $\sigma$ ) of four measurable diagnostics with time for all of the stochastic realizations. These are “microscopic indicators” number of fingers (NOF) and depth of penetration of the deepest finger (DPF) and “macroscopic indicators” center of mass (COM) and the Sherwood number ( $Sh$ ). The maximum and minimum values of all diagnostic variables are also plotted for comparison. Figure and figure caption modified from Xie and others (2012). Reprinted from Water Resources Research, 48(2), Y. Xie and others, Prediction and uncertainty of free convection phenomena in porous media, Copyright (2012), with permission from John Wiley and Sons.

The Rayleigh number in this system is  $3.4 \times 10^5$ , which is well into the transient oscillatory convection regime. Nevertheless, the variability demonstrated is surprisingly small with a coefficient of variation,  $CV$ , less than 0.31 for all the variables considered. The  $CV$  is highest for NOF ranging from 0.1 to 0.3 overtime, while the  $CV$ 's for DPF, COM, and  $Sh$ , hover around 0.1, confirming that the uncertainty associated with microscopic indicators is greater than the uncertainty associated with the macroscopic indicators.

In summary, certain plume features are predictable despite the apparent randomness associated with the semi-chaotic fingering processes, at least in homogeneous systems. One should not expect to match the precise locations of fingers in space and time but predicting the number of fingers or their depth is feasible. Even greater confidence can be placed on integrated variables such as the center of mass or the flux. Rather than taking a deterministic view, free convection processes should be treated stochastically which is consistent with their fundamental physical nature. Predictions and comparisons of statistical properties based on multiple stochastic realizations must form the fundamental basis for prediction and uncertainty analysis. This shift from deterministic thinking to stochastic thinking suggests a paradigm shift is needed in the way free convection processes in groundwater systems are conceptualized, measured, modeled, and predicted.

## Heterogeneity

Discussion in the previous section focused on homogeneous systems. Spatial heterogeneity, however, exerts a ubiquitous and critical control on groundwater flow and solute transport. Many of the classical papers on free convection were developed under highly idealized conditions and more often than not conducted in homogeneous layers. Whilst some studies examined layering in geological systems and anisotropy (e.g., Nield and Bejan, 2006) these were fairly simple in comparison to the complex geologic conditions encountered in groundwater systems. However, insights from early work suggested that geologic heterogeneity and anisotropy are important controls on the conditions for onset of instability, as well as growth and decay of density-driven flow patterns. It is therefore critical to understand how the realistic geologic heterogeneity encountered in groundwater systems may influence free convection processes. Regardless of whether the geological medium consists of mixtures of sand and clay, fractured rock, or karstic limestone, the heterogeneity of the material is of fundamental importance.

Various papers have studied the effect of heterogeneity on unstable plume development (Schincariol and Schwartz (1990); Simmons et al. (2001); Prasad and Simmons (2003); Simmons et al. (2008); Nield and Simmons (2007); Simmons et al., 2010; Niederau et al., 2019). Figure 26 summarizes some of the key types of geologic structures that have been considered. These include “traditional” homogeneous materials, trending and continuous sedimentary structures, continuous vertical conduits, discrete vertical fractures, orthogonal

fracture networks, and random distributions of fracture networks (of variable aperture and spacing).

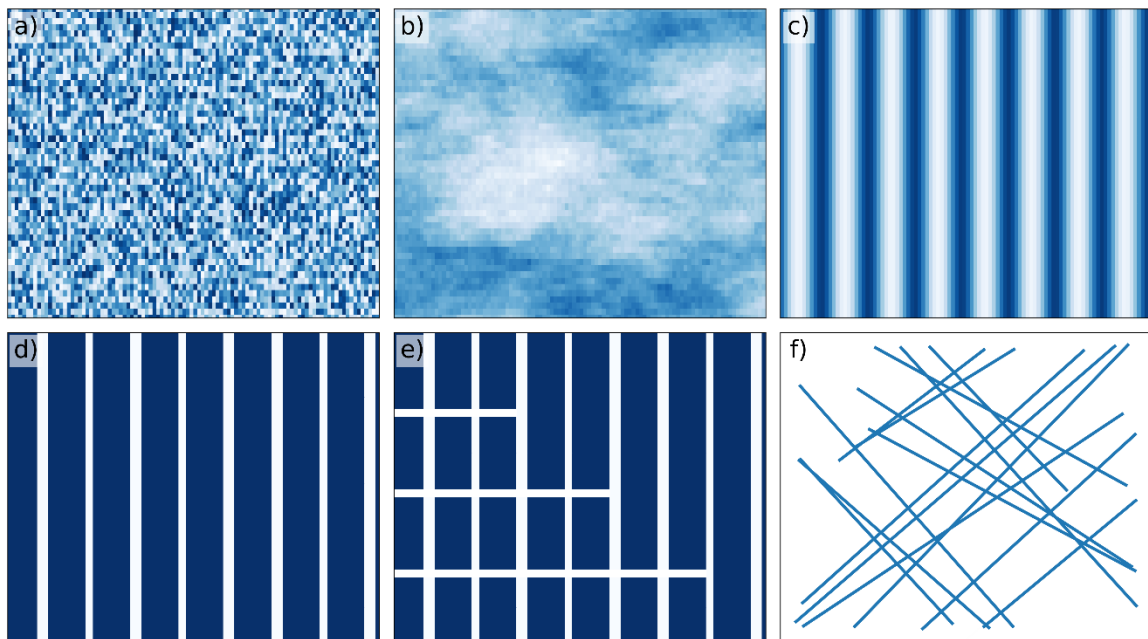


**Figure 26** - A pictorial summary of some key studies that have examined the effect of geologic heterogeneity on free convection processes. These images show general categories of permeability variations that have been studied including: a) traditional homogeneous materials; b) trending and continuous sedimentary structures; c) continuous vertical conduits; d) discrete vertical fractures; e) orthogonal fracture networks; and, f) random distributions of fracture networks (of variable aperture and spacing).

Some early insights into the problems associated with applying Rayleigh numbers to predict the onset of instability in heterogeneous systems were provided by comparing model results for statistically equivalent permeability realizations (i.e., sampled from a log-normal distribution with the same mean and standard deviation) as shown in Figure 27. The top row of Figure 27 illustrates how realizations generated from the same distribution can vary, with low permeability regions shown as dark blue and high permeability regions as light green to yellow. The next four rows show simulation results after 700 years first for a homogeneous case and then for 3 cases with increasing heterogeneity. All the systems have the same Rayleigh number  $Ra = 490$ . A solute boundary condition is defined at the top of the model with a  $5 \text{ kg m}^{-3}$  density difference between the boundary and the background, ambient, groundwater. Instabilities were triggered by adding noise to the source concentration along the top model boundary (concentrations in each cell were randomly perturbed by up to  $\pm 0.01$  percent). The salt finger pattern differs for the four homogeneous simulations due to the random noise added to the source, but the penetration depth and finger number are comparable.

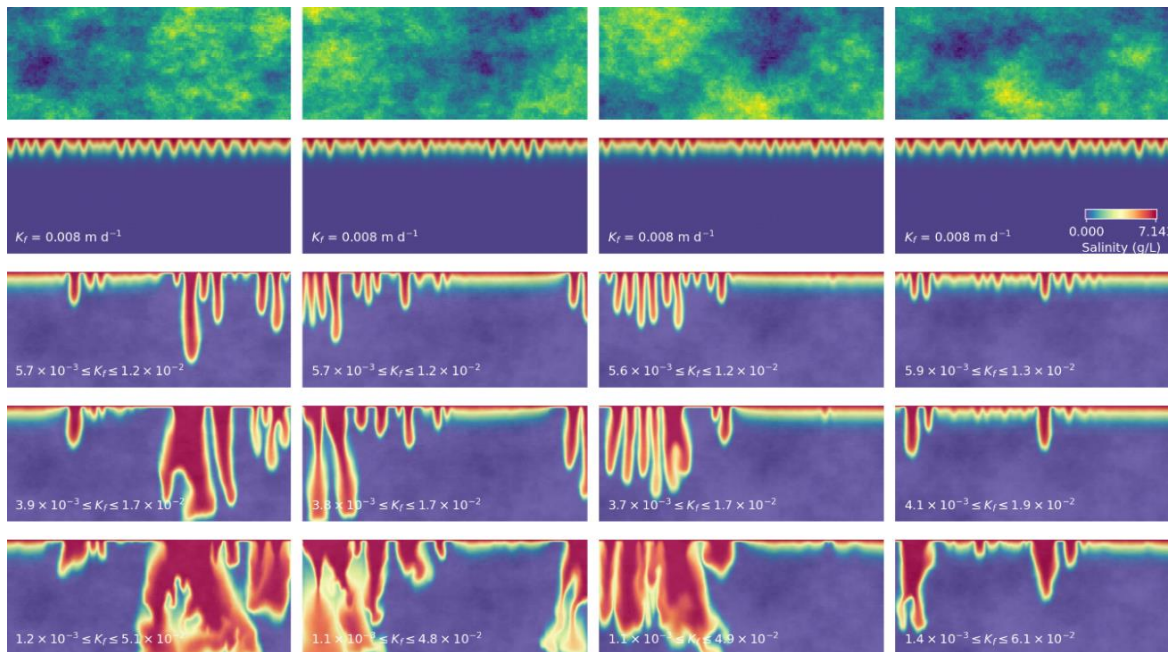


**Figure 27** – Top row: Four realizations of a random permeability field. Second row: finger patterns for the homogeneous case. Third to fifth row: finger patterns for standard deviation of the log  $k$  field of  $\sigma=0.1$ ,  $0.2$  and  $0.5$ . For the heterogeneous simulations, the permeability field is overlaid in transparent black and white so that less permeable parts can be discerned by slightly darker zones, and more permeable parts by lighter zones. An animated version of this image is provided [here](#) .

As the variance of the permeability field is increased, the role of heterogeneity becomes clear. The lower three rows in Figure 27 show the simulation result for a standard deviation of the log  $k$  field of  $\sigma = 0.1$ ,  $0.2$  and  $0.5$ , respectively. Differences are distinct for even variability as low as  $\sigma = 0.1$ , where salt fingers preferentially occur in more permeable zones and fingering is suppressed where low-permeability zones are located near the source. As the standard deviation increases to  $\sigma = 0.5$ , the geological heterogeneity essentially dictates the fingering pattern. Instead of many small fingers, much larger structures have formed inside the more permeable parts of the aquifer. They have also traveled much deeper than the fingers in the more homogeneous simulations because the maximum permeability is higher in the zone occupied by the salt fingers than the mean permeability, allowing the salt water to sink faster. These simulation results are consistent with the findings of Prasad and Simmons (2003), who studied a stochastic version of the Elder problem and found that increased heterogeneity tends to reduce the number of fingers that form.

Not shown in Figure 27, but visible in the animation ([video](#) ) is that the onset of free convection occurs after approximately four years for  $\sigma = 0.5$  while for the homogeneous case, salt fingers do not become perceptible until 350 years. So, on the one hand, heterogeneity promotes fingering by providing the perturbations needed for instabilities to form. On the other hand, it reduces the number of fingers by channeling the salt water into

more permeable zones of the aquifer. Also, where zones of low permeability are located near the solute source, the onset of free convection is delayed or prevented altogether.

It is evident that geologic heterogeneity exerts an important control on unstable plumes. Converting the  $k$  values to  $K_f$  in  $\text{cm s}^{-1}$  and calculating the variance of the natural logarithm  $\sigma_{\ln K_f}^2$  allows comparing the degree of heterogeneity of the simulations of Figure 27 to values reported in the literature for well-investigated sedimentary aquifers. The fields considered here have  $\sigma_{\ln K_f}^2 = 0.05, 0.21$  and  $1.32$ , respectively. The relatively homogeneous sediments that make up the well-characterized Borden aquifer have  $\sigma_{\ln K_f}^2$  between  $0.24$  and  $0.37$  (Sudicky, 1986; Woodbury and Sudicky, 1991) while the sand and gravel aquifer at the Cape Cod test site has  $\sigma_{\ln K_f}^2 = 0.26$  (LeBlanc et al., 1991). This is on the same order as the values for the realizations in the third row of Figure 27, in which the heterogeneity has an important influence on finger development. It follows that even in relatively homogeneous aquifers, free convection is likely to be influenced by the local-scale variability of the permeability field. The more heterogeneous sediments of the MADE site (Rehfeldt et al., 1992) have  $\sigma_{\ln K_f}^2 = 4.5$ , which is much higher than the highest value considered when creating Figure 27. Under those conditions, sedimentary heterogeneity may be expected to dominate the free convection processes entirely.

A number of studies have examined free convection in fractured media (e.g., Graf and Therrien, 2007a, 2005; Murphy, 1979; Sharp and Shi, 2009; Shikaze et al., 1998; Simmons et al., 2008). Graf and Therrien (2007b) observed that concentration distributions were very sensitive to the number of equidistantly distributed fractures near the source, and that fracture connection pathways and fracture permeabilities controlled the depth to which the dense plume ultimately migrated. Simmons and others (2008) studied the possible modes of free convection in fractured media. Inter-fracture convection (Mode 1), intra-fracture convection perpendicular to the face of the fracture (Mode 2A) and intra-fracture convection parallel to the face of the fracture (Mode 2B) were considered. These are illustrated in Figure 28.

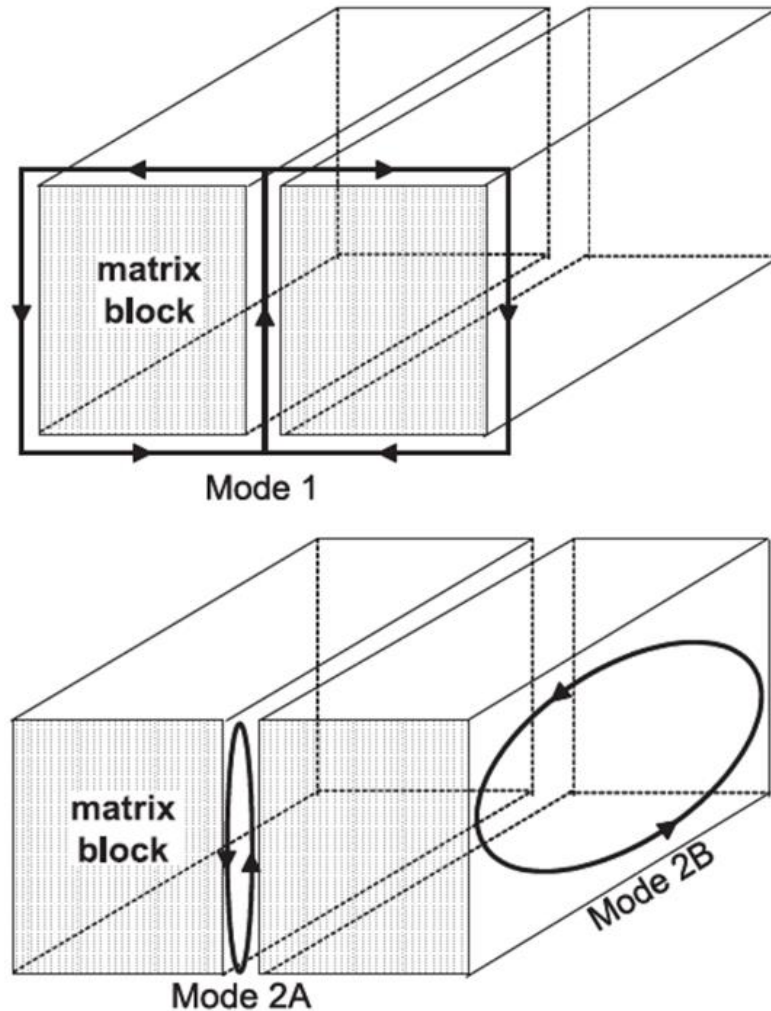


**Figure 28** - Modes of free convection in fractured media (Simmons et al., 2008). Reprinted from *Water Resources Research*, 44(3), C.T. Simmons et al., Modes of free convection in fractured low-permeability media, Copyright (2008), with permission from John Wiley and Sons.

By developing and applying Rayleigh numbers for each possible mode of convection, the likelihood of each mode was determined. All modes of convection are theoretically possible in fractured rock aquifers at extremely small density contrasts. Mode 2B is the most likely mode followed by Mode 1 and then Mode 2A. Three-dimensional simulation is required to permit all convection modes to occur but is computationally expensive. The findings have consequences for the simulation of convection in fracture networks. For example, fractures represented by one-dimensional fracture elements cannot simulate Mode 2A convection.

Finally, providing a short note on spatial dimensionality is useful. Many studies have been undertaken in two-dimensions but natural systems are three-dimensional where geometry becomes critical. Simply put, in general, all things equivalent, it is easier to get convection in a three-dimensional than a two-dimensional domain. Thus,

three-dimensional systems have lower critical  $Ra_c$  than their two-dimensional counterparts. This does not always hold true. For example, for large height/width ratios (vertical slots) the propensity for convection is severely reduced. Further discussion of the effects of spatial dimensionality on free convection is provided by Nield and Bejan (2006), Voss and others (2010), and Knorr and others (2016).

## 7 Selected Research Topics

### 7.1 Field Scale Detection of Free Convection

Free convection has been observed in laboratories and predicted by models for over a century. There are hundreds of papers on the theory, modeling and laboratory experiments of finger instabilities associated with free convection. Thus, finger instabilities are surmised to exist in field-based settings, but there is a lack of conclusive field-based evidence and data. A range of *secondary inferences* for the existence of free convection has been made in various studies. These include, but are not limited to:

- *“Numerical experiments demonstrate the existence of a convection cell...”* (Duffy and Al-Hassan, 1988);
- *“The observation that tritium exists throughout the profile is consistent with vertical circulation resulting from the density instability”* (Wood et al., 2002);
- *“The salt deficit may be accounted for by the slow downward convection of dense saline water beneath salt lake beds...”* (Teller et al., 1982);
- *“Abundant data indicate high fluid and solute fluxes in shaly sediments and account for the observed level of sediment diagenesis”* (Sharp et al., 1988);
- *“Assuming a critical Rayleigh number of  $4\pi^2$  ... both regions are predicted a priori to be unstable, and solute moves more rapidly by way of convective fingering”* (Simmons et al., 2002); and,
- *“Contamination from a waste dump at Noordwijk, Netherlands, resulted in a plume with downward velocity 45 times higher than the vertical velocity due to natural recharge”* (Koooper, 1983).

None of these observations constitute primary evidence for the existence, or otherwise, of free convection. Numerical experiments do not demonstrate the existence of free convection in a field-based setting. Given the limitations in using the Rayleigh number in field settings as discussed in Section 5.2, compliance with Rayleigh stability criteria is also not a sufficient test. Rayleigh number calculations are supportive and suggestive of the existence of instabilities leading to convective cells in field settings, but they are not conclusive.

Some studies provide more direct indications for free convective phenomena in groundwater, for example, based on groundwater salinity measurements taken after the flooding of freshwater aquifers by seawater. During the preparation for a deliberate seawater intrusion experiment in Denmark, the field site of Andersen and others (2008) was flooded by brackish water from a fjord during a storm surge on 29 and 30 January 2000. The site was equipped with a network of approximately 100 observation wells that were installed along a 120 m transect across a beach. The brackish water flooded the beach up to 90 m from the coast and pooled for some days in the depressions. Before the storm surge, the electrical conductivity measurements indicated the presence of a saltwater wedge near the shoreline (Figure 29a). Twenty-eight days after the storm, high groundwater salinities were measured between 70 to 90 m from the coastline (Figure 29b). The shape of the high-salinity zone resembles that of a finger.

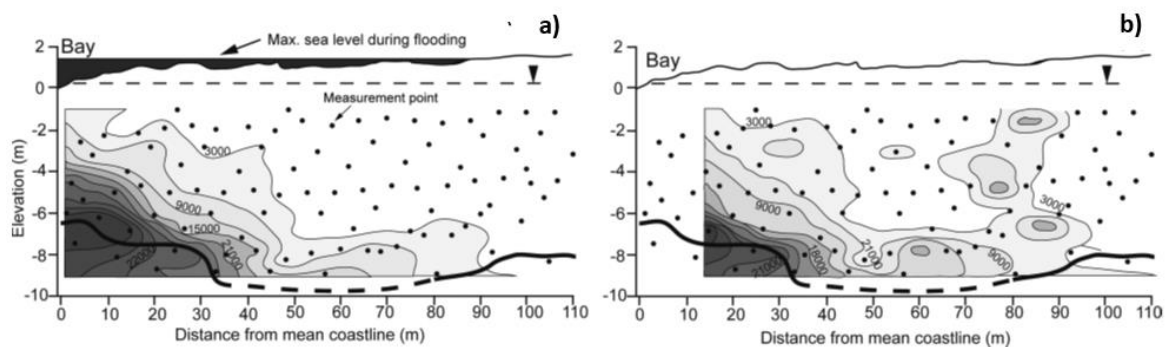


**Figure 29** - Vertical cross sections of the specific conductance (in  $\mu\text{S cm}^{-1}$ ) of groundwater along a transect of a beach aquifer in Denmark on a) 28 August 1999 and b) 27 February 2000 (Andersen et al., 2008). The black dots indicate piezometer screens from which groundwater could be sampled. The thick black line at the bottom of the images indicates the base of the aquifer. Modified from Andersen MS, Jakobsen R, Nyvang V, Christensen FD, Engesgaard P & Postma D (2008), Density-driven seawater plumes in a shallow aquifer caused by a flooding event – field observations, consequences for geochemical reactions and potentials for remediation schemes. [IAHS Website](#) Copyright © 2008 IAHS Press, reprinted with permission from IAHS Limited.

To support the interpretation of their data, Andersen and others (2008) conducted a numerical modeling study. They found that they had to consider the heterogeneity of the hydraulic conductivity field to obtain salt lobes with similar dimensions as in Figure 29b. While the homogeneous model predicted downward density-driven flow, its results did not match the field data. Andersen and others (2008) had hydraulic conductivity data from the slug tests at each of their piezometers so they could incorporate a heterogeneous hydraulic conductivity field in their model. While the heterogeneous model reproduced the observed salinity distribution in an overall sense, even with this information the modeled salinity profiles did not capture the small-scale variability of the observed salinity distribution. This finding is consistent with the discussion from the previous section, that is, while macroscopic features are amenable to prediction, microscopic features are not.

Somewhat similarly, Post and Houben (2017) investigated the salinization of a fresh groundwater lens on the northern German island of Baltrum following a storm flood that occurred in February 1962. They based their analysis on unpublished data that were collected by Otto Rülke, who had been doing geoelectrical measurements on the island before the flood (Rülke, 1969) and went over as soon as he could to install shallow observation wells. Chloride concentrations were measured in these wells at irregular intervals up to 8 years after the flood. The time series have an erratic shape with concentrations going up and down in the months after the flood. Based on numerical modeling, Post and Houben (2017) concluded that this must have been due to convective fingering. As the seawater inundated the lens, salt fingers moved down and as they grew vertically, they also migrated laterally (Figure 30). At a single point, this results in salt concentrations increasing or decreasing depending on the transient flow dynamics and finger geometry. Because of the difficulty in comparing model results to measured concentration versus time curves, they made comparisons between model-predicted concentration ranges for the depths of measurements. By comparison with density-invariant models, they could demonstrate that the free-convective model of salinization formed a much better explanation of the data than the density-invariant model.

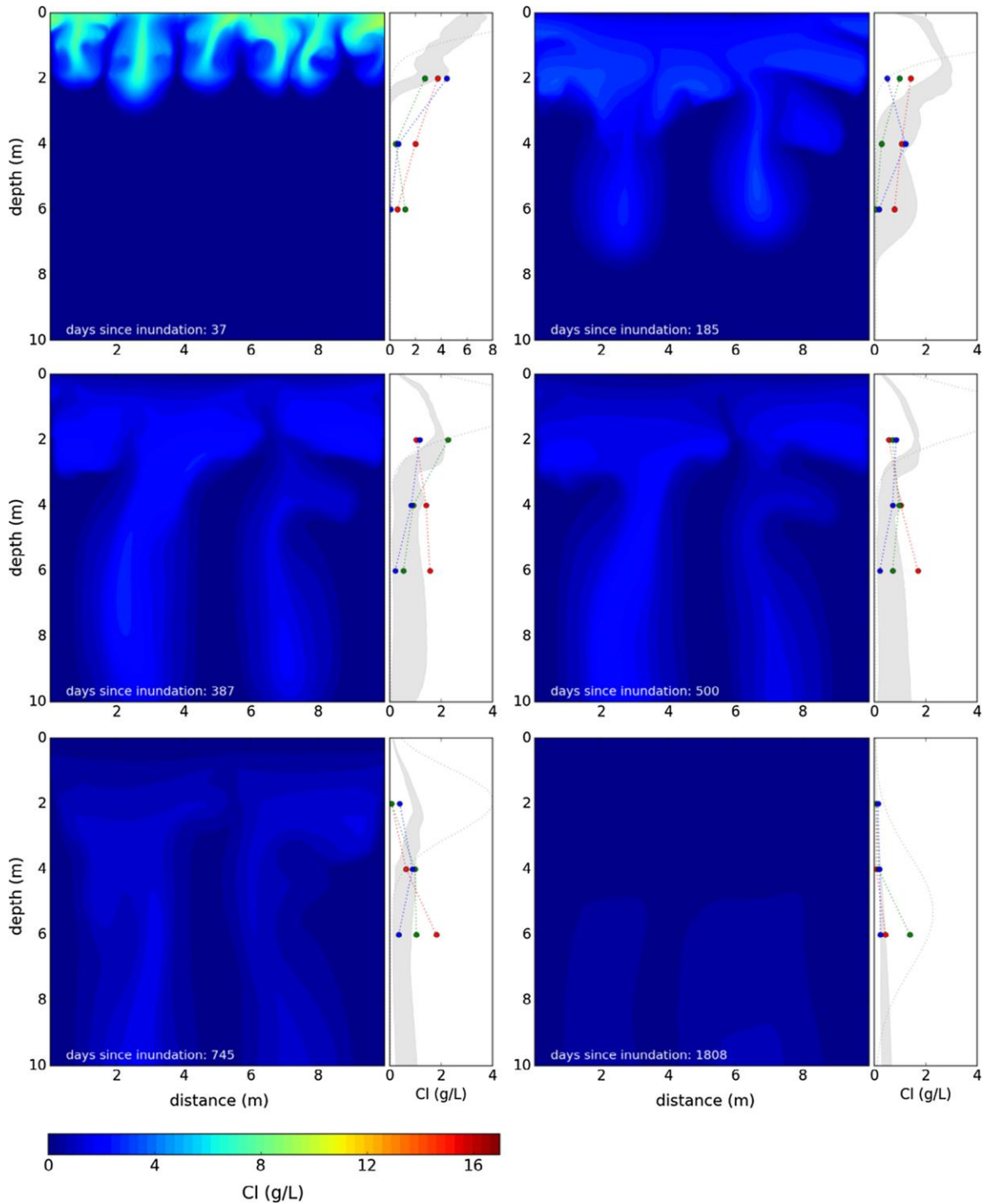


**Figure 30** - Contour plots of chloride concentrations and concentration versus depth curves for different times after the 1962 Baltrum storm flood. Measured data are shown for three multi-level observation wells together with shaded areas which represent the 25 to 75 percentile concentration range along each model layer. The thin dashed line in the chloride versus depth profiles (which sometimes goes off-scale) shows the results for the density-invariant model. Reprinted from Journal of Hydrology, 551, V.E.A. Post & G.J. Houben, Density-driven vertical transport of salt water through the freshwater lens on the island of Baltrum (Germany) following the 1962 storm flood, 689 – 702, Copyright (2017), with permission from Elsevier.

While the studies by Andersen and others (2008) and Post and Houben (2017) provide strong indications for convective fingering, their data still do not provide direct

evidence of the presence of salt fingers. Geophysical tomography techniques can provide snapshot images of the electrical resistivity of the subsurface and provide a way to visualize fingers in the field. These techniques have had success. Examples include the studies in the Okavango Delta in Botswana (Bauer Gottwein et al., 2007) and Padre Island, Texas (Stevens et al., 2009).

Around the same time, van Dam and others (2009) documented the existence of free convective fingering in the Sabkha Aquifer in the United Arab Emirates (Figure 31). This site was chosen because it is extensively characterized, homogeneous, density inversions exist and an unusual tritium distribution (Wood et al., 2002) was previously documented (van Dam et al., 2009). Large precipitation events helped to dissolve the halite crust at the surface and formed hypersaline brines seven weeks before data collection.



**Figure 31** - On the quest to find fingers in the sabkhat of Abu Dhabi in 2008. A range of hydrogeophysical methods were employed. (Photos courtesy Remke van Dam, David Hyndman and Warren W. Wood).

The electrical tomography results (Figure 32) show low resistivity ‘saline fingers’ (red) that protrude in higher resistivity background (green). The vadose zone and water table (~0.7 m below ground) show up as the layer with the highest resistivity (blue). Importantly, the near-perfectly homogeneous sedimentary sandy system means that geologic variation cannot be used to explain these lobe-shaped structures. Further work by van Dam and others (2014) has shown excellent agreement between field-based geophysical results and modeling. These results provide compelling field-based evidence for the existence of free convection in a groundwater field setting. Fascinatingly, the saline fingers have moved downwards about 15 meters in about seven weeks, a speed of approximately  $0.3 \text{ m d}^{-1}$  on average. Both diffusive migration and downward flow due to

recharge are much slower processes than free convection and cannot explain this significant solute transport rate nor its finger shape.

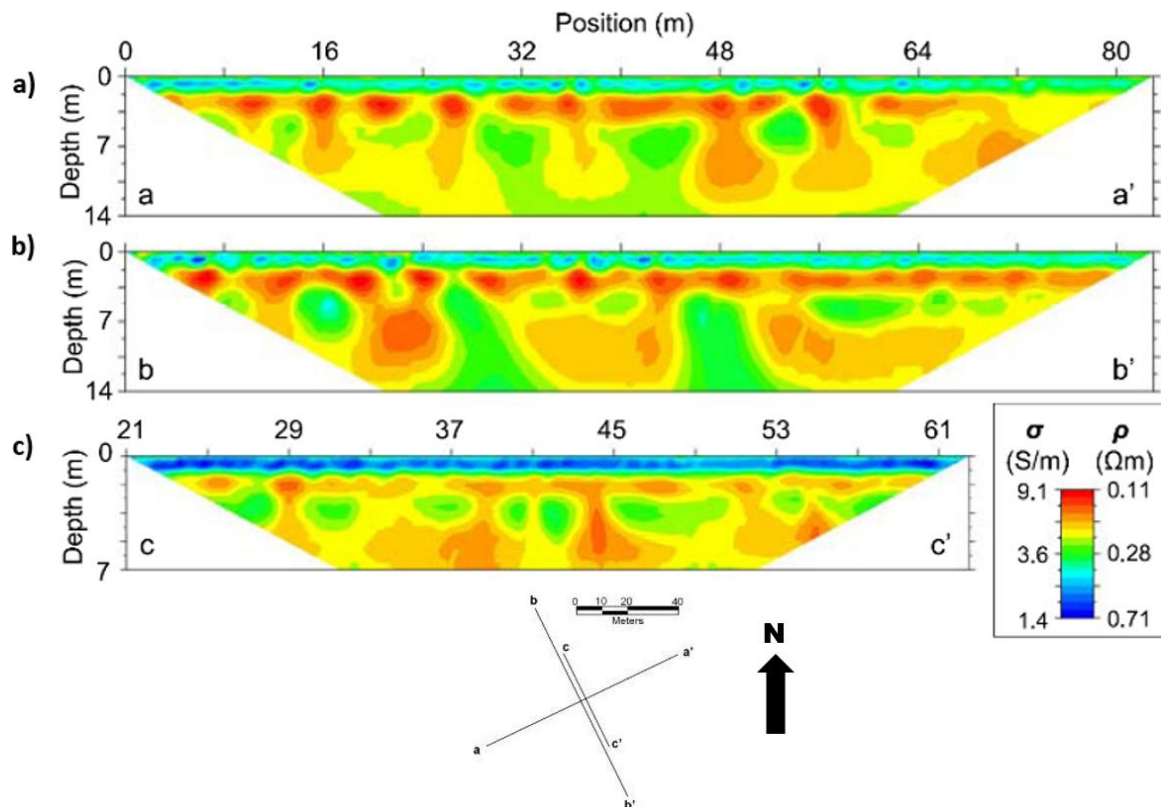


**Figure 32** - Electrical tomography results in the sabkha aquifer, Abu Dhabi, United Arab Emirates (van Dam et al., 2009). High salinity fingers (red) protrude into the lower salinity (green) background waters in lobe shapes typical of convective instabilities. The near perfectly homogeneous sandy aquifer means that these protrusions cannot be explained using geologic variability. The vadose zone and water table are identified by the high resistivity region in the top 0.7 m (blue). The cross sections a-a', b-b' and c-c' are also shown. Reprinted from *Geophysical Research Letters*, 36(11), R. van Dam and others, Natural free convection in porous media: First field documentation in groundwater, Copyright (2009), with permission from John Wiley and Sons.

## 7.2 Chemical Reactions in Variable-density Flow Systems

Geochemical reactions and groundwater flow and transport processes are closely linked. On the one hand, flow and transport redistribute solutes across the subsurface, thereby affecting the delivery of reactants for, and removal of reaction products of chemical reactions. On the other hand, chemical reactions may alter the fluid composition in such a profound way, that its density changes (e.g., as shown by the deviation of some data points from the theoretical relationship in Figure 4 of Section 2), and thereby, the flow field changes. Mixing by dispersion and diffusion is a key driver for geochemical reactions. The greater contact area between fluids of different density during convective fingering enhances mixing and thus promotes reactions.

Some of the early classical hydrochemical studies in a variable-density groundwater setting focused on the dissolution of calcite in freshwater-saltwater mixing zones in coastal

areas (Sanford and Konikow, 1989; Wigley and Plummer, 1976). Ore formation controlled by thermal convection has been studied in basin-scale geology (Person et al., 1996; Raffensperger and Garven, 1995). The mobilization of arsenic in groundwater storage and recovery in brackish aquifers has received attention (Wallis et al., 2011). Precipitation of minerals, such as carbonates, has been extensively studied in geothermal problems due to its relevance for aquifer thermal energy storage (Brons et al., 1991).

The equation of state as given by Equation 35 is valid for a single species. For a multispecies solution, density is no longer a function of the concentration of a single solute but now depends on the concentrations of all solutes present. In that case, the density can be calculated using a relationship of the type presented in Equation 38.

$$\rho = \rho_0 + \sum_{i=1}^{NS} \left( \frac{\partial \rho}{\partial C} \right)_i (C_i - C_{i,0}) \quad (38)$$

where:

$\rho_0$  = fluid density when  $C_i = C_{i,0}$  ( $\text{kg m}^{-3}$ )

$NS$  = total number of solutes that contribute to the density

$\left( \frac{\partial \rho}{\partial C} \right)_i$  = slope of the density-concentration relationship for species  $i$

$C_i$  = species concentration ( $\text{kg m}^{-3}$ )

$C_{i,0}$  = reference concentration of species  $i$  ( $\text{kg m}^{-3}$ )

Models based on this type of relationship have been used previously in studies by Zhang and Schwartz (1995) and Mao and others (2006). It is also possible to compute fluid density using a thermodynamic framework (Monnin, 1994, 1989), which was implemented in the studies by Freedman and Ibaraki (2002), Hamann and others (2015), and Post and Prommer (2007).

To assess and quantify the potential effects of reactive transport in a variable-density flow problem, Post and Prommer (2007) converted the Elder problem into a reactive multispecies transport problem to examine the importance of density changes induced by cation exchange and calcite equilibrium reactions on free convection processes. They found that chemical reactions were important only at low density contrasts. This is because the change in density induced by chemical reactions was only significant for low density contrasts, and negligible for high density contrasts.

Bauer-Gottwein and others (2007) investigated how variable-density flow, evapotranspiration and geochemical reactions work together to control the hydrology, and solute transport processes underneath salt pans on the islands in the Okavango Delta. In these systems evapoconcentration triggers (i) mineral precipitation and (ii) convective, density-driven downward transport of the salt into deeper aquifer systems. Their modeling

results showed that the time to onset of density driven flow can increase with mineral precipitation and carbon dioxide degassing. Hamann and others (2015) studied a playa system to gain insights into the feedback between density-driven flow and the spatiotemporal patterns of precipitating evaporites and brine evolution. By comparing their results to nonreactive models, they found that the nonreactive simulations could overestimate the solute mass in the aquifer below the playa by up to 20 percent compared to the reactive multicomponent transport simulations. Both studies highlight the important role those chemical reactions may have on the flow field in systems where solute concentrations are so high that salts will precipitate from the solution.

Free convection may also be expected to exert a strong control on tracer concentrations that are used to infer groundwater ages. As an example, Figure 33 shows the results of a simulation of a semi-confined aquifer that was originally fresh and suddenly became inundated by seawater. An age stratification was present before the inundation, with groundwater age increasing with depth, as reflected by decreasing  $^{14}\text{C}$  concentration of the groundwater. Some of the original stratification can still be recognized after 1500 years but it is also apparent that free convection has completely overhauled the pre-existing tracer concentration patterns that were present in the aquifer. Young, high-salinity water has sunk to the bottom of the aquifer, and old, fresher water ascends between the descending salt plumes. In this process, mixing of water of various ages is taking place. Consequently, where convective flows are important, the interpretation of tracer concentration patterns will be infinitely more complex than in settings with forced convection. Moreover, the mixing of the fluids is likely to trigger hydrochemical reactions that could have their bearing on the tracers of interest as well. For  $^{14}\text{C}$  it is well known that the interaction between the groundwater and carbon sources in the aquifer will bias the inferred age. Therefore, failing to recognize the role of convective flow may lead to serious misinterpretation of age tracer data.

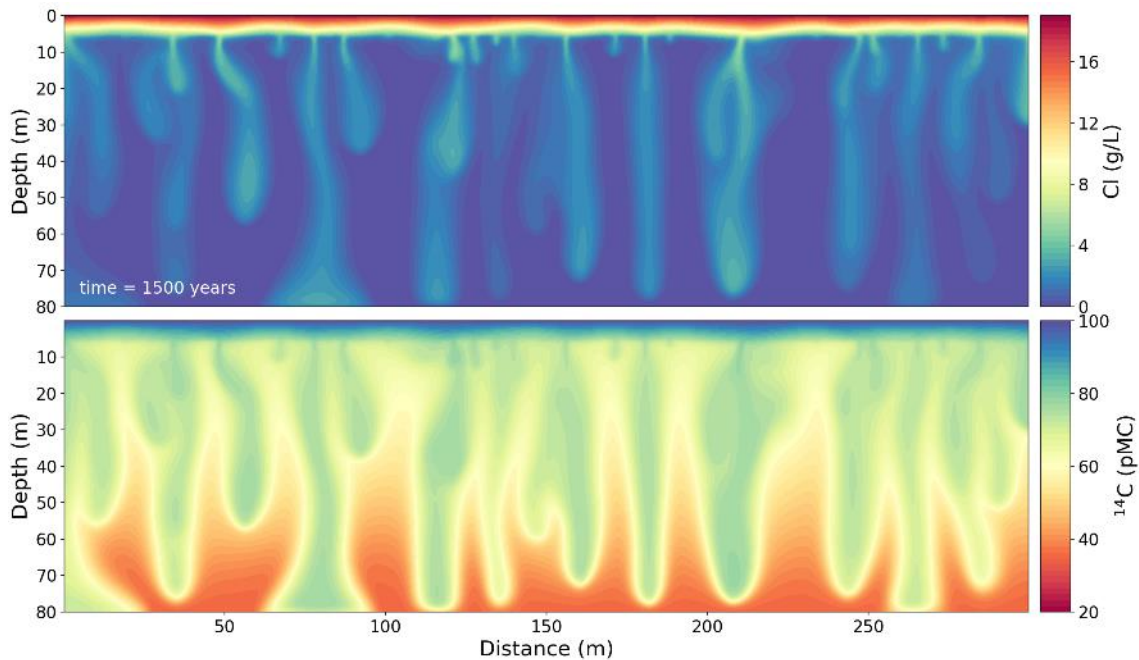


**Figure 33** - Numerical model results of a freshwater aquifer after 1500 years since it became inundated by seawater. Top: Chloride distribution. Bottom:  $^{14}\text{C}$  concentration.

Free convection is also important in the storage of  $\text{CO}_2$  in underground reservoirs. The injected  $\text{CO}_2$  tends to be lighter than the resident groundwater and floats to the top of the target rock layer and accumulates below the confining unit that acts as a seal of the reservoir. The  $\text{CO}_2$  dissolves in the brine, creating a fluid that is one to two percent denser as a result, and therefore tends to sink (Hidalgo and Carrera, 2009). Because the  $\text{CO}_2$  lowers the pH of the groundwater, carbonate minerals like calcite and dolomite can dissolve, which has the potential to enhance porosity and permeability (Islam et al., 2016; Sainz-Garcia et al., 2017).

Finally, free convection also has relevance for the emission of greenhouse gases from peat layers. Rappoldt and others (2003) found that nocturnal cooling of a water-saturated peat moss layer resulted in downward flow of the relatively cold surface water, and upward flow of the warmer water from below. This results in a periodic flow and mixing regime that has consequences for  $\text{CO}_2$  and methane transport in the upper layers of water-saturated peat.

### 7.3 Future Research Directions

Understanding, conceptualizing, measuring, predicting, and modeling variable-density processes in groundwater remains a challenge and an opportunity. This book shows that there are important differences in the implicit and explicit assumptions and approaches made between the earliest free convection studies in classical fluid mechanics and those in hydrogeology. Geologic heterogeneity especially presents a

challenge, as it controls the onset, growth and/or decay of plumes. This means that there are problems with application of Rayleigh numbers to evaluate the potential for unstable flow conditions because the Rayleigh number is based on mean quantities, and it is difficult to quantify relevant average properties in heterogeneous media. Furthermore, the Rayleigh number is based on a steady-state analysis to determine the onset of convection. It is difficult to identify relevant length scales and the appropriate critical Rayleigh numbers are unknown in most practical settings. It is unlikely that critical Rayleigh numbers based on highly idealized conditions such as the famous value of  $4\pi^2$  are likely to be appropriate.

Rayleigh numbers computed in many groundwater settings with a potentially unstable density stratification are well above the range of critical Rayleigh numbers identified by Nield (1968). This suggests that highly transient oscillatory regimes, which are the most difficult to characterize, are commonplace in nature. Heterogeneity can suppress convection in potentially unstable systems but its role in field settings is still unclear. All these results suggest that, despite the scientific progress that has been made to date, there are challenges to conceptual understanding and prediction of convective flow and transport processes. Some other topics that are likely to be important in the future include:

- better understanding quantification and controls of dispersion;
- better links with geological constraints (e.g., sedimentary facies data/structural geology);
- thermohaline (double-diffusive) and multi-species transport problems; and,
- complex geochemical reactions, fluid-matrix interactions and multiphase flow in carbon sequestration processes.

As a final word, we note that there are hundreds of modeling and theory papers and far fewer field-based papers that attempt to measure free convection directly. The “measurement to theory” ratio needs to be increased. Rigorous field-based studies and detailed measurements, coupled with state-of-the-art modeling approaches, will help to further enhance both conceptual understanding and predictive capabilities. More studies should focus on direct, explicit evidence, such as field observations of fingering patterns, or upwelling and downwelling circulation associated with free convection cells. Secondary inference for the existence of convection is a good indirect starting point but there is a continuing need to develop field techniques to gather better data that can constrain and validate numerical models. Important discoveries still need to be made, so the prognosis for better understanding variable-density flow is good.

## 8 Exercises

### Exercise 1

Derive the Ghijben-Herzberg relationship  $y = 40 h$  (see Figure 1) Hint: Use Equation 1 to calculate the pressure at depth in both the freshwater and saltwater leg of the U-tube.

[Click for solution to Exercise 1](#) ↴

### Exercise 2

Calculate the Ghijben-Herzberg relationship for the Baltic Sea ( $\rho = 1005 \text{ kg m}^{-3}$ ) and for the Dead Sea ( $\rho = 1240 \text{ kg m}^{-3}$ ).

[Click for solution to Exercise 2](#) ↴

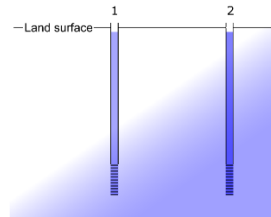
### Exercise 3

Verify that Equation 18 gives  $q_z = 0$  in an aquifer filled with stagnant seawater ( $\rho = \rho_s = 1025 \text{ kg m}^{-3}$ ).

[Click for solution to Exercise 3](#) ↴

## Exercise 4

Two piezometers located near an inland saline lake are screened 60 mbls and are 200 m apart as shown in the image below. The land surface is at 100 masl and the aquifer has a hydraulic conductivity of  $10 \text{ m d}^{-1}$ .



Measured hydraulic heads and densities are shown in the following table.

Piezometer	Hydraulic head (masl)	Density ( $\text{kg/m}^3$ )
1	100.4	1010
2	100	1020

Questions:

1. What is the direction of groundwater flow?
2. What is the specific discharge?

[Click for solution to Exercise 4](#) ↴

## Exercise 5

The following data are available for a multi-level observation well in which the screens and hydraulic heads are below sea level (data courtesy of Frank Smits, Waternet, The Netherlands). Calculate the vertical, specific discharge  $q_z$  in  $\text{mm d}^{-1}$ . The aquifer has a hydraulic conductivity of  $20 \text{ m d}^{-1}$ .

Screen	$z_i$ (m)	$h_i$ (m)	$\rho_i$ ( $\text{kg/m}^3$ )
1	-76.41	-3.13	1004.3
2	-96.44	-3.08	1004.3
3	-118.93	-3.04	1004.3

[Click for solution to Exercise 5](#) ↴

## Exercise 6

Calculate the Rayleigh number for a ten-meter-thick freshwater aquifer that has  $K_f = 10 \text{ m d}^{-1}$ , which is overlain by seawater (e.g., following an overtopping event due to a storm surge). *Hint:* Look up the definition of the freshwater hydraulic conductivity in the Section titled *Horizontal Flow*. Assume that  $\frac{\mu_f}{\mu} = 1$ .

[Click for solution to Exercise 6](#) ↴

## Exercise 7

Calculate the Rayleigh number for the unstable case shown in Figure 9b. Assume that  $\mu = 1 \times 10^{-3} \text{ kg m}^{-1} \text{ s}^{-1}$ ,  $k = 1 \times 10^{-10} \text{ m}^2$ ,  $D_T = 1 \times 10^{-6} \text{ m}^2 \text{ s}^{-1}$  and  $\Delta\rho = 3 \text{ kg m}^{-3}$ . This value of  $\Delta\rho$  is the approximate density difference at the moment when the boundary layer becomes unstable after about 2400 years. Compare your evaluation with the [animated version](#)  of this problem.

[Click for solution to Exercise 7](#) ↴

## Exercise 8

Calculate the Rayleigh number for the experiment in Figure 8b. The density was  $\rho = 1235 \text{ kg m}^{-3}$  and the sand had an intrinsic permeability of  $k = 1.25 \times 10^{-10} \text{ m}^2$ .

[Click for solution to exercise 8](#) ↴

## 9 References

- Adams, J.J. and S. Bachu, 2002, Equations of state for basin geofluids: Algorithm review and intercomparison for brines. *Geofluids*, volume 2, issue 4, pages 257-271, [doi: 10.1046/j.1468-8123.2002.00041.x](https://doi.org/10.1046/j.1468-8123.2002.00041.x).
- Andersen, M.S., R. Jakobsen, and V. Nyvang, F.D. Christensen, P. Engesgaard, and D. Postma, 2008, Density-driven seawater plumes in a shallow aquifer caused by a flooding event—Field observations, consequences for geochemical reactions and potentials for remediation schemes. International Association of Hydrological Sciences (IAHS) publication, pages 483-490.
- Bachmat, Y. and D.E. Elrick, 1970, Hydrodynamic instability of miscible fluids in a vertical porous column. *Water Resources Research*, volume 6, issue 1, pages 156–171, [doi: 10.1029/WR006i001p00156](https://doi.org/10.1029/WR006i001p00156).
- Bachu, S., 1995, Flow of variable-density formation water in deep sloping aquifers: review of methods of representation with case studies. *Journal of Hydrology*, volume 164, issues 1-4, pages 19–38, [doi: 10.1016/0022-1694\(94\)02578-Y](https://doi.org/10.1016/0022-1694(94)02578-Y).
- Bachu, S. and K. Michael, 2002, Flow of variable-density formation water in deep sloping aquifers: minimizing the error in representation and analysis when using hydraulic-head distributions. *Journal of Hydrology*, volume 259, issues 1-4, pages 49-65, [doi: 10.1016/S0022-1694\(01\)00585-6](https://doi.org/10.1016/S0022-1694(01)00585-6).
- Bakker, M., G.H.P.O. Essink, and C.D. Langevin, 2004, The rotating movement of three immiscible fluids—A benchmark problem. *Journal of Hydrology*, volume 287, issues 1-4, pages 270–278, [doi: 10.1016/j.jhydrol.2003.10.007](https://doi.org/10.1016/j.jhydrol.2003.10.007).
- Bauer, P., R. Supper, S. Zimmermann, and W. Kinzelbach, 2006, Geoelectrical imaging of groundwater salinization in the Okavango Delta, Botswana. *Journal of Applied Geophysics*, volume 60, issue 2, pages 126–141, [doi: 10.1016/j.jappgeo.2006.01.003](https://doi.org/10.1016/j.jappgeo.2006.01.003).
- Bauer-Gottwein, P., T. Langer, H. Prommer, P. Wolski, and W. Kinzelbach, 2007, Okavango Delta Islands: Interaction between density-driven flow and geochemical reactions under evapo-concentration. *Journal of Hydrology*, volume 335, issues 3-4, pages 389-405, [doi: 10.1016/j.jhydrol.2006.12.010](https://doi.org/10.1016/j.jhydrol.2006.12.010).
- Bear, J., 1972, *Dynamics of fluids in porous media*. Dover Publications, Incorporated, New York, USA, 800 pages.
- Bear, J., A.H.D. Cheng, D. Ouazar, S. Sorek, and I. Herrera, 1999, *Seawater intrusion in coastal aquifers - concepts, methods and practices in Theory and applications of transport in porous media*, editor, S.M. Hassanizadeh, Springer, Dordrecht, Netherlands.

- Bénard, H., 1900, Étude expérimentale des courants de convection dans une nappe liquide. - Régime permanent: tourbillons cellulaires. *Journal de Physique Théorique et Appliquée*, volume 9, issue 1, pages 513-524.
- Boblaye, M., 1833, Des depots Terrestres ou Epigeiques a la surface de la Moree (On the terrestrial and epigeic deposits on the surface of Morea). *Annales des Mines, Troisieme Serie, Tome IV*, pages 99–126.
- Brons, H.J., J. Griffioen, C.A.J. Appelo, and A.J.B. Zehnder, 1991, (Bio)geochemical reactions in aquifer material from a thermal energy storage site. *Water Research*, volume 25, issue 6, pages 729–736, [doi: 10.1016/0043-1354\(91\)90048-U](https://doi.org/10.1016/0043-1354(91)90048-U) ↗.
- Brutsaert, W., 2005, *Hydrology, an introduction*. Cambridge University Press, 618 pages, [doi: 10.1017/CBO9780511808470](https://doi.org/10.1017/CBO9780511808470) ↗.
- Cheng, A.H.D. and D. Ouazar, 2004, *Coastal aquifer management-monitoring, modeling, and case studies*, CRC Press, 296 pages, [doi: 10.1201/9780203493496](https://doi.org/10.1201/9780203493496) ↗.
- Cheng, P., 1979, Heat transfer in geothermal systems. *Advances in Heat Transfer*, volume 14, pages 1–105, [doi: 10.1016/S0065-2717\(08\)70085-6](https://doi.org/10.1016/S0065-2717(08)70085-6) ↗.
- Christensen, T.H., P. Kjeldsen, P.L. Bjerg, D.L. Jensen, J.B. Christensen, A. Baun, H.J. Albrechtsen, and G. Heron, 2001, Biogeochemistry of landfill leachate plumes. *Applied Geochemistry*, volume 16, issues 7-8, pages 659–718, [https://doi.org/10.1016/S0883-2927\(00\)00082-2](https://doi.org/10.1016/S0883-2927(00)00082-2) ↗.
- Combarous, M.A. and S.A. Bories, 1975, Hydrothermal convection in saturated porous media. *Advances in Hydrosience*, volume 10, pages 231-307, [doi: 10.1016/B978-0-12-021810-3.50008-4](https://doi.org/10.1016/B978-0-12-021810-3.50008-4) ↗.
- Du Commun, J., 1828, On the cause of fresh water springs, fountains, etc. *American Journal of Science*, 14, pages 174-176.
- van Dam, R.L., B.P. Eustice, D.W. Hyndman, W.W. Wood, and C.T. Simmons, 2014, Electrical imaging and fluid modeling of convective fingering in a shallow water-Table aquifer. *Water Resources Research*, volume 50, issue 2, pages 954-968, [doi: 10.1002/2013WR013673](https://doi.org/10.1002/2013WR013673) ↗.
- van Dam, R.L., C.T. Simmons, D.W. Hyndman, and W.W. Wood, 2009, Natural free convection in porous media: first field documentation in groundwater. *Geophysical Research Letters*, volume 36, issue 11, <https://doi.org/10.1029/2008GL036906> ↗.
- DZRD, 1936, Dienst der Zuiderzeewerken and Rijksbureau voor Drinkwatervoorziening [Zuiderzee Service Works and National Office for Drinking Water Supply], *Geo-hydrologische gesteldheid van de Wieringermeer*. Rijksuitgeverij dienst van de Nederlandsche Staatscourant [Geohydrological condition of the Wieringermeer. Government publishing service of the Dutch Government Gazette] (in Dutch).
- Diersch, H.J., 1981, Primitive variable finite element solutions of free convection flows in porous media. *ZAMM - Journal of Applied Mathematics and Mechanics*, volume 61, issue 7, pages 325–337, [doi: 10.1002/zamm.19810610707](https://doi.org/10.1002/zamm.19810610707) ↗.

- Diersch, H.J.G. and O. Kolditz, 2002, Variable-density flow and transport in porous media: approaches and challenges. *Advances in Water Resources*, volume 25, issues 8-12, pages 899–944, [doi: 10.1016/S0309-1708\(02\)00063-5](https://doi.org/10.1016/S0309-1708(02)00063-5).
- Drabbe, J. and W. Badon Ghijben, 1889, Nota in verband met de voorgenomen putboring nabij Amsterdam [Note concerning the intended well drilling near Amsterdam]. On the Cause of Fresh Water Springs, Fountains, *American Journal of Science*, volume 14, pages 174-176.
- Duffy, C.J. and S. Al-Hassan, 1988, Groundwater circulation in a closed desert basin: topographic scaling and climatic forcing. *Water Resources Research*, volume 24, issue 10, pages 1675–1688, [doi: 10.1029/WR024i010p01675](https://doi.org/10.1029/WR024i010p01675).
- Elder, J.W., 1967a, Steady free convection in a porous medium heated from below. *Journal of Fluid Mechanics*, volume 27, issue 1, pages 29–48, [doi: 10.1017/S0022112067000023](https://doi.org/10.1017/S0022112067000023).
- Elder, J.W., 1967b, Transient convection in a porous medium. *Journal of Fluid Mechanics*, volume 27, issue 3, pages 609–623, [doi: 10.1017/S0022112067000576](https://doi.org/10.1017/S0022112067000576).
- Elder, J.W., C.T. Simmons, H.J. Diersch, P. Frolkovic, E. Holzbecher, and K. Johannsen, 2017, The elder problem. *Fluids*, volume 2, issue 1, 11 pages, [doi: 10.3390/fluids2010011](https://doi.org/10.3390/fluids2010011).
- Fisher, A.T. and C. Geoffrey, 2010, Seamounts as conduits for massive fluid, heat, and solute fluxes on ridge flanks. *Oceanography*, volume 23, issue 1, pages 74–87, [doi: 10.5670/oceanog.2010.63](https://doi.org/10.5670/oceanog.2010.63).
- Freedman, V. and M. Ibaraki, 2002, Effects of chemical reactions on density-dependent fluid flow: On the numerical formulation and the development of instabilities. *Advances in Water Resources*, volume 25, issue 4, pages 439–453, [doi: 10.1016/S0309-1708\(01\)00056-2](https://doi.org/10.1016/S0309-1708(01)00056-2).
- Freeze, R.A. and J.A. Cherry, 1979, *Groundwater*. Prentice-Hall Incorporated, Englewood Cliffs, New Jersey, USA, 604 pages.
- Frolkovič, P. and H. de Schepper, 2000, Numerical modelling of convection dominated transport coupled with density driven flow in porous media. *Advances in Water Resources*, volume 24, issue 1, pages 63–72, [doi: 10.1016/S0309-1708\(00\)00025-7](https://doi.org/10.1016/S0309-1708(00)00025-7).
- Garcia-Fresca, B., F. Jerry Lucia, J.M. Sharp, and C. Kerans, 2012, Outcrop-constrained hydrogeological simulations of brine reflux and early dolomitization of the Permian San Andres Formation. *American Association of Petroleum Geologists (AAPG) Bulletin*, volume 96, issue 9, pages 1757–1781, [doi: 10.1306/02071210123](https://doi.org/10.1306/02071210123).
- Garven, G., J.P. Raffensperger, J.A. Dumoulin, D.A. Bradley, L.E. Young, K.D. Kelley, and D.L. Leach, 2003, Coupled heat and fluid flow modeling of the Carboniferous Kuna Basin, Alaska: Implications for the genesis of the Red Dog Pb-Zn-Ag-Ba ore district. *Journal of Geochemical Exploration*, volumes 78–79, pages 215–219, [doi: 10.1016/S0375-6742\(03\)00109-2](https://doi.org/10.1016/S0375-6742(03)00109-2).

- Graf, T. and R. Therrien, 2007a, Coupled thermohaline groundwater flow and single-species reactive solute transport in fractured porous media. *Advances in Water Resources*, volume 30, issue 4, pages 742–771, [doi: 10.1016/j.advwatres.2006.07.001](https://doi.org/10.1016/j.advwatres.2006.07.001).
- Graf, T. and R. Therrien, 2007b, Variable-density groundwater flow and solute transport in irregular 2D fracture networks. *Advances in Water Resources*, volume 30, issue 3, pages 455–468, [doi: 10.1016/j.advwatres.2006.05.003](https://doi.org/10.1016/j.advwatres.2006.05.003).
- Graf, T. and R. Therrien, 2005, Variable-density groundwater flow and solute transport in porous media containing nonuniform discrete fractures. *Advances in Water Resources*, volume 28, issue 12, pages 1351–1367, [doi: 10.1016/j.advwatres.2005.04.011](https://doi.org/10.1016/j.advwatres.2005.04.011).
- Greskowiak, J., 2014, Tide-induced salt-fingering flow during submarine groundwater discharge. *Geophysical Research Letters*, volume 41, issue 18, pages 6413–6419, [doi: 10.1002/2014GL061184](https://doi.org/10.1002/2014GL061184).
- Guo, W. And C.D. Langevin, 2002, User's guide to SEAWAT; a computer program for simulation of three-dimensional variable-density ground-water flow. United States Geological Survey (USGS), Techniques of Water-Resources Investigations 06-A7, [doi: 10.3133/twri06A7](https://doi.org/10.3133/twri06A7).
- Hamann, E., V. Post, C. Kohfahl, H. Prommer, and C.T. Simmons, 2015, Numerical investigation of coupled density-driven flow and hydrogeochemical processes below playas. *Water Resources Research*, volume 51, issue 11, pages 9338–9352, [doi: 10.1002/2015WR017833](https://doi.org/10.1002/2015WR017833).
- Herzberg, A., 1888, Erläuterungs-Bericht zum Entwässerungs- und Wasserversorgungs-Projekt des Inseldorfes Nordeney (Explanatory report on the dewatering and water supply project of the island village Nordeney). Niedersächsisches Landesarchiv Aurich, Germany, volume 16, issue 3.
- Herzberg, A., 1901, Die Wasserversorgung einiger Nordseebäder (The water supply of some North Sea spas). *Journal für Gasbeleuchtung und Wasserversorgung XLIV*, pages 815-819, pages 842-844, [doi: 10.1007/s10040-018-1772-8](https://doi.org/10.1007/s10040-018-1772-8).
- Hett, W.S., 1957, Problems II Books XXII - XXXVIII. William Heinemann Limited, London & Harvard University Press, Cambridge, Massachusetts, 456 pages.
- Hidalgo, J.J. and J. Carrera, 2009, Effect of dispersion on the onset of convection during CO<sub>2</sub> sequestration. *Journal of Fluid Mechanics*, volume 640, issue 10, pages 441-452, [doi: 10.1017/S0022112009991480](https://doi.org/10.1017/S0022112009991480).
- Holzbecher, E., 1991, Numerische modellierung von Dichteströmungen im porösen Medium. Technische Universität Berlin, Institut für Wasserbau und Wasserwirtschaft, Berlin, Germany, 160 pages.
- Holzbecher, E., 1996, Convective Heat and Mass Flow in Porous Media in Sixth V.M. Goldschmidt Conference, Heidelberg, Germany, pages 271–271.

- Holzbecher, E.O., 1998, Modeling density-driven flow in porous media. Springer Berlin, Heidelberg, Berlin, 286 pages, [doi: 10.1007/978-3-642-58767-2](https://doi.org/10.1007/978-3-642-58767-2).
- Holzbecher, E., 2005, Groundwater flow pattern in the vicinity of a salt lake. *Hydrobiologia*, volume 532, pages 233-242, [doi: 10.1007/s10750-004-6421-7](https://doi.org/10.1007/s10750-004-6421-7).
- Horton, C.W. and F.T. Rogers, 1945, Convection currents in a porous medium. *Journal of Applied Physics*, volume 16, pages 367–370, [doi: 10.1063/1.1707601](https://doi.org/10.1063/1.1707601).
- Hubbert, M.K., 1957, Darcy's law and the field equations of the flow of underground fluids. *International Association of Scientific Hydrology Bulletin*, volume 2, issue 1, pages 23–59, [doi: 10.1080/02626665709493062](https://doi.org/10.1080/02626665709493062).
- Illangasekare, T., S.W. Tyler, T.P. Clement, K.G. Villholth, A.P.G.R.L. Perera, J. Obeysekera, A. Gunatilaka, C.R. Panabokke, D.W. Hyndman, K.J. Cunningham, J.J. Kaluarachchi, W.W.G. Yeh, M.T. van Genuchten, and K. Jensen, 2006. Impacts of the 2004 tsunami on groundwater resources in Sri Lanka. *Water Resources Research*, volume 42, issue 5, [doi: 10.1029/2006WR004876](https://doi.org/10.1029/2006WR004876).
- Ingebritsen, S.E., W.E. Sanford, and C.E. Neuzil, 2006, *Groundwater in Geologic Processes*. Second Edition, Cambridge University Press, Cambridge, United Kingdom, 536 pages.
- Inglis, G., 1817, On the cause of ebbing and flowing springs. *The philosophical Magazine*, volume 50, issue 232, pages 81–83, [doi: 10.1080/14786441708637732](https://doi.org/10.1080/14786441708637732).
- IOC, 2010, Intergovernmental Oceanographic Commission. The international thermodynamic equation of seawater - 2010: Calculation and use of thermodynamic properties. Intergovernmental Oceanographic Commission, 218 pages.
- Islam, A., A.Y. Sun, and C. Yang, 2016, Reactive transport modeling of the enhancement of density-driven CO<sub>2</sub> convective mixing in carbonate aquifers and its potential implication on geological carbon sequestration. *Scientific Reports*, volume 6, issue 24768, [doi: 10.1038/srep24768](https://doi.org/10.1038/srep24768).
- Jiao, J. and V. Post, 2019, *Coastal hydrogeology*. Cambridge University Press, [doi: 10.1017/9781139344142](https://doi.org/10.1017/9781139344142).
- Johannsen, K., 2003, On the validity of the Boussinesq Approximation for the Elder Problem. *Computational Geosciences*, volume 7, pages 169-182, <https://doi.org/10.1023/A:1025515229807>.
- Jones, G.D., F.F. Whitaker, P.L. Smart, and W.E. Sanford, 2004, Numerical analysis of seawater circulation in carbonate platforms: II. The dynamic interaction between geothermal and brine reflux circulation. *American Journal of Science*, volume 304, issue 3, pages 250–284, [doi: 10.2475/ajs.304.3.250](https://doi.org/10.2475/ajs.304.3.250).
- Knorr, B., Y. Xie, C. Stumpp, P. Maloszewski, and C.T. Simmons, 2016, Representativeness of 2D models to simulate 3D unstable variable density flow in porous media. *Journal of Hydrology*, volume 542, pages 541–551, [doi: 10.1016/j.jhydrol.2016.09.026](https://doi.org/10.1016/j.jhydrol.2016.09.026).

- Konikow, L.F., Campbell, P.J., and Sanford, W.E., 1996. Modelling brine transport in a porous medium: A re-evaluation of the HYDROCOIN Level 1, Case 5 problem. International Association of Hydrological Sciences (IAHS), AISH Publication number 237, pages 363–372.
- Kooi, H., J. Groen, and A. Leijnse, 2000a, Modes of seawater intrusion during transgressions. *Water Resources Research*, volume 36, issue 12, pages 3581–3589, doi: [10.1029/2000WR900243](https://doi.org/10.1029/2000WR900243).
- Kooi, H., J. Groen, and A. Leijnse, 2000b, Modes of seawater intrusion during transgressions. *Water Resources Research*, volume 36, issue 12, pages 3581–3589, <https://doi.org/10.1029/2000WR900243>.
- Kooper, W.F., 1983, Dichtheidsstroming in het watervoerend pakket onder de vuilstortplaats te Noordwijk. Instituut voor Drinkwatervoorziening, intern report, pages 25–83.
- Labat, J.B., 1724, *Nouveau voyage aux isles de l'Amérique* (New voyage to the islands of America). Tome Second, The Hague, the Netherlands.
- Langevin, C.D. and W. Guo, 2006, MODFLOW/MT3DMS-based simulation of variable-density ground water flow and transport. *Groundwater*, volume 44, issue 3, pages 339–351, doi: [10.1111/j.1745-6584.2005.00156.x](https://doi.org/10.1111/j.1745-6584.2005.00156.x).
- Lapwood, E.R., 1948, Convection of a fluid in a porous medium. *Mathematical Proceedings of the Cambridge Philosophical Society*. Cambridge University Press, volume 44, issue 4, pages 508–521, doi: [10.1017/S030500410002452X](https://doi.org/10.1017/S030500410002452X).
- LeBlanc, D.R., S.P. Garabedian, K.M. Hess, L.W. Gelhar, R.D. Quadri, K.G. Stollenwerk, and W.W. Wood, 1991, Large-scale natural gradient tracer test in sand and gravel, Cape Cod, Massachusetts: 1. Experimental design and observed tracer movement. *Water Resources Research*, volume 27, issue 5, pages 895–910, doi: [10.1029/91WR00241](https://doi.org/10.1029/91WR00241).
- Liang, Y., B. Wen, M.A. Hesse, and D. DiCarlo, 2018, Effect of dispersion on solutal convection in porous media. *Geophysical Research Letters*, volume 45, issue 18, pages 9690–9698, <https://doi.org/10.1029/2018GL079849>.
- van Lopik, J.H., N. Hartog, and W.J. Zaadnoordijk, 2016, The use of salinity contrast for density difference compensation to improve the thermal recovery efficiency in high-temperature aquifer thermal energy storage systems. *Hydrogeology Journal*, volume 24, pages 1255–1271, doi: [10.1007/s10040-016-1366-2](https://doi.org/10.1007/s10040-016-1366-2).
- Luszczynski, N.J., 1961, Head and flow of ground water of variable density. *Journal of Geophysical Research*, volume 66, issue 12, pages 4247–4256, doi: [10.1029/JZ066i012p04247](https://doi.org/10.1029/JZ066i012p04247).
- Mao, X., H. Prommer, D.A. Barry, C.D. Langevin, B. Panteleit, and L. Li, 2006, Three-dimensional model for multi-component reactive transport with variable density

- groundwater flow. *Environmental Modelling and Software*, volume 21, issue 5, pages 615–628, [doi: 10.1016/j.envsoft.2004.11.008](https://doi.org/10.1016/j.envsoft.2004.11.008).
- Mazzia, A., L. Bergamaschi, and M. Putti, 2001, On the reliability of numerical solutions of brine transport in groundwater: analysis of infiltration from a salt lake. *Transport in Porous Media*, volume 43, pages 65–86, [doi: 10.1023/A:1010665609617](https://doi.org/10.1023/A:1010665609617).
- Missimer, T.M., W. Guo, C.W. Walker, and R.G. Maliva, 2002, Hydraulic and density considerations in the design of aquifer storage and recovery systems. *Florida Water Resources Journal*, volume 55, pages 30–36.
- Monnin, C., 1989, An ion interaction model for the volumetric properties of natural waters: Density of the solution and partial molal volumes of electrolytes to high concentrations at 25°C. *Geochimica et Cosmochimica Acta*, volume 53, issue 6, pages 1177–1188, [doi: 10.1016/0016-7037\(89\)90055-0](https://doi.org/10.1016/0016-7037(89)90055-0).
- Monnin, C., 1994, Density calculation and concentration scale conversions for natural waters. *Computers and Geosciences*, volume 20, issue 10, pages 1435–1445, [doi: 10.1016/0098-3004\(94\)90103-1](https://doi.org/10.1016/0098-3004(94)90103-1).
- Murphy, H.D., 1979, Convective instabilities in vertical fractures and faults. *Journal of Geophysical Research*, volume 84, issue B11, pages 6121–6129, [doi: 10.1029/JB084iB11p06121](https://doi.org/10.1029/JB084iB11p06121).
- NEA, 1992, Nuclear Energy Agency, The International hydrocoin project Groundwater hydrology modelling strategies for performance assessment of nuclear waste disposal Summary report. Nuclear Energy Agency of the OECD (NEA), Paris, France, <https://inis.iaea.org/collection/NCLCollectionStore/Public/24/002/24002761.pdf> (accessed on February 1, 2022).
- NEA, 1990, Nuclear Energy Agency, 1990, The international hydrocoin project Groundwater hydrology modelling strategies for performance assessment of nuclear waste disposal. Nuclear Energy Agency of the Organisation for Economic Co-Operation and Development (OECD-NEA), Paris, France,
- Niederau, J., J.F. Wellmann, and N. Börsing, 2019, Analyzing the influence of correlation length in permeability on convective systems in heterogeneous aquifers using entropy production. *Geothermal Energy*, volume 7, issue 35, [doi: 10.1186/s40517-019-0151-6](https://doi.org/10.1186/s40517-019-0151-6).
- Nield, D.A., 1968, Onset of thermohaline convection in a porous medium. *Water Resources Research*, volume 4, issue 3, pages 553–560, [doi: 10.1029/WR004i003p00553](https://doi.org/10.1029/WR004i003p00553).
- Nield, D.A. and A. Bejan, 2006, *Convection in porous media*. Springer New York, 640 pages, [doi: 10.1007/0-387-33431-9](https://doi.org/10.1007/0-387-33431-9).
- Nield, D.A. and C.T. Simmons, 2007, A discussion on the effect of heterogeneity on the onset of convection in a porous medium. *Transport in Porous Media*, volume 68, pages 413–421, [doi: 10.1007/s11242-006-9045-8](https://doi.org/10.1007/s11242-006-9045-8).

- Oostrom, M., J.S. Hayworth, J.H. Dane, and O. Güven, 1992, Behavior of dense aqueous phase leachate plumes in homogeneous porous media. *Water Resources Research*, volume 28, issue 8, pages 2123–2134, [doi: 10.1029/92WR00711](https://doi.org/10.1029/92WR00711).
- Pawlowicz, R., 2012, The electrical conductivity of seawater at high temperatures and salinities. *Desalination*, volume 300, pages 32–39, [doi: 10.1016/j.desal.2012.06.001](https://doi.org/10.1016/j.desal.2012.06.001).
- Person, M., B. Dugan, J.B. Swenson, L. Urbano, C. Stott, J. Taylor, and M. Willett, 2003, Pleistocene hydrogeology of the Atlantic continental shelf, New England. *Geological Society of America Bulletin*, volume 115, issue 11, pages 1324–1343, [doi: 10.1130/B25285.1](https://doi.org/10.1130/B25285.1).
- Person, M., J.P. Raffensperger, S. Ge, G. Garven, 1996, Basin-scale hydrogeologic modeling. *Reviews of Geophysics*, volume 34, issue 1, pages 61–87, [doi: 10.1029/95RG03286](https://doi.org/10.1029/95RG03286).
- Post, V.E.A., 2012, Electrical conductivity as a proxy for groundwater density in coastal aquifers. *Groundwater*, volume 50, issue 5, pages 785–792, [doi: 10.1111/j.1745-6584.2011.00903.x](https://doi.org/10.1111/j.1745-6584.2011.00903.x).
- Post, V.E.A. and J.R. von Asmuth, 2013, Review: Hydraulic head measurements - new technologies, classic pitfalls. *Hydrogeology Journal*, volume 21, pages 737–750, [doi: 10.1007/s10040-013-0969-0](https://doi.org/10.1007/s10040-013-0969-0).
- Post, V.E.A., E. Banks, and M. Brunke, 2018a, Groundwater flow in the transition zone between freshwater and saltwater: a field-based study and analysis of measurement errors. *Hydrogeology Journal*, volume 26, pages 1821–1838, <https://doi.org/10.1007/s10040-018-1725-2>.
- Post, V.E.A. and G.J. Houben, 2017, Density-driven vertical transport of saltwater through the freshwater lens on the island of Baltrum (Germany) following the 1962 storm flood. *Journal of Hydrology*, volume 551, pages 689–702, [doi: 10.1016/j.jhydrol.2017.02.007](https://doi.org/10.1016/j.jhydrol.2017.02.007).
- Post, V.E.A., G.J. Houben, and J. van Engelen, 2018b, What is the Ghijben-Herzberg principle and who formulated it? *Hydrogeology Journal*, volume 26, pages 1801–1807, [doi: 10.1007/s10040-018-1796-0](https://doi.org/10.1007/s10040-018-1796-0).
- Post, V.E.A. and H. Kooi, 2003, Rates of salinization by free convection in high-permeability sediments: Insights from numerical modeling and application to the Dutch coastal area. *Hydrogeology Journal*, volume 11, pages 549–559, [doi: 10.1007/s10040-003-0271-7](https://doi.org/10.1007/s10040-003-0271-7).
- Post, V., H. Kooi, and C. Simmons, 2007, Using hydraulic head measurements in variable-density groundwater flow analyses. *Groundwater*, volume 45, issue 6, pages 664–671, [doi: 10.1111/j.1745-6584.2007.00339.x](https://doi.org/10.1111/j.1745-6584.2007.00339.x).
- Post, V.E.A. and H. Prommer, 2007, Multicomponent reactive transport simulation of the Elder problem: effects of chemical reactions on salt plume development. *Water Resources Research*, volume 43, issue 10, [doi: 10.1029/2006WR005630](https://doi.org/10.1029/2006WR005630).

- Post, V.E.A. and C.T. Simmons, 2010, Free convective controls on sequestration of salts into low-permeability strata: Insights from sand tank laboratory experiments and numerical modelling. *Hydrogeology Journal*, volume 18, pages 39-54, [doi: 10.1007/s10040-009-0521-4](https://doi.org/10.1007/s10040-009-0521-4).
- Prasad, A. and C.T. Simmons, 2005, Using quantitative indicators to evaluate results from variable-density groundwater flow models. *Hydrogeology Journal*, volume 13, pages 905–914, [doi: 10.1007/s10040-004-0338-0](https://doi.org/10.1007/s10040-004-0338-0).
- Prasad, A. and C.T. Simmons, 2003, Unstable density-driven flow in heterogeneous porous media: a stochastic study of the *Elder* [1967b] “short heater” problem. *Water Resources Research*, volume 39, issue 1, [doi: 10.1029/2002WR001290](https://doi.org/10.1029/2002WR001290).
- Raffensperger, J.P. and G. Garven, 1995, The formation of unconformity-type uranium ore deposits 2. Coupled hydrochemical modeling. *American Journal of Science*, volume 295, pages 639–696, [doi: 10.2475/ajs.295.6.639](https://doi.org/10.2475/ajs.295.6.639).
- Rappoldt, C., G.J.J.M. Pieters, E.B. Adema, G.J. Baaijens, A.P. Grootjans, and C.J. van Duijn, 2003, Buoyancy-driven flow in a peat moss layer as a mechanism for solute transport. *Proceedings of the National Academy of Sciences*, volume 100, issue 25, pages 14937-14942, [doi: 10.1073/pnas.1936122100](https://doi.org/10.1073/pnas.1936122100).
- Rayleigh, O.M.F.R.S.L, 1916, LIX. On convection currents in a horizontal layer of fluid, when the higher temperature is on the under side. *The London, Edinburgh, and Dublin Philosophical Magazine and Journal of Science*, volume 32, issue 192, pages 529-546, [doi: 10.1080/14786441608635602](https://doi.org/10.1080/14786441608635602).
- Rees, D.A.S., A. Selim, and J.P. Ennis-King, 2008, The instability of unsteady boundary layers in porous media *in* *Emerging topics in heat and mass transfer in porous media*, Springer, Dordrecht, Netherlands, pages 85–110, [doi: 10.1007/978-1-4020-8178-14](https://doi.org/10.1007/978-1-4020-8178-14).
- van Reeuwijk, M., S.A. Mathias, C.T. Simmons, and J.D. Ward, 2009, Insights from a pseudospectral approach to the *Elder* problem. *Water Resources Research*, volume 45, issue 4, [doi: 10.1029/2008WR007421](https://doi.org/10.1029/2008WR007421).
- Rehfeldt, K.R., J.M. Boggs, and L.W. Gelhar, 1992, Field study of dispersion in a heterogeneous aquifer: 3. Geostatistical analysis of hydraulic conductivity. *Water Resources Research*, volume 28, issue 12, pages 3309-3324, <https://doi.org/10.1029/92WR01758>.
- Reilly, T.E. and A.S. Goodman, 1985, Quantitative analysis of saltwater-freshwater relationships in groundwater systems - A historical perspective. *Journal of Hydrology*, volume 80, issues 1-2, pages 125-160, [doi: 10.1016/0022-1694\(85\)90078-2](https://doi.org/10.1016/0022-1694(85)90078-2).
- Riaz, A., M. Hesse, H.A. Tchelepi, and F.M. Orr, 2006, Onset of convection in a gravitationally unstable diffusive boundary layer in porous media. *Journal of Fluid Mechanics*, volume 548, pages 87-111, [doi: 10.1017/S0022112005007494](https://doi.org/10.1017/S0022112005007494).
- Ringrose, P.S., A.K. Furre, S.M. Gilfillan, S.M.V. Krevor, M. Landrø, R. Leslie, T. Meckel, B. Nazarian, and A. Zahid, 2021, Storage of carbon dioxide in saline aquifers:

- physicochemical processes, key constraints, and scale-up potential. *Annual Review of Chemical and Biomolecular Engineering*, volume 12, pages 471-494, [doi: 10.1146/annurev-chembioeng-093020-091447](https://doi.org/10.1146/annurev-chembioeng-093020-091447).
- Rülke, O., 1969, Die Auswirkungen der Sturmflut von 1962 auf ein Süßwasservorkommen auf der Insel Baltrum [The consequences of the storm flood of 1962 on the freshwater resources of the island of Baltrum], *Geologisches Jahrbuch*, volume 87, pages 427-444.
- Sainz-Garcia, A., E. Abarca, A. Nardi, F. Grandia, and E.H. Oelkers, 2017, Convective mixing fingers and chemistry interaction in carbon storage. *International Journal of Greenhouse Gas Control*, volume 58, pages 52-61, [doi: 10.1016/j.ijggc.2016.12.005](https://doi.org/10.1016/j.ijggc.2016.12.005).
- Sanford, W.E. and L.F. Konikow, 1989, Simulation of calcite dissolution and porosity changes in saltwater mixing zones in coastal aquifers. *Water Resources Research*, volume 25, issue 4, pages 655-667, <https://doi.org/10.1029/WR025i004p00655>.
- Santing, G., 1980, Een probleem bij de stroming van zoet en zout grondwater: de correcties op de stijghoogten. *H2O*, volume 13, pages 544-548.
- Schincariol, R.A. and F.W. Schwartz, 1990, An experimental investigation of variable density flow and mixing in homogeneous and heterogeneous media. *Water Resources Research*, volume 26, issue 10, pages 2317-2329, [doi: 10.1029/WR026i010p02317](https://doi.org/10.1029/WR026i010p02317).
- Segol, G., 1994, *Classic groundwater simulations: proving and improving numerical models*. Prentice Hall, 531 pages.
- Sharp, J.M., W.E. Galloway, L.S. Land, E.F. McBride, P.E. Blanchard, D.P. Bodner, S.P. Dutton, M.R. Farr, P.B. Gold, T.J. Jackson, P.D. Lundegard, G.L. Macpherson, and K.L. Milliken, 1988, Diagenetic processes in northwestern Gulf of Mexico sediments. *Developments in Sedimentology, Diagenesis*, volume 43, pages 43-113, [doi: 10.1016/S0070-4571\(08\)70006-2](https://doi.org/10.1016/S0070-4571(08)70006-2).
- Sharp, J.M. and M. Shi, 2009, Heterogeneity effects on possible salinity-driven free convection in low-permeability strata. *Geofluids*, volume 9, pages 263-274, [doi: 10.1111/j.1468-8123.2009.00262.x](https://doi.org/10.1111/j.1468-8123.2009.00262.x).
- Shikaze, S.G., E.A. Sudicky, and F.W. Schwartz, 1998, Density-dependent solute transport in discretely-fractured geologic media: is prediction possible? *Journal of Contaminant Hydrology*, volume 34, issue 3, pages 273-291, [doi: 10.1016/S0169-7722\(98\)00080-1](https://doi.org/10.1016/S0169-7722(98)00080-1).
- Simmons, C.T., 2005, Variable density groundwater flow: from current challenges to future possibilities. *Hydrogeology Journal*, volume 13, pages 116-119, [doi: 10.1007/s10040-004-0408-3](https://doi.org/10.1007/s10040-004-0408-3).
- Simmons, C.T. and J.W. Elder, 2017, The Elder Problem. *Groundwater*, volume 55, issue 6, pages 926-930, [doi: 10.1111/gwat.12593](https://doi.org/10.1111/gwat.12593).
- Simmons, C.T., T.R. Fenstemaker, and J.M. Sharp, 2001, Variable-density groundwater flow and solute transport in heterogeneous porous media: approaches, resolutions

- and future challenges. *Journal of Contaminant Hydrology*, volume 52, issues 1-4, pages 245-275, doi: [10.1016/S0169-7722\(01\)00160-7](https://doi.org/10.1016/S0169-7722(01)00160-7).
- Simmons, C.T., A.V. Kuznetsov, and D.A. Nield, 2010, Effect of strong heterogeneity on the onset of convection in a porous medium: importance of spatial dimensionality and geologic controls. *Water Resources Research*, volume 46, issue 9, doi: [10.1029/2009WR008606](https://doi.org/10.1029/2009WR008606).
- Simmons, C.T., K.A. Narayan, and R.A. Wooding, 1999, On a test case for density-dependent groundwater flow and solute transport models: the Salt Lake problem. *Water Resources Research*, volume 35, issue 12, pages 3607-3620, doi: [10.1029/1999WR900254](https://doi.org/10.1029/1999WR900254).
- Simmons, C.T., K.A. Narayan, J.A. Woods, and A.L. Herczeg, 2002a, Groundwater flow and solute transport at the Mourquong saline-water disposal basin, Murray Basin, southeastern Australia. *Hydrogeology Journal*, volume 10, pages 278-295, doi: [10.1007/s10040-002-0192-x](https://doi.org/10.1007/s10040-002-0192-x).
- Simmons, C.T., M.L. Pierini, and J.L. Hutson, 2002b, Laboratory investigation of variable-density flow and solute transport in unsaturated-saturated porous media. *Transport in Porous Media*, volume 47, pages 215-244, doi: [10.1023/A:1015568724369](https://doi.org/10.1023/A:1015568724369).
- Simmons, C.T., J.M. Sharp, and D.A. Nield, 2008, Modes of free convection in fractured low-permeability media. *Water Resources Research*, volume 44, issue 3, doi: [10.1029/2007WR006551](https://doi.org/10.1029/2007WR006551).
- Stevens, J.D., J.M. Sharp, C.T. Simmons, and T.R. Fenstemaker, 2009, Evidence of free convection in groundwater: Field-based measurements beneath wind-tidal flats. *Journal of Hydrology*, volume 375, issues 3-4, pages 394-409, doi: [10.1016/j.jhydrol.2009.06.035](https://doi.org/10.1016/j.jhydrol.2009.06.035).
- Sudicky, E.A., 1986, A natural gradient experiment on solute transport in a sand aquifer: spatial variability of hydraulic conductivity and its role in the dispersion process. *Water Resources Research*, volume 22, issue 13, pages 2069-2082, doi: [10.1029/WR022i013p02069](https://doi.org/10.1029/WR022i013p02069).
- Teller, J.T., J.M. Bowler, and P.G. Macumber, 1982, Modern sedimentation and hydrology in Lake Tyrrell, Victoria. *Journal of the Geological Society of Australia*, volume 29, issues 1-2, pages 159-175, doi: [10.1080/00167618208729202](https://doi.org/10.1080/00167618208729202).
- Verruijt, A., 1980, The rotation of a vertical interface in a porous medium. *Water Resources Research*, volume 16, issue 1, pages 239-240, <https://doi.org/10.1029/WR016i001p00239>.
- Versluys, J., 1918, *Hydrologie van het Nederlandsche Kustgebied*. Den Haag, Moormans, 28 pages.
- Voss, C.I., 1984, A finite-element simulation model for saturated-unsaturated, fluid-density-dependent ground-water flow with energy transport or

- chemically-reactive single-species solute transport. United States Geological Survey (USGS), Water-Resources Investigations Report 84-4369, 429 pages, [doi: 10.3133/wri844369](https://doi.org/10.3133/wri844369).
- Voss, C.I., 1999, USGS SUTRA Code - History, practical use, and application in Hawaii *in* Seawater intrusion in coastal aquifers – concepts, methods and practices, Springer, Dordrecht, pages 249–313, [doi: 10.1007/978-94-017-2969-79](https://doi.org/10.1007/978-94-017-2969-79).
- Voss, C.I., C.T. Simmons, and N.I. Robinson, 2010, Three-dimensional benchmark for variable-density flow and transport simulation: matching semi-analytic stability modes for steady unstable convection in an inclined porous box. *Hydrogeology Journal*, volume 18, pages 5–23, [doi: 10.1007/s10040-009-0556-6](https://doi.org/10.1007/s10040-009-0556-6).
- Voss, C.I. and W.R. Souza, 1987, Variable density flow and solute transport simulation of regional aquifers containing a narrow freshwater-saltwater transition zone. *Water Resources Research*, volume 23, issue 10, pages 1851–1866, [doi: 10.1029/WR023i010p01851](https://doi.org/10.1029/WR023i010p01851).
- Wallis, I., H. Prommer, T. Pichler, V. Post, S.B. Norton, M.D. Annable, and C.T. Simmons, 2011, Process-based reactive transport model to quantify arsenic mobility during aquifer storage and recovery of potable water. *Environmental Science and Technology*, volume 45, issue 16, pages 6924–6931, [doi: 10.1021/es201286c](https://doi.org/10.1021/es201286c).
- Ward, J.D., C.T. Simmons, and P.J. Dillon, 2007, A theoretical analysis of mixed convection in aquifer storage and recovery: how important are density effects? *Journal of Hydrology*, volume 343, issues 3-4, pages 169–186, [doi: 10.1016/j.jhydrol.2007.06.011](https://doi.org/10.1016/j.jhydrol.2007.06.011).
- Ward, J.D., C.T. Simmons, P.J. Dillon, and P. Pavelic, 2009, Integrated assessment of lateral flow, density effects and dispersion in aquifer storage and recovery. *Journal of Hydrology*, volume 370, pages 83–99, [doi: 10.1016/j.jhydrol.2009.02.055](https://doi.org/10.1016/j.jhydrol.2009.02.055).
- Werner, A.D., M. Bakker, V.E.A. Post, A. Vandenbohede, C. Lu, B. Ataie-Ashtiani, C.T. Simmons, and D.A. Barry, 2013, Seawater intrusion processes, investigation and management: recent advances and future challenges. *Advances in Water Resources*, volume 51, pages 3–26, [doi: 10.1016/j.advwatres.2012.03.004](https://doi.org/10.1016/j.advwatres.2012.03.004).
- Werner, A.D., H.K. Sharp, S.C. Galvis, V.E.A. Post, and P. Sinclair, 2017, Hydrogeology and management of freshwater lenses on atoll islands: review of current knowledge and research needs. *Journal of Hydrology*, volume 551, pages 819–844, [doi: 10.1016/j.jhydrol.2017.02.047](https://doi.org/10.1016/j.jhydrol.2017.02.047).
- Wigley, T.M.L. and L.N. Plummer, 1976, Mixing of carbonate waters. *Geochimica et Cosmochimica Acta*, volume 40, issue 9, pages 989–995, [doi: 10.1016/0016-7037\(76\)90041-7](https://doi.org/10.1016/0016-7037(76)90041-7).
- Wilson, A.M., W. Sanford, F. Whitaker, and P. Smart, 2001, Spatial patterns of diagenesis during geothermal circulation in carbonate platforms. *American Journal of Science*, volume 301, issue 8, pages 727–752, [doi: 10.2475/ajs.301.8.727](https://doi.org/10.2475/ajs.301.8.727).

- Wood, W.W., W.E. Sanford, and A.R.S. al Habshi, 2002, Source of solutes to the coastal sabkha of Abu Dhabi. *Geological Society of America Bulletin*, volume 114, issue 3, pages 259-268, [doi: 10.1130/0016-7606\(2002\)114%3C0259:SOSTTC%3E2.0.CO;2](https://doi.org/10.1130/0016-7606(2002)114%3C0259:SOSTTC%3E2.0.CO;2).
- Woodbury, A.D. and E.A. Sudicky, 1991, The geostatistical characteristics of the Borden aquifer. *Water Resources Research*, volume 27, issue 4, pages 533-546, [doi: 10.1029/90WR02545](https://doi.org/10.1029/90WR02545).
- Wooding, R.A., 1959, The stability of a viscous liquid in a vertical tube containing porous material. *Proceedings of the Royal Society, Series A, Mathematical, Physical and Engineering Sciences*, pages 120-134, [doi: 10.1098/rspa.1959.0141](https://doi.org/10.1098/rspa.1959.0141).
- Wooding, R.A., 1960, Rayleigh instability of a thermal boundary layer in flow through a porous medium. *Journal of Fluid Mechanics*, volume 9, issue 2, pages 183-192, [doi: 10.1017/S0022112060001031](https://doi.org/10.1017/S0022112060001031).
- Wooding, R.A., 1962, The stability of an interface between miscible fluids in a porous medium. *Zeitschrift für angewandte Mathematik und Physik ZAMP*, volume 13, pages 255-266, <https://doi.org/10.1007/BF01601087>.
- Wooding, R.A., 1963, Convection in a saturated porous medium at large Rayleigh number or Peclet number. *Journal of Fluid Mechanics*, volume 15, issue 4, pages 527-544, [doi: 10.1017/S0022112063000434](https://doi.org/10.1017/S0022112063000434).
- Wooding, R.A., 1969, Growth of fingers at an unstable diffusing interface in a porous medium or Hele-Shaw cell. *Journal of Fluid Mechanics*, volume 39, issue 3, pages 477-495, [doi: 10.1017/S002211206900228X](https://doi.org/10.1017/S002211206900228X).
- Wooding, R.A., S.W. Tyler, I. White, and P.A. Anderson, 1997, Convection in groundwater below an evaporating Salt Lake: 2. Evolution of fingers or plumes. *Water Resources Research*, volume 33, issue 6, pages 1219-1228, [doi: 10.1029/96WR03534](https://doi.org/10.1029/96WR03534).
- Xie, Y., C.T. Simmons, A.D. Werner, and H.J.G. Diersch, 2012, Prediction and uncertainty of free convection phenomena in porous media. *Water Resources Research*, volume 48, issue 2, [doi: 10.1029/2011WR011346](https://doi.org/10.1029/2011WR011346).
- Zhang, H. and F.W. Schwartz, 1995, Multispecies contaminant plumes in variable density flow systems. *Water Resources Research*, volume 31, issue 4, pages 837-847, [doi: 10.1029/94WR02567](https://doi.org/10.1029/94WR02567).
- Zhang, H., F.W. Schwartz, W.W. Wood, S.P. Garabedian, and D.R. LeBlanc, 1998, Simulation of variable-density flow and transport of reactive and nonreactive solutes during a tracer test at Cape Cod, Massachusetts. *Water Resources Research*, volume 34, issue 1, pages 67-82, [doi: 10.1029/97WR02918](https://doi.org/10.1029/97WR02918).
- Zheng, C. and G.D. Bennett, 2002, *Applied Contaminant Transport Modeling*. Wiley, second edition, 656 pages.

## 10 Boxes

### Box 1 - Free Convection Cake

The recipe to create the free convection cake (also known as marble cake) shown in the photograph of Figure 10 was included in Post (2004). As some of us nowadays prefer a plant-based diet, a vegan version of the recipe is provided below. It was kindly shared by André Nogueira and Rita Parente who included it in their cookbook "[Vegan Para Todos](#)" (Vegan for Everybody).



Vegan marble cake. Photograph copyright (2021), with permission from André Nogueira and Rita Parente.

#### Ingredients

- 1/4 cup (16 g) raw cacao powder
- 3–4 Table spoons lukewarm water
- 2 1/2 cups (340 g) all-purpose flour
- 2 teaspoons baking powder
- 1/2 teaspoon baking soda
- 1/4 teaspoon fine Himalayan salt
- 1 cup (250 ml) dairy-free milk

- 3/4 cup (approximately 200 g) granulated sugar
- 1/2 cup (125 ml) dairy-free yoghurt
- 1/3 cup (80 ml) sunflower oil
- 1 teaspoon apple cider vinegar
- 1 teaspoon vanilla extract

### Preparation

- Preheat the oven to 180 °C and line a rectangular loaf pan with parchment paper.
- In a small bowl, combine the cacao powder and two table spoons of lukewarm water and mix to obtain a thick paste. Add the remaining water to thin the paste slightly.
- Sift the flour, baking powder, baking soda and salt into a large mixing bowl. In another mixing bowl, combine the milk, sugar, yoghurt, oil, vinegar and vanilla extract.
- Pour the wet mixture onto the dry ingredients and mix until the ingredients are well incorporated. The batter should be smooth and pourable. Transfer half of your batter into your spare mixing bowl, add the cacao mixture and fold it in until it is combined.
- Use two large spoons to dollop the chocolate and vanilla cake batters into the pre lined pan alternately.
- Bake the cake in the oven for 45 minutes or until a toothpick comes out clean.
- Allow the cake to cool completely before removing it from the pan and cutting into it.

[Back to the main text](#) ↑

## 11 Exercise Solutions

### Solution Exercise 1

For the fresh water:  $p = \rho_f g(y + h)$

For the seawater:  $p = \rho_s g y$

Equating the pressures and rearranging gives:  $y = \frac{\rho_f}{\rho_s - \rho_f} h = 40h$

[Return to Exercise 1](#) ↑

### Solution Exercise 2

Baltic Sea:  $y = \frac{1000}{1005 - 1000} h = 200h$

Dead Sea:  $y = \frac{1000}{1240 - 1000} h = 4.17h$

[Return to Exercise 2](#) ↑

### Solution Exercise 3

Inserting Equation 12 in the bracketed term of Equation 18 shows that the terms cancel, thus yielding  $q_z = 0$ :

$$\frac{\rho_f - \rho_s}{\rho_f} + \frac{\rho_s - \rho_f}{\rho_f} = 0$$

[Return to Exercise 3](#) ↑

## Solution Exercise 4

The freshwater head can be calculated using  $h_f = z_i + (h_i - z_i) \frac{\rho_i}{\rho_f}$ , which gives (noting that  $z_i = 100 - 60 = 40$  m):

$$1. \quad h_{f,1} = 40 + (100.4 - 40) \frac{1010}{1000} = 101 \text{ m}$$

$$h_{f,2} = 40 + (100 - 40) \frac{1020}{1000} = 101.2 \text{ m}$$

The freshwater head is higher at piezometer 2 than at piezometer 1, so the flow is from piezometer 2 to 1. This is opposite to what one would conclude from uncorrected hydraulic head measurements.

2. The specific discharge follows from

$$q_x = -K_f \frac{\Delta h_f}{\Delta x} = -10 \times \frac{101.2 - 101}{200} = -0.01 \text{ m d}^{-1}$$

which is a negative number because flow is in the direction of declining head.

[Return to Exercise 4](#) ↑

## Solution Exercise 5

It can be seen that the density does not vary between the screens, so this means the point water hydraulic heads can be used directly in the calculation of  $q_z$  with Darcy's law. Given the negative numbers, the smallest absolute value is the highest hydraulic head so the hydraulic head increases with depth, thus flow is upward from screen 3 to screen 2. The factor of 1000 in the equation converts meters to millimeters.

$$q_z = -20 \frac{(-3.08 - -3.04)}{(-96.44 - -118.93)} \times 1000 = 36 \text{ mm d}^{-1}$$

While from screen 2 to 1 it is

$$q_z = -20 \frac{(-3.13 - -3.08)}{(-76.41 - -96.44)} \times 1000 = 50 \text{ mm d}^{-1}$$

For the more general case where the density varies, one would first convert the hydraulic heads to freshwater heads using  $h_f = z_i + (h_i - z_i) \frac{\rho_i}{\rho_f}$ , which yields (three decimals are provided to prevent large rounding errors in the calculation of  $q_z$ ):

Screen	$h_f$
1	-2.815
2	-2.679
3	-2.542

Using  $q_z = -K_f \left( \frac{\Delta h_f}{\Delta z} + \frac{\rho_{mean} - \rho_f}{\rho_f} \right)$  one finds for the flow between piezometer 3 and 2:

$$q_z = -20 \left( \frac{(-2.679 - -2.542)}{(-96.44 - -118.93)} + \frac{1004.3 - 1000}{1000} \right) \times 1000 = 36 \text{ mm d}^{-1}$$

And for the flow between piezometer 2 and 1

$$q_z = -20 \left( \frac{(-2.815 - -2.679)}{(-76.41 - -96.44)} + \frac{1004.3 - 1000}{1000} \right) \times 1000 = 5 \text{ mm d}^{-1}$$

Which is the same answer as before (note that the unrounded result has a 0.43 percent error because  $K_f$  was equated to the hydraulic conductivity).

[Return to Exercise 5](#) ↑

## Solution Exercise 6

$K_f = 10 \text{ m d}^{-1}$ , which is  $1.2 \times 10^{-4} \text{ m s}^{-1}$ , so with

$$K_f = \frac{k\rho_f g}{\mu_f}$$

The Rayleigh number can be calculated as

$$Ra = \frac{\Delta\rho g k H}{\mu D_C} = \frac{K_f \Delta\rho g H}{\rho_f D_C} = \frac{1.2 \times 10^{-4} \times 25 \times 9.81 \times 10}{1000 \times 5.0 \times 10^{-10}} = 5.7 \times 10^5$$

Where it was assumed that  $D = D_C = 5.0 \times 10^{-10} \text{ m}^2 \text{ s}^{-1}$  and the representative density values for fresh water and seawater were taken as provided in the text of this book.

[Return to Exercise 6](#) ↗

## Solution Exercise 7

The value for  $H$  can be obtained from Figure 9, with which the Rayleigh number can be calculated as:

$$Ra = \frac{\Delta\rho g k H}{\mu D_T} = \frac{3 \times 9.81 \times 10^{-10} \times 100}{1.0 \times 10^{-3} \times 1.0 \times 10^{-6}} = 2.9 \times 10^2$$

[Return to Exercise 7](#) ↗

## Solution Exercise 8

From the photograph it can be inferred that  $H = 1 \text{ m}$ , so:

$$Ra = \frac{\Delta\rho g k H}{\mu D_C} = \frac{235 \times 9.81 \times 1.25 \times 10^{-10} \times 1}{1 \times 10^{-3} \times 5.0 \times 10^{-10}} = 6 \times 10^5$$

[Return to Exercise 8](#) ↗

## 12 Notations

$C$	solute concentration ( $M/L^3$ )
$c$ and $c_s$	specific heat capacities of the groundwater and rock, respectively ( $ML^2/(T^2\theta)$ )
$C_0$	initial concentration of the groundwater ( $M/L^3$ )
$C_i$	concentration species $i$ ( $M/L^3$ )
$C_{i,0}$	reference concentration of species $i$ ( $M/L^3$ )
$c_p$	volumetric heat capacity ( $M/(LT^2\theta)$ )
$C_{ss}$	concentration associated with a source ( $M/L^3$ )
$D$	diffusion coefficient ( $L^2/T$ ); for solutes, $D=D_C$ the molecular diffusion coefficient; for heat, $D=D_T$ the thermal diffusion coefficient
$\overline{D}_{h,c}$	solute dispersion tensor ( $L^2/T$ ) which includes the effect of both molecular diffusion and mechanical dispersion
$D_C$	solute diffusion coefficient in the bulk medium which is decreased from the diffusion coefficient in open water by the factors of connected porosity ( $n$ ) and tortuosity ( $\tau$ ) ( $L^2/T$ )
$\Delta C$	concentration difference ( $M/L^3$ )
$\Delta\rho$	density difference ( $M/L^3$ )
$\Delta T$	temperature difference ( $\theta$ )
$D_T$	thermal diffusivity ( $L^2/T$ )
$\overline{D}_C$	dispersion tensor which includes the combined effects of thermal conduction and mechanical dispersion ( $L^2/T$ )
$g$	gravitational acceleration ( $L/T^2$ )
$\vec{g}$	gravitational acceleration vector ( $L/T^2$ )
$H$	thickness of the layer (L)
$h_p$	pressure head (L)

$h_{p,i}$	pressure head for a piezometer at location $i$ containing a fluid column with density $\rho_i$ (L)
$\vec{J}_C$	solute mass flux (M/(L <sup>2</sup> T))
$\vec{J}_e$	heat flux (M/T <sup>3</sup> )
$k$	intrinsic permeability (L <sup>2</sup> )
$K_d$	distribution coefficient (L <sup>3</sup> /M)
$k_T$	thermal conductivity (ML/(T <sup>3</sup> Θ))
$\mu$	dynamic viscosity (M/(LT))
$n$	porosity (dimensionless)
$\nabla$	gradient operator which represents the rate of change of a variable per unit of distance in the $x$ , $y$ and $z$ direction
$NS$	total number of solutes that contribute to the fluid density
$p$	pressure (M/(LT <sup>2</sup> ))
$p_0$	initial fluid pressure (M/(LT <sup>2</sup> ))
$\left(\frac{\partial \rho}{\partial C}\right)_i$	slope of the density-concentration relationship for species $i$
$\vec{q}$	specific discharge (L/T)
$Q_h$	heat flow across the source boundary (M/T <sup>3</sup> )
$Q_m$	mass flux across the source boundary (M/(TL <sup>2</sup> ))
$q_{ss}$	discharge rate per unit of volume of water source, or sink (1/T)
$\rho$	groundwater density (M/L <sup>3</sup> )
$\rho_0$	density of the fluid at initial concentration, temperature and pressure (M/L <sup>3</sup> )
$\rho_b$	dry bulk density of the rock (M/L <sup>3</sup> )
$\rho_r$	density of the rock (M/L <sup>3</sup> )
$\rho_{ss}$	density of water source, or sink (M/L <sup>3</sup> )
$t$	time (T)

$T$	temperature ( $\theta$ )
$T_0$	initial temperature of the groundwater ( $\theta$ )
$T_{ss}$	temperature associated with a source ( $\theta$ )
$z$	elevation relative to a datum (L)

## 13 About the Authors



**Vincent Post** is a hydrogeologist specializing in coastal groundwater systems and the development and application of reactive transport models. He obtained his Doctor of Philosophy degree in 2004 and has worked as an assistant professor in hydrogeology at the VU University in Amsterdam. Between July 2010 and December 2015, he worked as a lecturer/senior lecturer at Flinders. From January 2016 to June 2021, he was a research associate at the Federal Institute of Geosciences and Natural Resources (Bundesanstalt für Geowissenschaften und Rohstoffe, BGR) in Hannover, Germany. In July 2022 he founded Edinsi Groundwater, a company aimed at providing hydrogeological knowledge to support the sustainable management of groundwater. He remains affiliated with Flinders University as an Adjunct Associate Professor.



Distinguished Professor **Craig T. Simmons** FTSE (Fellow of the Australian Academy of Technology and Engineering) is a leading groundwater scientist, recognized for major contributions to groundwater science, science leadership, education and policy reform. Craig is Matthew Flinders Distinguished Professor of Hydrogeology, Schultz Chair in the Environment at Flinders University and Foundation Director of the ARC National Centre for Groundwater Research and Training in Australia. From July 2020, he is seconded to the Australian Research Council in the role of Executive Director for Mathematics, Physics, Chemistry and Earth Sciences. Craig is a Fellow of both the Australian Academy of Technology and Engineering (ATSE) and the American Geophysical Union (AGU). His work has been recognized by numerous national and international research and teaching awards including the Anton Hales Medal for outstanding contributions to research in the Earth Sciences awarded by the Australian Academy of Science, and an Australian Award for University Teaching. In 2015 Craig was named South Australian Scientist of the Year, and in 2017 he was awarded Australian Water Professional of the Year. He is a 2017 Convocation Medalist of Flinders University and 2017 Biennial Medalist of the Modelling and Simulation Society of Australia and New Zealand. He is a member of the U.S. National Academies of Sciences, Engineering, and Medicine Roundtable on Unconventional Hydrocarbon Development. He has served and/or continues to serve as an Editor and Associate Editor for numerous major international journals including *Water Resources Research*, *Journal of Hydrology*, *Hydrogeology Journal*, *Groundwater* and *Vadose Zone Journal*.

Please consider signing up for the GW-Project mailing list to stay informed about new book releases, events and ways to participate in the GW-Project. When you sign up for our email list it helps us build a global groundwater community. [Sign up](#)<sup>↗</sup>.



# Modifications to Original Release

## Changes from the Original Version to Version 2

Original Version: June 2022, Version 2: January 2023

### Specific changes:

Page numbers refer to the original pdf

page ii, is now page i and subsequent roman numeral pages are each decreased by i

page iii, added notation that this is version 2

page iv, updated wording of Groundwater Project book usage and email sign-up

page iv, after the ISBN number, DOI corrected

page 7, end of Figure 5 caption, subscripts  $s$  and  $f$  changed to italic font

page 8, parameter definitions for Equation 1, ' $z = 0$ ' and  $m$  at the end of the definition changed to upright font

page 9, first line after definitions for Equation 4, ' $z$ , is the elevation' changed  $z$  to italic font

page 13, last paragraph, 3rd line, 'which applied' changed to 'which is applied'

page 19, last sentence of caption to Figure 9, 'video' capitalized to 'Video'

page 27, last paragraph, 5th line, '0.5 mm d' changed to '0.5 mm  $d^{-1}$ '

page 37, parameter definitions after Equation 33,  $\rho_b$  and  $K_d$  subscripts changed to italic font

page 50, first paragraph, 5th line,  $Sh$  changed to italic font

page 50, caption of Figure 25,  $\mu$  and  $\sigma$  changed to italic font

page 51, first paragraph, 5th line,  $Sh$  changed to italic font

page 66, Exercise 1, 40 changed to upright font

page 66, Exercise 2, 1005 changed to upright font

A

page 68, Exercise 8, 'Figure 5b' changed to 'Figure 8b'

page 83, bottom of page, 'Return to main text' link corrected so it works

page 89, definition of  $\rho_{ss}$ , changed  $\rho$  to italic font

page 92, updated wording of email sign-up